COPPER, SILVER, AND GOLD ETCHING WITH H_2 AND CH_4 BASED PLASMAS

A Thesis
Presented to
The Academic Faculty

by

Tae-Seop Choi

In Partial Fulfillment
of the Requirements for the Degree
Doctor of Philosophy in the
School of Chemical & Biomolecular Engineering

Georgia Institute of Technology
December 2014

COPPER, SILVER, AND GOLD ETCHING WITH H_2 AND CH_4 BASED PLASMAS

Approved by:

Dr. Dennis W. Hess, Advisor
School of Chemical & Biomolecular Engineering
Georgia Institute of Technology

Dr. Pradeep K. Agrawal
School of Chemical & Biomolecular Engineering

Georgia Institute of Technology

Dr. Elsa Reichmanis
School of Chemical & Biomolecular Engineering
Georgia Institute of Technology

Dr. Michael A. Filler
School of Chemical & Biomolecular Engineering
Georgia Institute of Technology

Dr. Younan Xia
School of Biomedical Engineering
Georgia Institute of Technology

Date Approved: September 30, 2014

ACKNOWLEDGEMENTS

Graduate students' life is like climbing a very high mountain obscured by thick clouds. We do not know what paths are waiting for us until the moment we actually face it. Sometimes it could be a stiff slope, cliff, gentle slope or just flat plain if you are very lucky. In thermodynamic point of view, there is always a way to avoid high barriers, like simply using a catalyst. However, if a person already know how to find the easy path, that means he already had a Ph.D. or he is just genius no needs for pursuing the degree. Anyway, that is the reason why climbers needs a good guide and graduate students should find a good advisor. I believe that I am very lucky not because I have walked through a flat plain but I met Dr. Hess.

Dr. Hess was differ from authoritative professors that I have met in my undergraduate school. Whenever we discussed about my research, he never ordered me to do something or taught me solutions directly. Rather, he carefully listened to my opinions and was willing to think about the problems along with me, which built up my own knowledge and problem solving capability. What I like the most of him was his attitude toward my research project. Our meetings have always begun with his smile and curiosity on my experimental results and analysis, like an innocent child waiting for his new present on the Christmas Eve. In many times, Dr. Hess was very excited about the results and made me felt that he was passionately participating our research. People feel more happiness when there is someone whom they can share their experiences and emotions. Dr. Hess' enthusiasm on my research was a strong driving force to motivate myself and led my last 4 years of research life. Someday, I hope to have opportunities to deliver what I learn from Dr. Hess to people who will walk through the path I have gone through, like a Santa Clause giving presents to children.

I would like to give my sincerest thanks to my advisor, Professor Dennis W. Hess for his dedication in my graduate school life.

I also thank the member of my thesis committee, Professor Pradeep K. Agrawal, Professor Elsa Reichmanis, Professor Michael A. Filler, and Professor Younan Xia, for their advice and suggestions on my research work.

I thanks to Georgia Tech cleanroom staffs, Tran-Vihn Nguyen, Gary Spinner, Thomas Johnson-Averette, and Charlie Suh for their unlimited supports on my experiments.

I am thoroughly grateful to my wife Chiwon, my parents and all of my friends Galit Levitin, Michael Casciato, Lester Li, Sonam Sherpa, Fangyu Wu, Zhenguan Tang, Won-Tae Choi, and Lu Jiang.

TABLE OF CONTENTS

LIST OF TABLES

LIST OF FIGURES

LIST OF SYMBOLS AND ABBREVIATIONS

D°	diatomic bond dissociation enthalpy
$\Delta_{at}H°$	crystal standard atomization enthalpy
$\Delta_{sub}H°$	standard sublimation enthalpy
CMOS	complementary metal oxide semiconductor
CMP	chemical mechanical planarization/polishing
DC	direct current
DFT	density function theory
E-beam	electron beam
EEDF	electron energy distribution function
FCC	face cubic center
FE-SEM	field emission scanning electron microscopy
FTIR	Fourier transform infrared spectroscopy
hafcH	hexafluoroacetylacetone
IC	Integrated circuit
ICP	inductively coupled plasma
IR	infrared
OES	optical emission spectroscopy
SPR	surface plasmon resonance
PECVD	plasma enhanced chemical vapor deposition
PMMA	Poly(methyl methacrylate)
PR	photoresist
PT-ICP	plasma therm inductively coupled plasma
RF	radio frequency

Sccm	standard cubic centimeter per minute
UV	ultra violet
VUV	vacuum ultra violet
UHV	ultra high vacuum
XPS	X-ray photonelectron spectroscopy

SUMMARY

This thesis describes investigations on Cu, Ag, and Au subtractive etching by H_2 and CH_4 plasmas below room temperature (10 ^oC). Both blanket film etching and patterning studies were performed. Results from these efforts generated insight into the mechanisms controlling the etch processes.

The unique electronic structure of Cu, Ag, and Au (group 11 metals) yields similar electrical and optical properties, which facilitate the use of these metals as interconnects in electronic devices and allows the design and fabrication of photonic devices. However, the inability to pattern Cu, Ag, and Au anisotropically with nm scale critical dimensions in traditional wet (liquid) etch processes precludes implementation for current and future device fabrication. The low volatility of etch products for halogenated plasma etch processes inhibits dry etching processes unless ion beams or sputtering approaches are invoked; these techniques suffer from low etch rates and limited selectivity. Such limitations led to an additive (Damascene) process for Cu patterning. Environmental concerns with disposal of the slurries used for Damascene patterning as well as an increase in the resistivity of Cu structures due to the nm scale patterns has led to a renewed interest in subtractive patterning methods for Cu.

In order to demonstrate that H_2 plasmas may be feasible to replace Damascene processes and other metal patterning schemes, nm scale Cu stack etching and various metal etching studies were performed. ~60 nm Ta/Cu/Ta stacks with ~70 ° wall slope were successfully patterned by a 3-step $CF_4/H_2/CF_4$ plasma sequence. In addition, the ability to etch the other group 11 metals, Ag and Au (33 nm/min and 26 nm/min of etch rate), in H_2 plasmas was demonstrated. In contrast, metals such as Ti, Ta, Ni, Cr, and Al, which are frequently employed in IC devices, were not

etched under the same H_2 plasma conditions, indicating that the chemistry based upon the similar electronic structure of group 11 metals plays an important role in H_2 plasma etching. Detailed masking studies demonstrated that an electronically excited state induced by photon enhancement facilitates the formation and desorption of hydrides of the group 11 metals. Unlike Cu removal, which depends to some extent upon chemical processes, effective removal of Ag and Au requires substantial enhancement by physical sputtering.

Photoresist (PR) mask degradation during reactive H_2 plasma etching was mitigated by invoking the residue-forming etchant CH_4. CH_4 plasmas also increased the Cu etch rate (17 nm/min), despite its well-known ability to form passivation layers that inhibit etching. Although gaseous CH_3Cu was not observed with optical emission spectroscopy (OES), the energetic momentum transfer from CH_x+ ion sputtering and the formation of a thermodynamically stable CH_3Cu moiety appear to be responsible for the increased Cu etch rate in CH_4 plasmas despite the hydrocarbon residue formation. Similarly, Ag and Au etching occurred in CH_4 plasmas with etch rates of 31 nm/min and 12 nm/min, respectively. Analogous to H_2 plasma etching, physical ion sputtering is the major contributor to Ag and Au etching in CH_4 plasmas although Au etch products have sufficient volatility to desorb from the surface even without ion bombardment. However, the enhanced Cu etch rate in CH_4 plasmas compared to the etch rate in H_2 (13 nm/min) and He (10 nm/min) plasmas confirms that chemical reactions play an important role in Cu etching in CH_4 plasmas.

CHAPTER 1.

INTRODUCTION

1.1 Unique Optical and Electrical Properties of Cu, Ag and Au

Copper (Cu), silver (Ag), and gold (Au) have drawn attention for a variety of applications because they share unique and similar properties such as high electrical conductivity, high corrosion resistance, and reflectivity. These features are consequences of the behavior of valence electrons which originate from the similar electronic structures of Cu, Ag, and Au in group 11 elements [1, 2].

Energy levels of electrons in a single atomic metal are quantized and each level is occupied by two electrons, one with spin up and the other with spin down, based on the Pauli exclusion principle [3]. The electrons are accommodated in the energy bands from the lowest energy level until all electrons in a metal have been placed in the higher levels. At absolute zero, the highest energy level occupied by an electron is called the Fermi energy or Fermi level. In this scenario, the probability of electron occupancy in an energy level above the Fermi energy is zero at T = 0 K. In addition, the filled space below the Fermi energy is known as the Fermi sphere and its surface is called the Fermi surface. However, when T > 0 K, thermal excitation of electrons occurs, thereby populating energy levels above the Fermi energy. Because the thermal energy available to an electron at room temperature is ~0.025 eV, only those electrons near the Fermi level or Fermi surface can be excited [3].

In diatomic molecules, each atomic level is split into two energy levels due to the influence of one atom on electrons in the other atom. Likewise, in a crystalline solid, the inter-atomic interaction influences electrons in other atoms; as a result, the atomic levels are split into

a number of closely spaced sublevels. Because the energy interval between two adjacent levels are very small, the individual sublevels are indistinguishable and electrons can move in what is regarded as a continuous energy band [3]. Like energy levels in an atom, each energy band can hold up two electrons per band [1]. Metal properties arise from the electrons near the Fermi surface or from interband transitions between filled electron levels below the Fermi energy and unfilled electron levels above the Fermi energy, because only electrons near the Fermi surface can response to a stimulus such as an electric field or optical-frequency photons [1].

The outer electron configuration of Group 11 elements, Cu, Ag, and Au, has one s-electron near the Fermi level which is above a filled d band. The strong tendency to completely fill a d band and the presence of an s-d band gap, accounts for monovalent chemical behavior, high electrical conductivity, and optical properties, analogous to the characteristics of monovalent alkali metals [1, 2].

The electrical conductivity of metals depends on the number of charge carriers and their mobility [2]. The charge carrier density of Cu, Ag, and Au is 1/atom because the number of electrons involved in the Fermi surface is one, unlike other noble metals(Ru, Rh, Pd, Os, IR, and Pt) whose charge carrier density is < 1/atom due to their d-s interband transition [2]. Thus, the high electrical conductivity of Cu, Ag, and Au originates from their free-electron-like monovalent behavior. In addition to the monovalent behavior, the high mobility of free electrons arises from the crystal compressibility and density, which leads to high electrical conductivity [1, 2]. Generally, the electrical resistivity of metals increases with an increase in metal temperature [3]. That is, lattice vibrations (phonons) by the metal ions result in enhanced electron scattering [3]. However, the low compressibility due to the completely filled d band and the dense crystal structure (face centered cubic) of Cu, Ag, and Au reduce the amplitude of phonons, which

contributes to the observed high electrical conductivity [1, 2]. The metal optical properties depend on the interactions of photons with s and d band electrons [2]. The electrons in the filled d band below the Fermi surface can be excited by absorbing photons. Therefore, the minimum energy which can be absorbed from a photon is determined by the energy difference between the d band and the Fermi level of metals [2]. For Cu, Ag, and Au, the energy difference between the lower filled d band and the Fermi level are 2.1 eV, 4 eV, and 2.17 eV, and corresponding photon wavelengths are 591 nm, 300 nm, and 560 nm, respectively. Thus, Cu and Au reflect light above 591 nm and 560 nm while no visible light is absorbed by Ag[1, 2]. This unique optical character generates the distinctive colors of red for Cu, white for Ag, and yellow for Au [1, 2] and causes surface plasmon resonance (SPR) of these nanostructures to occur at visible frequencies [4, 5].

Table 1.1 describes a variety of physical, chemical, electrical, and optical properties of Cu, Ag, and Au and compares them to them to the properties of aluminum (Al) [1, 2, 6-13]. These data offer information that relates to potential electrical and optical applications and show the similarities that might be exploited in chemical and physical processing methods for group 11 elements. Specific comparisons among these elements are discussed in following sections.

Table 1.1 Properties of Cu, Ag, Au, and Al; data are obtained from [11, 12] except resistivities [7, 8], self-diffusivities [6], reflectances [1, 2, 13], metal hydrides formation and atomization enthalpy [9, 10].

	Cu	Ag	Au	Al
Atomic number	29	47	79	13
Group	11	11	11	13
Period	4	5	6	3
Atomic mass	63.5	107.9	197	27
Crystal structure	fcc	fcc	fcc	fcc
Atomic radius (pm)	135	160	135	125
Bond length (pm)	272	290	288	242
Electron configuration	[Ar] $3d^{10}$ $4s^{1}$	[Kr] $4d^{10}$ $5s^{1}$	[Xe] $5d^{10}$ $6s^{1}$	[Ne] $3s^{2}p^{1}$
Resistivity ($\mu\Omega$ cm)	1.7	1.6	2.2	2.7
Self- Diffusivity (cm2/s at 1000 K)	1.67E-09	1.07E-08	6.15E-09	2.37E-06
Wave length of reflectance >85% (nm)	591	300	560	104
Electron work function (eV)	4.65	4.26	5.1	4.28
Electronegativity	1.9 (Pauling); 1.75 (Allrod Rochow)	1.93 (Pauling); 1.42 (Allrod Rochow)	2.54 (Pauling); 1.42 (Allrod Rochow)	1.61 (Pauling) 1.47 (Allrod Rochow)
Melting point (K)	1357.75	1234	1337.73	933.4
Enthalpy of fusion (kJ/mol)	13.01	11.3	12.55	10.67
Enthalpy of atomization (kJ/mol at 25°C)	338.9	284.5	364	322.2
Formation enthalpy of metal hydride crystal (kJ/mol)	CuH: 87±17	AgH: 86±19	AuH: 67±19	AlH_3: -11.4
Atomization enthalpy of metal hydride crystal (kJ/mol)	467±17	417±19	519±19	unknown
Lattice energy (kJ/mol)	CuH: 1254 (thermochemical cycle) or 828 (calculated) CuH_2: 2941(calculated)	AgH: 941 (calculated)	AuH: 1033(calculated)	AlH_3: 5924 (calculated)
Bond energy in gaseous diatomic species (kJ/mol)	CuCu: 176.52 ±2.38 CuH: 277.8 CuO: 269.0 ±20.9	AgAg: 160.3 ±3.4 AgH: 215.1 ±8 AgO: 220.1 ±20.9	AuAu: 224.7 ±1.5 AuH: 292.±6.7l AuO :221.8 ±20.9	AlAl: 133 ±6 AlH: 284.9 ±6.3 AlO: 511 ±3

1.2 Interconnects in Integrated Circuits

An integrated circuit (IC) is comprised of a set of electronic devices where active (transistor) and passive (resistor, capacitor, and inductor) units are assembled on a single silicon substrate and interconnected by conducting films [14, 15]. The interconnect materials must have

high electrical conductivity, which led to the use of aluminum (Al) for this purpose beginning in the early 1960s [15].

Historically, the performance of an IC chip was dominated by the time delay introduced by operation of a complementary metal oxide semiconductor (CMOS) transistor. However, the IC evolved based upon the idea of increasing the number of devices and their packing density by reducing the pattern size of films that comprise circuits and devices [16]. Although the time delay of CMOS transistors decreased as the channel length of CMOS transistors was reduced, the time delay from the parasitic resistance due to the capacitance of interlayer dielectric films that serve as electrical isolation between metal layers and to the resistance of the metal film, remained constant [17]. As a result, the wiring resistance and capacitance (RC) delay of interconnects increasingly affected IC performance as the device sizes became submicron [17]. Therefore, a combination of lower resistivity metal interconnect materials and interlayer materials with dielectric constants lower than that of SiO_2 were desired to reduce RC time delays [15].

In addition, as the critical dimension of devices fell below one micron, electromigration-related circuit failures became a concern in ICs [15]. The smaller cross-section of Al interconnects caused larger current densities, which enhanced electron momentum transfer to Al ions. As a result, Al transport created hillocks and voids in the film, which led to short-circuits or open circuits and thereby reliability failures of the interconnects [15].

Because of these problems with IC speed and reliability, Al was replaced by copper (Cu) as an interconnect material in 1993 due to its lower resistivity (1.7 μΩ-cm for Cu and 2.7 μΩ-cm for Al) [7] and better resistance to electromigration compared to Al [15]. However, Cu does not show the highest conductivity of noble metals nor does it have the best electromigration

resistance. Specifically, Ag and Au can be considered viable candidates for future interconnects. The electrical resistivity of Ag is the lowest among all metals (1.6 μΩ-cm) and the oxidation resistance of Ag also exceeds that of Cu and Al [7]. In addition, the electromigration resistance of Ag is as at least one order of magnitude higher than that of Al [7]. Although the electrical resistivity of Au (2.2 μΩ-cm) [8] is higher than that of Cu, the chemical inertness and a factor of ~3 improvement in electromigration resistance relative to Al [18] suggests that Au can be considered a potential interconnect material.

1.3 Surface Plasmon Resonance and Optical Applications

When incident light is absorbed by spherical metallic nanostructures, the oscillating electric field invokes the collective oscillation of free electrons; this phenomenon is known as surface plasmon resonance [19]. As described in Figure 1.1, the electron cloud in the metal is displaced relative to the nuclei by the electric field, and is restored by the columbic force between electrons and nuclei. This restoring motion causes free electron oscillation relative to the nuclei [19]. The resonance (oscillation) frequency depends upon the polarizability, size and shape of the metal nanoparticle, and by inter-nanoparticle coupling interactions [5]. Because SPR occurs at visible frequencies for Cu, Ag, and Au [4], these metals can be employed in optical devices and applications [5].

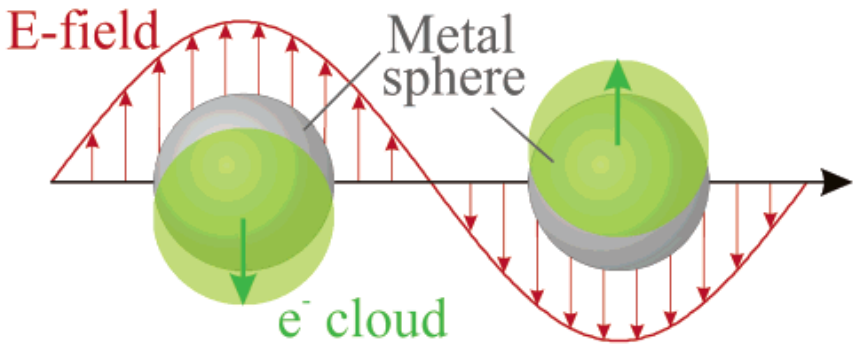

Figure 1.1 Schematic of surface plasmon resonance for a nanosphere. The electric field displaces the free electrons relative to the nuclei [19].

Optical applications for nanoparticles often arise from the damping process of SPR [20]. There are two major energy decay paths of SPR (Figure 1.2); radiative transformation of SPR and a nonradiative path where SPR decays into electron-hole excitations via intraband transitions or interband transitions (For noble metals, interband excitation occurs between the s band and d band near Fermi level) [20]. The electromagnetic wave from the radiative decay path of SPR, whose oscillating frequency is the same as the surface plasmon frequency, results in elastic/Rayleigh scattering by the nanoparticle [5]. On the other hand, the nonradiative path comprises light absorption by the nanoparticle [5]. These extinction paths are dependent on particle size [21]. Light absorption dominates the decay path for smaller nanoparticle that do not scatter, while strong light scattering and absorption contribute to the SPR extinction for larger particles [21]. The tunability of light absorption and scattering of noble nanoparticles makes possible a variety of applications [5]. For example, because the light scattering intensity from Au nano particles is 4 - 5 orders of magnitude higher than that of efficient fluorophores [21], Au nanoparticles can be employed as tags replacing conventional fluorophores in optical imaging [22]. Moreover, the strong dependency of SPR on the dielectric constant of the local environment of nanoparticles [19] such as solvent, substrate and adsorbates, provides potential application to biosensing [23-25]. Also, as a result of the nonradiative extinction path, the

absorbed light is converted to heat by electron- electron and electron-phonon relaxations [26], which can be utilized for the photothermal therapy of cancer cells [27].

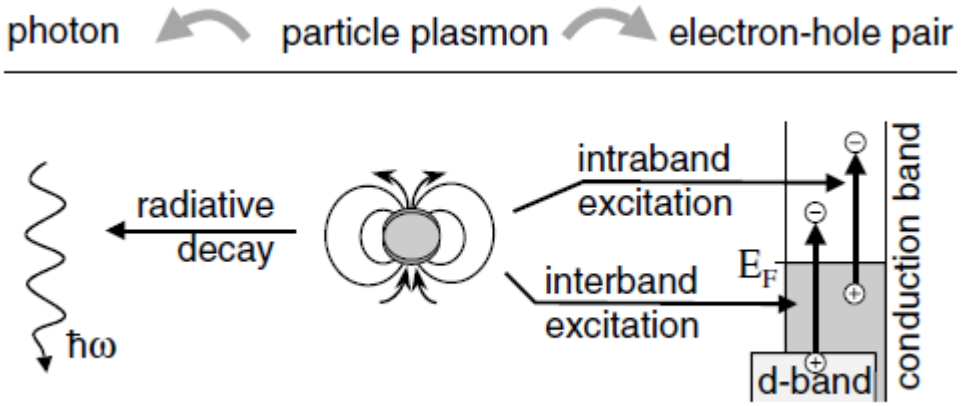

Figure 1.2 Scheme of radiative and nonradiative (intra or inter band transition) decay of surface plasmon resonance of nanoparticles [20].

Several methods have been reported to prepare nanoparticles or structures for optical applications. The traditional methods for preparing Ag and Au nanoparticles involve the precipitation of colloidal nanoparticles [28]. The first synthetic process is the reduction of metallic ions by electron transfer from a reducing agent [29]. These metal atoms gradually aggregate to form stable nuclei, which continue to grow by diffusion of metal atoms from solution [29]. The other approach invokes patterning of nanostructure by a lift-off method, which consist of three major processes; patterning of a mask layer, deposition of the metal film into the patterned trench, and removal of the mask layer [30]. The widely used mask material is a monolayer of polystyrene particles [24] or the patterning of an electron sensitive polymer such as Poly(methyl methacrylate) (PMMA) by electron beam lithography which degrades the exposed area of PMMA [30]. Metal films can be deposited by physical vapor deposition, where a metal source is either heated by a filament, coil or electron beam, or sputtered by energetic ions accelerated into the metal target [31]. Alternatively, metal films can be deposited

electrochemically from solution where metal ions from the anode diffuse to the cathode where they are reduced to form a metal film [32].

1.4 Plasmas and Plasma Etching Processes

Plasma etching has been used in IC fabrication since the early 1980s due to the ability to achieve high etch selectivity and anisotropic etch profiles. This technique generates free radicals and ions through electron impact collisions in an ionized gas, and is capable of high etch rates through ion enhanced chemical reaction of free radicals with film surfaces. This method allows improved dimensional resolution, tolerances, and control relative to what can be achieved by wet-chemical etching [33].

A plasma is a state of gas composed of electrons, ions, and neutral chemical species in ground and in excited states. The plasmas employed in IC fabrication are partially ionized gases, since only a fraction of the gas is ionized and dissociated. Generally, the power required for this purpose is provided by a radio frequency (RF) electromagnetic field. Electrons generated from the ionization are accelerated by the RF field; during oscillation within the field, they collide with gaseous species to form a variety of chemical moieties. Specifically, inelastic electron impact collisions generate chemically reactive species such as radicals and excited state atoms or molecules and energetic radiation (ions, electrons, and photons) by transferring energy to molecules or atoms [34, 35].

Plasma etching consist of 3 steps: (1) formation of reactive species by electron collisions; (2) transport and adsorption of the reactive species at the film surface followed by reaction with the surface material in order to form volatile products; (3) desorption of the volatile products which are removed from the chamber by convection through the vacuum pump [34].

There are four basic processes that can occur when a surface is exposed to a plasma: sputtering, pure chemical etching, energetic ion-enhanced etching, and protective ion-enhanced etching (Figure 1.3 [34]). Sputtering is the mechanical ejection of substrate material from surfaces by momentum transfer from energetic ion bombardment. Although sputter etch rates are low and display essentially no selectivity to the mask layer or underlying film materials, high directionality induced by acceleration of ions due to an established electric field makes sputtering anisotropic and assists removal of low volatility etch products. In pure chemical etching, neutral radicals react with substrate materials to form volatile products, which leads to high selectivity, but isotropic etch profiles similar to those from wet etching due to the lack of ion bombardment to enhance vertical etch rates. Energetic ion-enhanced etching is a synergistic process which combines chemical and physical effects of plasma-generated species, and thus promotes reaction between etchant and the substrate material. Generally, etch rates increase with increases in ion energy although anisotropy and selectivity can be reduced. Finally, protective ion-enhanced etching is the combination of material deposition and etching. Fragments from dissociated gas phase precursors form films over all substrate surfaces. This protective coating inhibits sidewall (lateral) etching, while ion bombardment removes the deposited layer on the surface perpendicular to the ion bombarding direction to enable anisotropic patterning or etching [35].

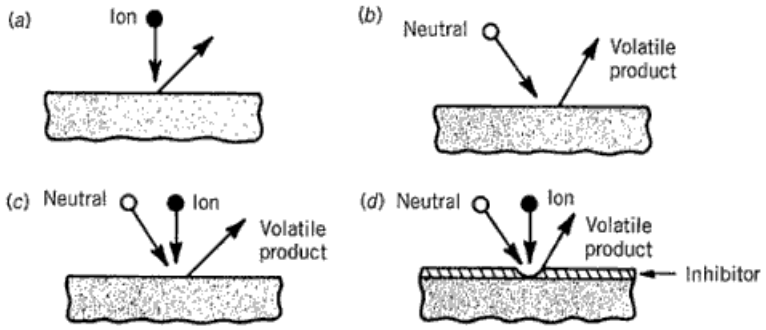

Figure 1.3 Four basic plasma-surface etch processes: (a) sputtering; (b) pure chemical etching; (c) energetic ion-enhanced etching; (d) protective ion-enhanced etching [35]

In this study, an inductively coupled plasma (ICP) system has been used to investigate metal etch processes. An ICP has two RF power supplies, one supplies power to the coil (Figure 1.4) and the other supplies power to the platen (or electrode) where the backside cooling system is incorporated. A mechanical chuck holds a 4" Si wafer on top of the platen and He gas flows through the trenches where the platen is contact with the underside of the Si wafer to maintain a constant Si wafer temperature (generally at 10 ℃) during plasma operation. The base pressure of the ICP system is 10^{-5} Torr and 5-80 mTorr pressure variation can be achieved during the etch process. The pressure and inlet gas flows are controlled by mechanical and turbo pumps, and mass flow controllers, respectively. The maximum gas flow was 75 sccm for each of the 6 gas lines(O_2, Ar, H_2,CF_4, C_4F_8, and CO_2, where He and CH_4 gas share the gas line with Ar and CO_2, respectively).

An ICP has two RF power supplies, one supplies power to the coil (Figure 1.4) and the other supplies power to the platen. An RF voltage applied to the coil creates an RF current that induces an electromagnetic field, and thereby generates a high plasma density, e.g., ~10^{12} electrons and ions per cm^3. Power applied to the platen increases the negative potential on the platen and thus the substrate, which enhances the positive ion bombardment flux and energy.

Between the glow discharge or plasma region and the substrate or platen surface, there is a region/layer called the 'sheath', which is a charge imbalance (electric field) regime that has a preponderance of positive ions [36]. The positive ions in the bulk (glow) discharge which reach the boundary of sheath are accelerated across the sheath by the negatively charged substrate and thus bombard the substrate or platen [36, 37]. In general, because the power applied to the platen is relatively small compared to the coil power, it does not effectively ionize and dissociate the low pressure gas. Thus, it is possible to nearly independently control the density of the plasma (ions, electrons, and neutral radicals) and the ion bombardment energy; in this way, etch processes can be optimized for specific results such as etch rate, anisotropy and selectivity [37].

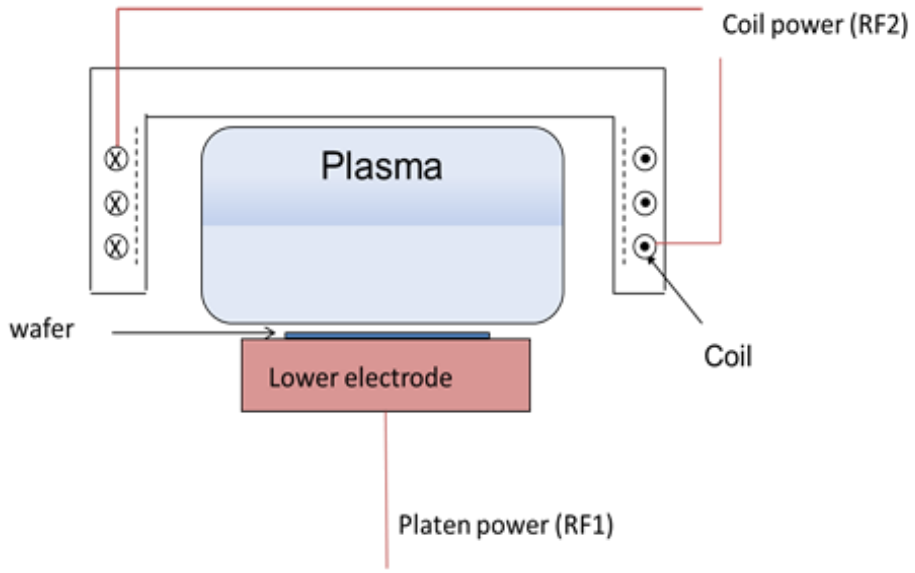

Figure 1.4 Schematic of a cylindrical inductively coupled plasma (ICP) reactor

1.5 Patterning Methods of Cu, Ag, and Au Films: from Wet to Dry.

1.5.1 Wet Etching

Etching or patterning is one of the most important processes for IC or microelectronic device fabrication [38]. Until the early 1980s, wet etching, which is simple and economical, was

the dominant method for pattern transfer through a mask to underlying semiconductor or metal layers [38]. Like many other metals, a variety of wet (liquid) etching solutions for Cu, Ag, and Au have been reported [39-47].

The basic principle of a wet etch process is the oxidization of metal by oxidizing agents followed by formation of metal-ligand complexes to remove the oxidized metal from the surface [40]. Thus, the wet etch rate is dependent upon the chemical reactivity of metals and the solubility of ligand complexes [39, 42]. Because the order of chemical reactivity decreases from Cu > Ag > Au, some etchants can dissolve Cu but not Ag and Au, or Cu and Ag but not Au [39]. For example, dilute aqua regia (3HCl: $1H_2O_2$:$2H_2O$ at 30 ℃) dissolves Cu, Ag and Au, piranha ($50H_2SO_4$: $1H_2O_2$ at 120 ℃) dissolves Cu and Ag but not Au, and a 30% $FeCl_3$ aqueous solution dissolves only Cu [41].

As mentioned above, a variety of liquid etchants can be used to etch Cu. An aqueous $FeCl_3$ solution with HCl is used to etch Cu at room temperature; in this solution, $FeCl_3$ is dissociated into Fe^{3+} (etchant) and Cl^- (coordinating ligand) and HCl assists the dissolution of copper chloride [39, 41].

$$Cu(s) + 2Fe^{3+} + 3Cl^- \rightarrow CuCl_3^- + 2Fe^{2+}$$

The reported Cu etch rate can reach 3900 nm/min depending upon the $FeCl_3$ and HCl concentrations [39, 41], and the narrowest Cu line width that could be defined was 600 nm [39]. Similarly, the addition of $2Fe(NO_3)_3$: $3SC(NH_2)_2$ (Thiourea) in deionized water to HCl permitted the definition of 200 nm line widths of Cu as well as Ag and Au, but the etch rate was not reported [40].

Xia at al. reported Ag wet etching with a variety of etchants (Fe^{3+}, O_2, and H_2O_2) combined with coordinating ligands ($S_2O_3^{2-}$, CN^-, I, Br, Cl, OH, and SCN) at room temperature [42]. The etch rate of standard $K_3Fe(CN)_3$ (0.01 M) aqueous solution was ~150 nm/min while the etch rate also depended on the types of coordinating ligands in the decreasing order $I^- > OH^- \approx Br^- \approx SCN^- > Cl^-$ [42]. The smallest size of Ag structures defined was ~200 nm.

$$Ag(s) + Fe(CN)_6^{3-} + X^- \rightarrow AgX(s) + Fe(CN)_6^{4-}$$,where X =I, Br, Cl, OH and SCN

Because of the precipitation of AgX, addition of $K_2S_2O_3$ was recommended to form soluble $Ag(S_2O_3^{2-})_2^{3-}$ [42]. When $Fe(NO_3)_3$ (0.05 M) was used as an etchant at room temperature, the reported Ag etch rate was ~100 nm but increased up to 2800 nm/min with 0.1 M $Fe(NO)_3$.

$$Ag(s) + Fe(NO_3)_3 \rightarrow AgNO_3 + Fe(NO_3)_2$$

Additional ligands were not necessary for this recipe due to the formation of soluble $AgNO_3$ [42]. Likewise, an aqueous solution with saturated O_2 (etchant) displayed a Ag etch rate of 25 nm/min, and the combination of H_2O_2 etchant and NH_4OH ligands can dissolve the Ag, although O_2 bubbles form on the Ag surface which generated non-uniform etch rates across the surface [42].

Traditionally, the solution used for Au wet etching has contained cyanide (CN^-) as a coordinating ligand [38]. Since the adsorption of CN^- lowers the oxidation potential of Au by 2 V, a mild oxidant such as O_2 or $Fe(CN)_6^{3-}$ can dissolve Au [47].

$$4Au(s) + 8CN^- + O_2 + 2H_2O \rightarrow 4[Au(CN)_2^-] + 4OH^-$$

$$Au(s) + 2CN^- + Fe(CN)_6^{3-} \rightarrow Fe(CN)_6^{4-} + Au(CN)^{2-}$$

Therefore, use of a 0.01 M aqueous solution of $K_3[Fe(CN)_6]$ containing 0.1 M KSCN or $K_2S_2O_3$ provided a Au etch rate of 6-18 nm/min and achieved 200 nm line width Au patterns [47]. Alternatively, an aqueous solution of KI and I^- has been widely utilized for Au etching [46].

$$2Au(s) + I_2 \rightarrow 2AuI$$

The Au etch rate obtained from 4 g of KI + 1g of I^- in 150 mL deionized water solution was 25.6 nm/min and the smallest Au line defined was 4 μm [46].

1.5.2. Dry (Plasma) Etching.

As film dimensions in devices decreased below one micron, isotropic wet (liquid) etching was unable to maintain the necessary critical device dimension due to undercutting of the mask materials (Figure 1.5), thereby leading to device failures [38]. This limitation established the need for plasma-based dry etching, where the etch rate is only partially controlled by chemistry and the vertical ion bombardment enables anisotropic etch profiles [48].

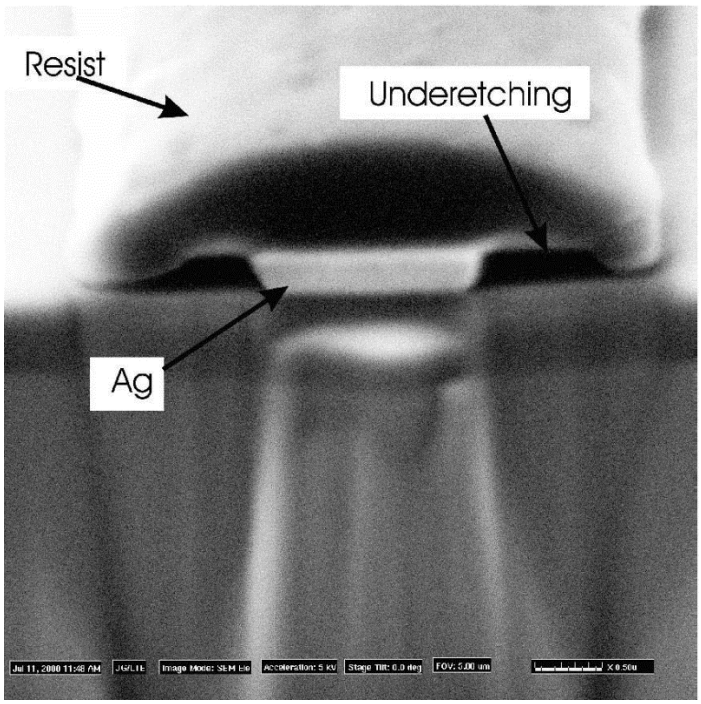

Figure 1.5 Cross sectional SEM image of an undercut Ag film after wet etching by 1.2% NH_4OH/H_2O_2 solution [44].

The basic principle of plasma etching involves the reaction between neutral gas-phase radicals and the solid (metal or semiconductor) surface to form volatile products that can be desorbed from the surface [34]. Because many metal or silicon halides are volatile (SiF_4, $SiCl_4$, CrO_2Cl_2, TaF_5, $AlCl_3$. etc…), halogen-based plasmas are typically used in plasma etching process [49-51]. However, Cu, Ag, and Au do not form volatile halogenated etch products in traditional halogen-based plasmas [52-54]. Therefore, additional methods to enhance removal of product species have been applied to assist etch product removal; these methods include increasing temperature [54-59], enhancement of ion bombardment energy [55, 60-64], photon exposure [65, 66], and wet etching [52, 53].

The effect of temperature on Cl_2 plasma etching of Cu is well established in the report of Miyazaki et al. [59]. The $CuCl_x$ products formed in a Cl_2 plasma began to sublime, apparently with the product species Cu_3Cl_3 at 180 ℃ at 20 sccm Cl_2, 1.3W/cm^2 power density, and 10

mTorr in a magnetically enhanced reactive ion etching system [59]. Because the growth rate of $CuCl_x$ is higher than the sublimation rate of Cu_3Cl_3 at temperatures <200°C, a thick layer of $CuCl_x$ residue remained under these etch conditions. At temperatures > 270 °C, chemical reaction rather than ion bombardment dominated the etch process, which led to an undercut or isotropic etch profile [59]. The maximum etch rate reported was 320 nm/min, with vertical (~90°) profiles of 250 nm Cu lines at 260 °C [59].

To avoid the need for a substantially elevated temperature process, several enhancements to the plasma process have been described. Lee at al. demonstrated that the addition of Ar to a Cl_2 plasma enhanced the ion bombardment energy and thereby provided sufficient momentum transfer to remove $CuCl_x$ at 200 °C [55]. The Cu line width and etch rate observed were 1000 nm and ~460 nm/min, respectively, with nearly vertical Cu sidewalls at 10 Cl_2 /5 Ar sccm, 1.5 mTorr, 150 W (platen)/ 800 W (source) power at 200 °C electrode temperature with an electron cyclotron resonance plasma system [66]. However, a subsequent H_2 plasma treatment was required to remove the $CuCl_x$ residues that remained after etching [55].

An alternative method to promote plasma-assisted metal etching uses photon exposure. The basic mechanisms of $CuCl_2$ desorption by photon impingement are localized heating or photochemical process; these processes can assist the formation of relatively volatile Cu_3Cl_3 and/or weaken the $CuCl_x$-Cu bond by electronic excitation of valence electrons in $CuCl_x$ [65, 66]. Exposure of the Cu surface to IR radiation at a wavelength of 1 µm while etching in a Cl_2-based plasma reduced the required temperature for Cu etching to 60 °C with an etch rate of 500 nm/min [65]; 400 nm/min Cu etch rate was achieved with UV (340 nm) exposure at room temperature [66]. When 488 nm laser or VUV photons were employed at room temperature, a 13-17 nm/min Cu etch rate was observed in Cl_2 without plasma ignition; laser heating of the Cu

surface enhanced both formation and desorption of $CuCl_x$, while VUV exposure directly dissociated gas phase or adsorbed Cl_2, thereby promoting etch rates [67, 68].

Because high temperature and/or high energy photon exposure prohibit the use of an organic photoresist(PR) mask, Lee and Kuo suggested a dry/wet process sequence at room temperature to etch/pattern Cu layers. This process used two steps: Cl_2 [52], HCl [69], or HBr [70] plasma exposure to halogenate the Cu surface, followed by dissolution of the halogenated layer with a dilute HCl solution. Although this room temperature dry/wet process enabled the use of a PR mask, Cu sidewall roughness attributed to the corrosion of Cu by chlorine or bromine can be difficult to avoid [70, 71]. Jain et al. studied a non-chlorine plasma system for Cu etching by utilizing a vapor mixture of H_2O_2 and hexafluoroacetylacetone(hafcH) [71]. Similar to a wet Cu etching process, H_2O_2 vapor oxidized Cu to form CuO follow by reaction with hafcH to form volatile $Cu(hafc)_2$ and H_2O vapor at 250 ℃ [71]. Although the measured etch rate was as high as 1000 nm/min, the formation of low density CuO initiated void formation or surface roughness and the high temperature needed prevented the use of a PR mask [71]. Furthermore, since the etch or removal process is analogous to wet (chemical) etch processes, isotropic etch profiles are expected, although profiles were not reported for this work.

Similar to Cu etching, the formation of non-volatile silver halide products limits the ability to dry etch Ag films [53, 62]. In an attempt to remove fluorinated silver products generated in a pure CF_4 plasma, a PR stripping solvent was used, but residues remained [62]. Gao at al. employed a CF_4/Ar plasma to etch Ag in an electron-cyclotron-resonance reactive-ion-beam-etching system [61]. At 0.1 mTorr, 180 W microwave power, 600 V beam voltage and room temperature, a Ag etch rate of 112.6 nm/min was achieved, although non-uniform sidewall profiles and roughness were observed [61]. In Cl_2-based plasma etching, an additional wet etch

step using a PR stripping solvent was also required; mask undercutting and side wall roughness resulted [53]. In an attempt to avoid halogen plasmas, Hauder at al. reported the use of O_2 plasma followed by H_2O_2 wet process to remove the oxidized silver film. However, due to degradation of the PR mask by the O_2 plasma, non-uniform pattern transfer to the underlying Ag film occurred [44].

A few studies that report plasma-assisted Au etching have appeared. Pure Cl_2 or a mixture of CF_4 and CCl_4 plasmas etched Au at 7 nm/min and 91 nm/min respectively, at 100 mTorr and 450 W power [38]. However, chlorination reactions generated surface roughness and poor mask selectivity to both PR and SiO_2 masks limited implementation of this process [38]. With HBr/Ar and Cl_2/Ar plasmas, nonvolatile Au etch products were sputtered/redeposited onto feature sidewalls, resulting in tapered etch profiles of ~75 ° [64]. Aldridge demonstrated a high selectivity (to SiO_2) anisotropic Au etch process with an etch rate up to 908 nm/min in a Cl_2 plasma at 125 °, 100 sccmCl_2, 100 mTorr and 400 W power [54]. Although a feature size of 0.5 µm was achieved, Cl_2 generated rough sidewalls and PR cannot be used as a mask due to the high temperature [54]. These investigations demonstrate that halogen- and oxidation-based dry etching processes have severe limitations for the nanometer scale patterning of Cu, Ag and Au features.

1.5.3 Ion-Beam Etching

An alternative approach for subtractive dry etching of Cu, Ag and Au films is ion beam etching. In this process, the etch mechanism is physical sputtering of metal species by incident ions. Provided that the energy (momentum) transfer from ions exceeds the sputtering threshold (normally 5-10 eV), the metal atoms are ejected from the surface without the need for chemical

reactions to generate volatile species [72]. This means that the relative mass difference between incoming ions and metal atoms, the ion energy, and the bond strength of metal atoms determine sputter yields and so etch rates [72]. These characteristics of ion beam etching provide several advantages for patterning processes such as high resolution (nanometer) etching for any material or multilayer combination without mask undercut, and the ability to control sidewall profiles [73]. For this reason, experimental and theoretical sputtering yields of semiconductors and metals including Cu, Ag and Au, with a variety of ions from hydrogen ion to Xe and ion energy ranges from several tens of eV to MeV have been studied since the early 1960s [72, 74]. However, ion beam etching presents several problems, specifically, etch selectivity is low since sputter yields for different materials differ by factors of only 2-4 (in principle, chemical etch selectivities can be nearly infinite), dependence of sputtering yield on the incident ion angle which therefore affects side wall slope when etching surfaces with steps and redeposition of sputtered materials onto wafer surfaces and etched sidewalls [73].

1.5.4 Damascene Technology

The difficulties involved in dry Cu etching/patterning processes led to the introduction of Damascene Technology by IBM in the mid 1990s [75]. In the Damascene process, instead of subtractive Cu etching, the dielectric material is etched to form trenches into which Cu is electroplated. Deposited Cu above the trench level is removed by chemical mechanical planarization/polishing (CMP) as shown schematically in Figure 1.6 [76].

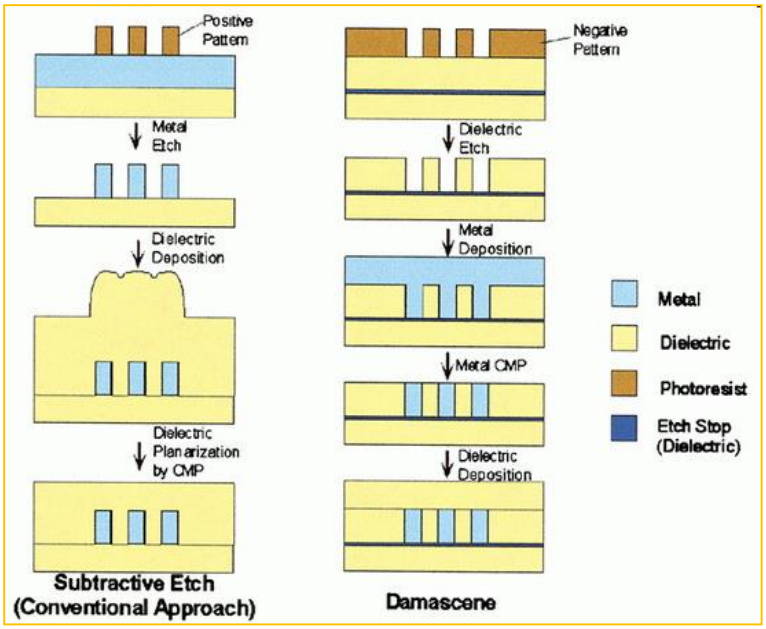

Figure 1.6 Comparison between subtractive plasma etch and Damascene process [77].

However, the Damascene process suffers from the 'size effect' (Figure 1.7). When lateral feature dimensions are reduced below 100 nm, the resistivity of Cu dramatically increases, since the feature size is approaching the electron mean free path in Cu (~40 nm at room temperature) [78]. The size effect is a result of electron scattering at sidewalls and grain boundaries which yields an increase in resistivity [79, 80]. This size effect can be reduced by increasing the grain size and mitigating the Cu sidewall/surface roughness. However, increasing the grain size is difficult in Damascene processes due to both narrow feature geometries [81] and to the introduction of impurities during the CMP step [82]. Therefore, development of a subtractive Cu plasma etching process at low temperatue is of much interest. Such a process is expected to alleviate one cause of the size effect and consequently suppress the dramatic increase in resistivity with Damascene-patterned sub-100 nm Cu lines; as a result, performance of microelectronic devices will likely improve.

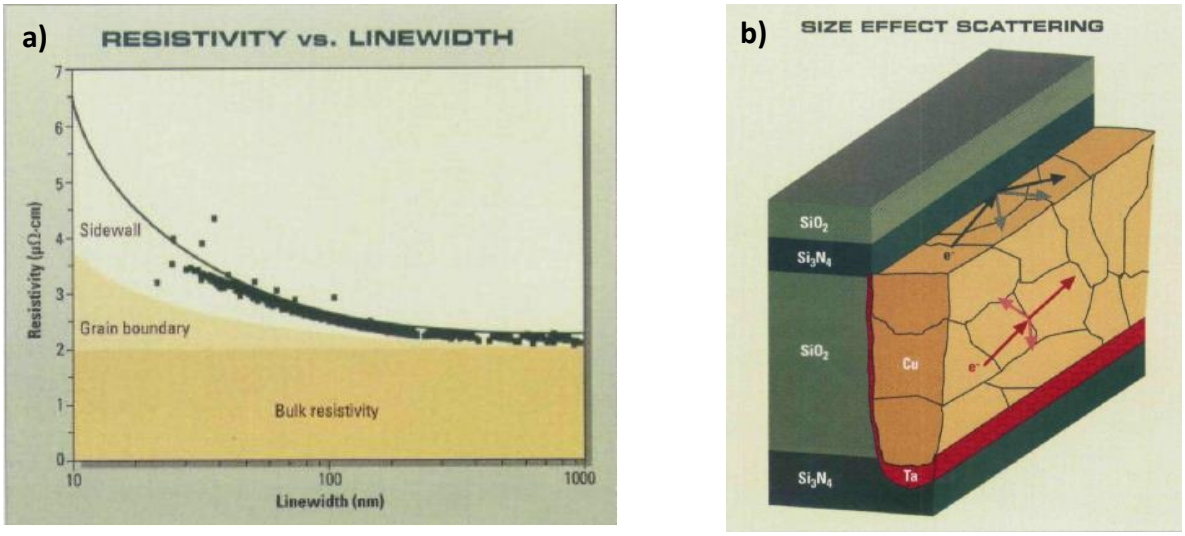

Figure 1.7 a) Dependence of the resistivity of damascene copper lines on line width. b) Size effect: electron scattering [83]

1.6 H_2-based Plasma Cu Etching

Recently, new approaches to low temperature subtractive Cu etching have been reported. Specifically, Kulkarni et al. reported a thermodynamic analysis of the Cu-Cl-H system , wherein $CuCl_2$, formed by chlorination of the Cu surface, might be converted to volatile Cu_3Cl_3 when exposed to H atoms [84]. Based on these equilibrium calculations, Wu et al. demonstrated a low temperature two-step etch process that used a Cl_2 plasma followed by an H_2 plasma treatment [85]. Further studies demonstrated that H_2 plasma exposure was the rate limiting step in this two-step process and that Cu could be etched by a pure H_2 plasma without a Cl_2 plasma pretreatment [86].

Figure 1.8 shows SEM images comparing the Cu etch profile generated by H_2 and Ar inductively coupled plasmas (ICP) [86]. The higher etch rate of an H_2 plasma relative to an Ar plasma (13 nm/min vs 4 nm/min) suggests that chemical reactions between Cu and H assists the etching processes with Cu hydrides being likely etch products. Since the atomic or molecular weight of hydrogen atoms and molecules is considerably lower than that of Ar, sputtering of Cu

by H species is minimal due to the low momentum transfer [86, 87]. However, Cu hydrides are thermodynamically unstable and easily decomposed even at 0 ℃ [88]. Furthermore, the vapor pressure of CuH_x species are reported to be low [84].

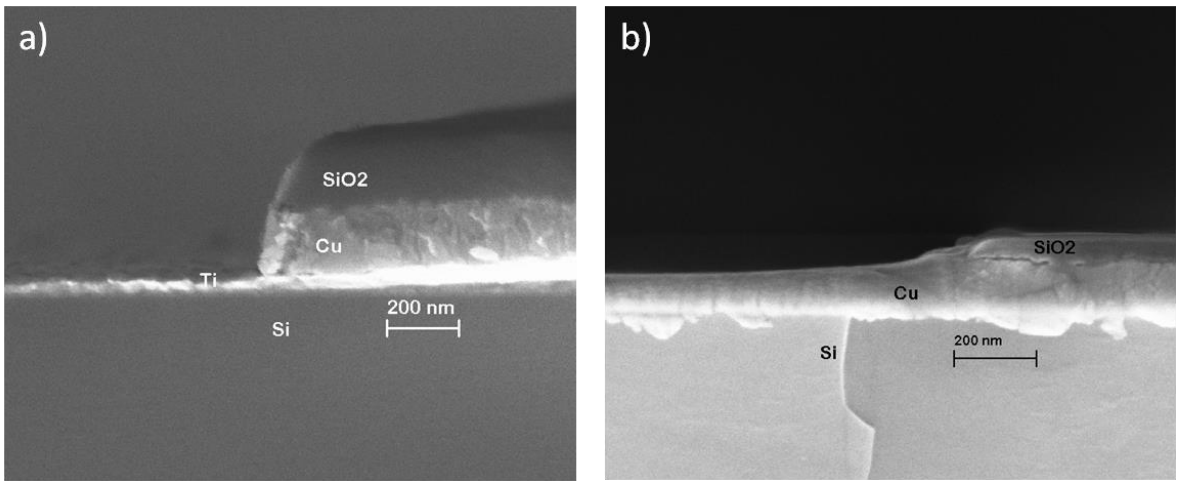

Figure 1.8 Cross-sectional SEMs of SiO_2 masked 100 nm Cu films. After 8 min plasma Cu etching with flows of (a) 50 sccm H_2, (b) 50 sccm Ar. Other etch conditions were 100 W(platen)/500 W(coil), 20 mTorr pressure, and 10 ℃ electrode temperature [86].

To gain insight into the role of Cu chemical and physical etch components in H_2 plasmas, zero platen power and zero coil power experiments were performed in an ICP reactor [87]. The concentrations of radicals and ions generated in the ICP system are determined by coil power, whereas ion bombardment energy (platen DC bias) is controlled by platen power [37]. When power was applied to both platen and coil (default power), reasonable etch rates were observed as shown in Figure 1.9; however, with zero coil or zero platen power, etch rates are only 5 % and 36 % of that for the case where simultaneous power application was used. The higher etch rate observed with zero coil power relative to that with zero platen power signifies the importance of ion bombardment in H_2 plasma etching of Cu [87].

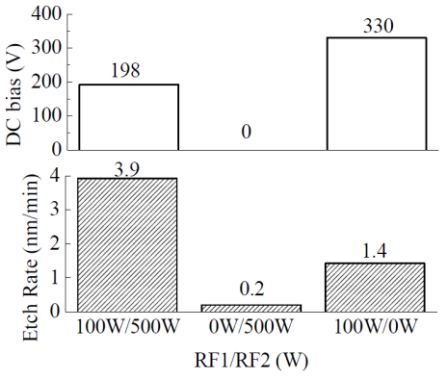

Figure 1.9 Cu etch rates and corresponding DC bias in H_2 plasma with default power, zero platen power, and zero coil power. The other conditions are 20 mTorr pressure, 50 sccm H_2 flow rate, and 20 ℃ electrode temperature in STS SOE ICP reatctor [87].

In addition to ion bombardment, the Cu surface is exposed to plasma-generated photons and radicals. Because the wavelength of these photons is relatively short, the high energy UV photons may promote chemical reactions between Cu and H and possibly enhance etch product ejection from the surface by electronic excitation[89, 90]. Initial etch experiments were performed to compare He plasma and Ar plasma ablation of Cu; higher etch rates of He plasma (10 nm/min) relative to Ar (4 nm/min) were observed despite the fact that Ar is a more efficient sputtering gas due to its higher atomic weight and so momentum transfer [87]. However, the intense atomic emission lines in UV wavelength range for He (50-60 nm) are more energetic than those of Ar (80-100 nm) [91], implying that the higher photon energy from He may contribute significantly to Cu ablation, analogous to reports of UV laser ablated Cu [92], since no chemical reactions occur in noble Ar and He gas plasmas [87].

Substrate temperature and optical emission studies offered further insight into the chemical and physical mechanisms involved in Cu plasma etching using H_2 plasmas. As shown in Figure 1.10-a, an Oxford ICP reactor was used to investigate substrate temperatures from -150 to 100 ℃. Over the temperature range -150 to 10 ℃, the Cu etch rate increased nearly linearly,

with a 0.05 eV effective activation energy. However, above 10 ℃, the etch rate decreased [93]. This surprising etch trend is likely a result of the instability of the expected etch product CuH, which is reported to be unstable at 0 ℃ [88] and rapidly decomposes above 50 ℃ [94]. Furthermore, 0.05 eV is a low activation energy that is characteristic of etch processes dominated by ion-enhanced etching [95]. These observations led to the postulate that the etch mechanism changes at a temperature of ~10 ℃. That is, up to that temperature, formation and ion-enhanced desorption of CuH_x is the dominant etch mechanism, but at higher temperatures, the Cu etch rate decreases due to the thermal instability of CuH. At higher temperatures, the etch rate increases, perhaps due to more efficient hydrogen ion sputtering that is promoted by the increased thermal energy [93].

To investigate possible etch products present in the plasma atmosphere, optical emission spectroscopy (OES) was used (Figure 1.10-b)). During H_2 plasma etching, OES indicated that atomic Cu species were present in the gas phase, but no Cu hydrides were detected [93]. This result is consistent with the instability of desorbed CuH_x, which should be readily dissociated when impacted by electrons in the plasma.

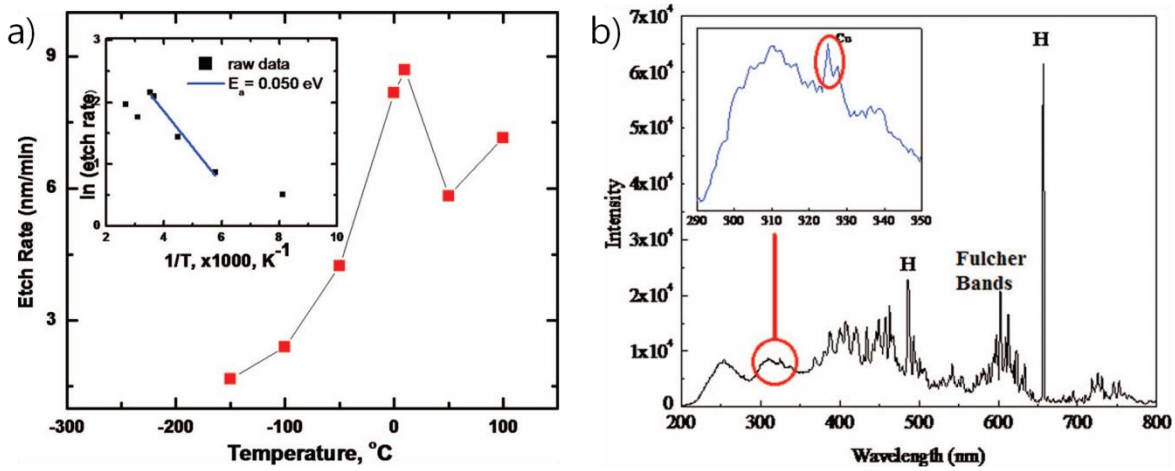

Figure 1.10 a) Substrate temperature vs Cu etch rate at 100 W(platen)/1800 W(coil), 20 mTorr pressure, and H_2 60 sccm flow rate for 10 minutes. The inside graph is Arrhenius plot of Cu etch. b) Optical emission spectrum of Cu etching with H_2 plasma at 100 W(platen)/1800 W(coil), 20 mTorr pressure, H_2 60 sccm flow rate, and 10 ℃ substrate temperature.

1.7 Thesis Objectives and Organization

This chapter addresses the unique material characteristics and potential applications of Cu, Ag, and Au films. Patterning methods for these metals have evolved due to the requirement for nanometer scale Cu, Ag, and Au structures. Investigations of H_2-based plasma etching of Cu at low temperature offers a possible approach to alleviate the size effect by replacing the current Damascene process with a subtractive all-dry etch process. Since Cu etch studies have demonstrated that a combination of chemical and physical etching mechanisms are operative in H_2 plasmas, Ag and Au etching in H_2 plasmas may also be possible due to the similarity of their electronic structures to that of Cu.

Highly selective Cu subtractive etching was achieved by H_2 plasma at 10 ℃ using an SiO_2 mask. However, the relatively low etch rate, ~ 80 ° sidewall profile, and inability to use a PR mask due to degradation by the H_2 plasma are obstacles for practical applications. Implementation of a residue-forming plasma, CH_4, offers an alternative method to overcome

some of these disadvantages. Specifically, a CH_4 plasma both supplies H atoms for etching and also protects the PR mask degradation and metal sidewalls as a result of hydrocarbon deposition.

In chapter 2, a three-step plasma etch sequence to achieve definition of a sub 100 nm Ta/Cu/Ta stack structure at low temperature is detailed. Chapter 3 describes Ag and Au film etching in an H_2 plasma at 10 ℃ and the similarities and differences in etching mechanisms between Ag, Au, and Cu are discussed. Chapter 4 describes the CH_4-based plasma etching of Cu at low temperature. The etching mechanism and the advantages of a CH_4 plasma process relative to an H_2 plasma process are discussed. Chapter 5 offers results of the investigation of the low temperature etching mechanism of Ag and Au using a CH_4 plasma. Finally, in chapter 6, a summary of the primary technological and scientific contributions from this thesis and possible future directions for this research are discussed.

CHAPTER 2.

HIGH ASPECT RATIO FEATURE OF Ta/Cu/Ta STACK ETCHING

2.1 Introduction

The previous Cu etching study by Fangyu Wu demonstrated the feasibility of Cu plasma etching by hydrogen based plasmas at low temperature and generated initial insight into possible etch mechanisms [86, 87, 93]. Ultimately, we wish to establish the controlling parameters in the etch process that will allow feature sizes on the order of 50 nm to be defined. However, etching ultra small metal (e.g., Cu) structure sizes presents a number of challenges. Specifically, when the etched feature depth is greater than the feature width (aspect ratio > 1), several issues arise which are unimportant during the plasma etching of large features or low aspect ratio structures. For instance, in plasma etching, substrates in contact with the plasma are negatively charged; the voltage is often increased by the application of platen power in order to enhance the energy of positive ions that bombard the substrate, thereby facilitating anisotropic etch profiles. In high aspect ratio structures, the electric field that results from negatively charged side walls substantially influences the ion directionality causing deflection from a perpendicular (to the substrate) path and thus sidewall collisions. In addition, diffusion of reactants to and etch products from the bottom of feature causes collisions with incoming ions, again causing deflection of the ions responsible for directionality or anisotropic etch profiles. As a result, control of feature profiles during plasma etching can be limited in high aspect ratio structures [96].

Therefore, accomplishments on this small size patterning will permit detailed evaluation of the suitability of subtractive Cu etch processes to mitigate the size effect in small Cu features.

2.2 Experimental

2.2.1 Structure of Ta/Cu/Ta stack Sample

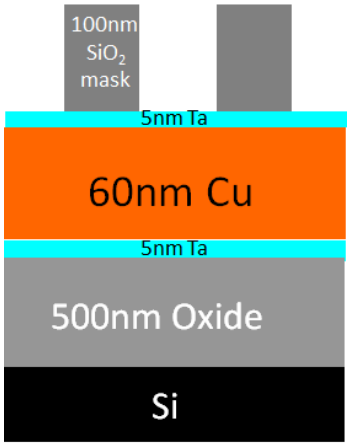

Figure 2.1 Cross section of Cu stack samples obtained from Applied Materials.

Due to the high diffusivity of Cu in most materials, Cu films must be encased when incorporated into IC structures to inhibit or prevent Cu diffusion to junctions or interfaces where this impurity deteriorates device reliability [97]. Typically, Ta, Ti, W, Cr, or Ni are used as diffusion barrier layers in metallization structures. This is an important issue for etch processes, since a metal stack consisting of layers of materials, rather than a simple Cu film, must be etched controllably if Cu patterns are to be generated. Figure 2.1 is such a stack structure supplied by Applied Materials(AMAT). The stack consists of a 100 nm thick patterned SiO_2 hard mask, 5 nm thick tantalum(Ta), 60 nm thick Cu, 5nm thick Ta, and a 500 nm thick SiO_2 layer on the Si substrate. The linewidth of SiO_2 mask patterns ranges from ~55 nm to ~670 nm across the sample.

2.2.2 Basis of 3-step Etching Process

In order to etch the 3 different stack layers(Ta/Cu/Ta), at least 3 different plasma etch processes are required. Tantalum can be etched by fluorine- (F) containing plasmas, because the surface reaction between Ta and F forms volatile products such as TaF_5[51, 98], but reaction of Cu with F does not form volatile products. Therefore, Ta was etched with a mixture of CF_4 and Ar or with pure CF_4. As described above, H_2 gas was then used to etch the Cu layer [86]. In 3 step etching experiments, another CF_4-based etch was used to remove the bottom Ta layer; this stack etch sequence was therefore composed of three steps. Specifically, 50 sccm CF_4 with or without 50 sccm Ar, 100-130 W (platen)/ 500 W (coil) power, 10 mTorr, 10 -16 ℃ electrode temperature with 7-15 sec etch time were applied for Ta etching step and 50 sccm H_2, 100-150 W (platen)/ 500 W (coil) power, 20 mTorr, 10 ℃ electrode temperature with 15 min etch time were applied for Cu etching step.

2.3 Results and Discussion

2.3.1 Two-step Large Structure (linewidth 670 nm) Etch Process

Initially, plasma etching of large structures with line width ~670 nm was performed using a two-step process (no etching of bottom Ta layer) in a Plasma Therm Inductively Coupled Plasma(PT-ICP) Reactor located in the Petit Cleanroom. Unlike Cu single layer etching, stack etching is difficult and complex because of the sequence of steps needed. Although the plasma etch gas (CF_4) during the previous step was evacuated from the chamber after the end of first step, fluorocarbon-containing residues are coated on chamber walls and perhaps on the substrate, which can affect the subsequent H_2 plasma etching step.

A mixture of 50 sccm CF_4 and 50 sccm Ar was employed to etch the Ta layer on top of Cu (first step). For this purpose, 100 W and 500 W power were applied to platen and coil respectively, while the chamber pressure and electrode temperature were maintained at 10 mTorr and 16 ℃ respectively for 7 seconds etch time. In the next step, 50 sccm of H_2 was utilized with 100 W(Platen)/500 W(Coil) power, 20 mTorr pressure, and 10 ℃ electrode temperature for 15 minutes to etch the Cu film. Although the etch rate of a blanket Cu film is 13 nm/min in the same reactor under the same conditions[86], a longer etch time (15 min) was required for the 60 nm thick Cu; this reduction in etch rate was ascribed to the limited transport of H into patterned structures[96] and perhaps to F residues that result from multiple etch steps in the same chamber.

The top Ta(5 nm) and Cu(60 nm) layers were successfully etched with this 2-step process (Figure 2.2). As expected, the 2-step etch terminated on the bottom Ta layer which remains essentially intact due to the selectivity of H_2 plasma between Cu and Ta. In addition, the sidewall angle was ~80 degrees, which is identical to that observed during the etching of a single Cu layer[86]. However, the CF_4 plasma etches SiO_2 with a high etch rate[99]; thus, significant loss of the SiO_2 hard mask cannot be avoided during the process especially on the edge where the mask layer is thinner than on a flat surface.

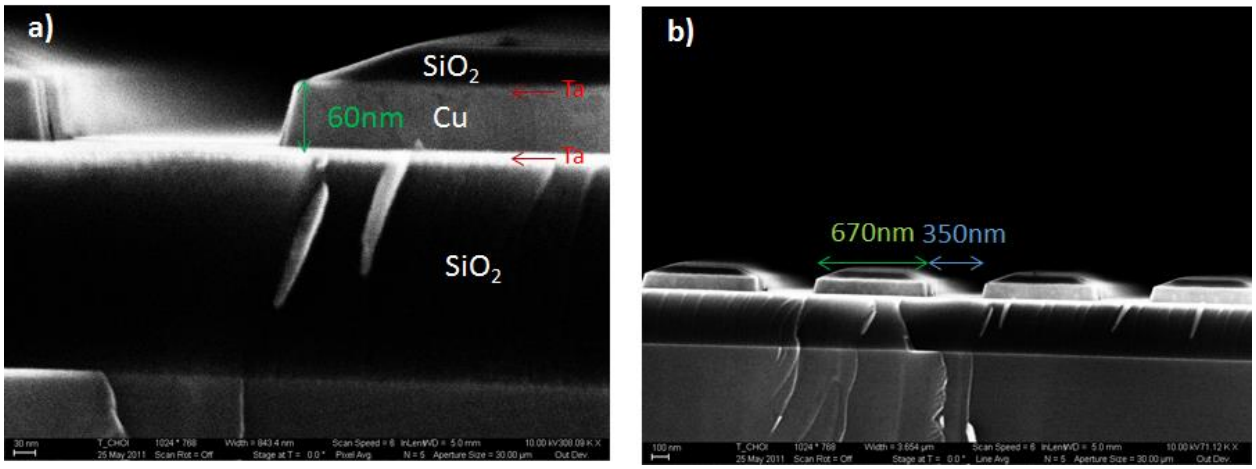

Figure 2.2 Cross sectional SEM images of 2-step etch process of large linewidth structures (670 nm) with 5 nm Ta/60 nm Cu/5 nm Ta thickness. a) higher and b) lower magnification images of the same structures.

2.3.2 Three-step Small Structure (linewidth 55 nm) Etch Process

Etching of smaller AMAT-supplied stack structures (55 nm linewidth) has also been studied. Due to the nm scale structures and thus increased aspect ratio, alternative etch conditions were required for the $CF_4/H_2/CF_4$ plasma etch of the Ta/Cu/Ta stack. The first step used 50 sccm CF_4 gas with 130 W (platen)/500 W (coil) power, 10 mTorr pressure, and 10 ℃ electrode temperature for 10 seconds. As mentioned above, high aspect ratio features are easily damaged by ion bombardment[96]; results indicated that the Ar ion kinetic energy for this small structure was too high. Thus, instead of a CF_4/Ar mixture, pure CF_4 gas was used in the Ta etching step, and higher platen power (130 W) than that used for the larger structures applied in order to increase the ion bombardment energy to achieve anisotropic etching. In addition, a longer etch time (10 seconds instead of 7 seconds) was employed to compensate for the removal of Ar gas. The second step condition was 50 sccm H_2 gas, 150 W (platen)/500 W (coil), 20 mTorr pressure, and 10 ℃ electrode temperature for 15 minutes Cu etch time. In the temperature dependent Cu etching studies with an H_2 plasma, Fangyu Wu demonstrated that below room temperature,

higher etch rates are observed[93]. Therefore, lower electrode temperature 10 ℃ was applied instead of 16 ℃ in this case to increase the etching rate. The third step (bottom Ta etch) is the almost same as the first step except with a longer etch time (15seconds). The need for a longer etch time is due to the Cu sidewall angle whose slope from the H_2 plasma is not vertical and thus the transport of ions and neutral species into this narrow trench limits the etch rate at the bottom Ta layer.

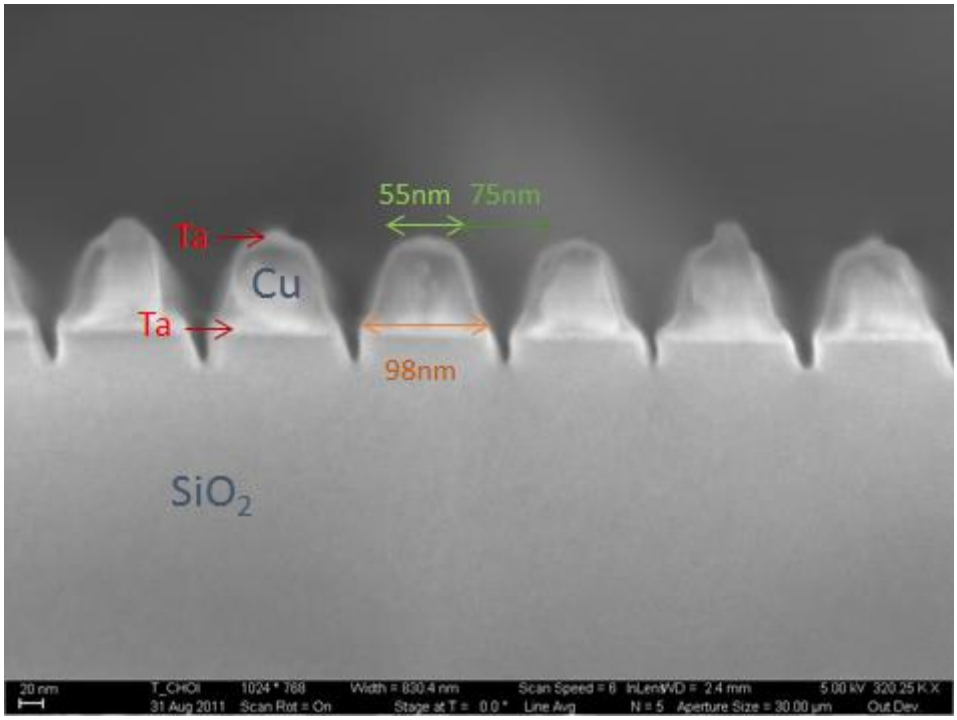

Figure 2.3 Cross sectional SEM images of small linewidth structures (55 nm) by 3-step etch process.

Clearly, Ta/Cu/Ta stack layers are etched by the 3-step process although the bottom Ta layers are clearly over etched resulting in attack of the SiO_2 layer (Figure 2.3). The Cu sidewall angle was ~73 degrees. However, the SiO_2 mask layer was removed during the second CF_4 etch process since the mask was exposed to two F-containing etch steps, unlike the larger structures which were subject to only one CF_4 etch. Because the side walls of the SiO_2 mask layer for small

features are closely spaced, the SiO_2 mask becomes narrow at the top SiO_2 surface which leads to rapid etching by CF_4/H_2 plasma exposure. Although considerable optimization is needed in order to establish a viable etch process for Cu stack etching at small dimensions, these initial results suggest that Cu patterning in H_2 plasmas is feasible in IC processing.

CHAPTER 3.

MECHANISTIC CONSIDERATIONS IN PLASMA-ASSISTED ETCHING OF Ag AND Au THIN FILMS

3.1 Introduction

In order to assess whether H_2 plasmas can effectively etch a variety of metal layers, several metal films (Ti, Ta, Ni, Cr, and Al) were exposed to H_2 plasmas; under the conditions used for Cu etching, no removal of any of these metals was observed. Such results suggest that the chemical properties and electronic structure of Cu may facilitate H_2 plasma etching. If this assumption is correct, then H_2-based plasma etching of other Group 11 elements (Ag and Au) should be possible. Indeed, Ag etching in H_2 plasmas has been demonstrated [100], although no etch rates or mechanistic information was offered.

In this chapter, we report Ag and Au etching rates and pattern profiles using H_2, He and Ar plasmas at low temperature (10 ℃). Comparison of the results of these etch studies with those of Cu allows assessment of the relative importance of sputtering versus chemical reactions that lead to desorption of etch products in the plasma-based etching of Group 11 metals. Possible similarities and differences in etch mechanisms for these metals are also discussed.

3.2 Experimental Procedures

Ag and Au thin films of 100 nm thickness were evaporated (CVC E-Bean Evaporator and CHA E-Beam Evaporator) onto a 20 nm thick Ti layer on a 4 inch Si wafer. Patterns were generated using a hard mask; a 150 nm SiO_2 layer was plasma deposited (Unaxis PECVD) onto

Ag and Au at a platen temperature of 250 ℃ and was subsequently patterned using a $C_4F_8/CO_2/Ar$ based plasma in a Plasma Therm (PT) ICP reactor. Ag and Au coated substrates were sectioned into etch samples ~1cm^2 and attached to a 4 inch Si carrier wafer by *cool grease* 7016 (AI Technology Inc.). In order to compare the Ag and Au etch results with the previously reported Cu etching studies, Ag and Au film etch studies were performed in the PT-ICP reactor under the same etch conditions as those used to etch Cu: 100 W(platen)/500 W(coil) power, 20 mTorr pressure, and 10 ℃ substrate temperature . Etch gases investigated were H_2, He, and Ar at 50 sccm flow rate.

Additional experiments were performed to investigate chemical reaction effects of H_2 plasmas. In these studies, blanket Cu, Ag, and Au films were either etched without a mask present, or were patterned with an H_2 plasma using a glass slide which served as a hard mask affixed at the edges by kapton tape onto the carrier wafer. The same plasma conditions used previously to pattern Ag and Au films were invoked for these experiments.

After etching, Cu, Ag, and Au film patterns were examined with a scanning electron microscope (Zeiss Ultra60 FE-SEM) and the etched thickness determined by both SEM and a Dektak 150 Profilometer after removing the SiO_2 mask by a dilute HF solution (2 volume %). Chemical analysis of the glass slide mask that was in contact with the metal layer was conducted using X-ray photoelectron spectroscopy (Thermo Scientific K-Alpha XPS).

3.3 Results and Discussion

In order to determine whether our masking process using plasma-deposited SiO_2 caused alterations to the metal film structure and composition, several control experiments were performed. After patterning the SiO_2 masking layers with a C_4F_8 plasma, XPS analyses of the

metal surfaces did not detect Si, indicating that either no Si has been transferred to the metal film, or its concentration is below the detectability limit of XPS. Furthermore, to ensure that metal morphology is unaffected by the dilute HF solution used to remove the SiO_2 masking layer after patterning, blanket Cu, Ag, and Au films were treated for 1 min. with a 2 % HF solution. No alteration of metal film morphologies relative to the as-deposited metal films was observed by SEM. These results indicate that any morphology changes observed after removal of the etch mask were due to the plasma etch process rather than SiO_2 deposition and HF removal of this masking layer.

3.3.1 Ag Etching Results

The results of etching 100 nm thick Ag films with H_2, He, and Ar plasmas are shown in Figure 3.1. Unlike Cu, Ag agglomerated into islands prior to the etch process, thereby inhibiting accurate film thickness changes and thus, etch rate measurements. Ag grains undergo growth and agglomeration in order to mitigate the surface and interfacial tension of Ag thin films [101, 102]. Since Ag self-diffuses rapidly above 150 ℃ [103] and SiO_2 mask layer deposition was performed at 250 ℃, grain growth results in non-uniform film thickness and grain size (30-300 nm) as shown in Figure 3.1-a2. In order to improve the accuracy of etch rate measurements for these rough layers, the Ag etch rates given below were estimated based upon the average etch depth as determined by both profilometer and cross sectional SEM images.

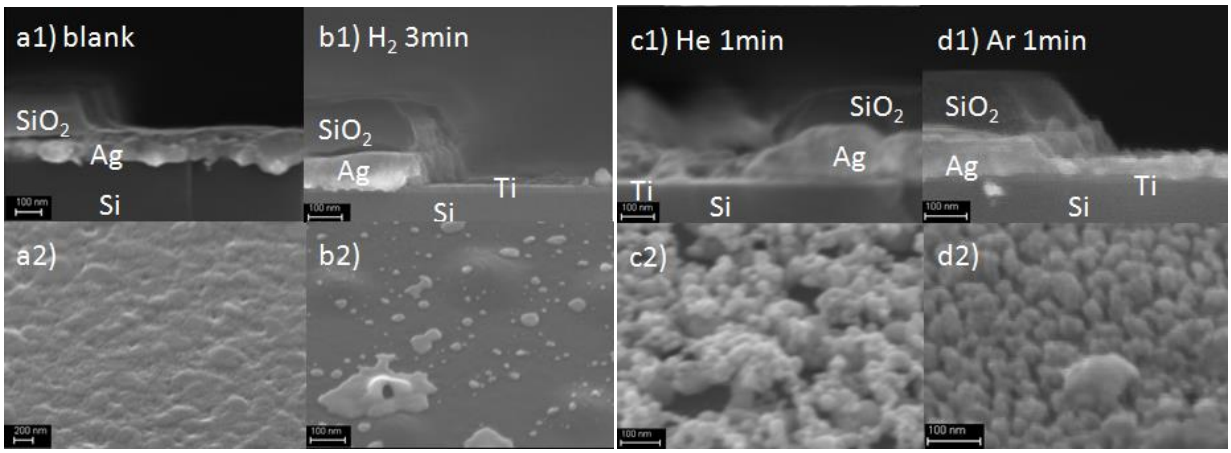

Figure 3.1 SEM images of cross sections and surfaces of 100 nm thick Ag films. a1) cross section and a2) Ag surface before plasma etching; b1) Ag cross section and b2) Ag surface after plasma etching with H_2 plasma for 3 min; c1) Ag cross section and c2) Ag surface after He plasma etching for 1 min; and d1) Ag cross section and d2) Ag etched surface after etching with an Ar plasma for 1 min. All the etch conditions were: 50 sccm gas flow, 100 W(platen)/500 W(coil) power, 20 mTorr pressure, and 10 ℃ electrode temperature.

The Ag etch rates estimated for H_2, He, and Ar plasmas are 33, 45, and 50 nm/min, respectively. These etch rates and etched Ag surface morphological features are different from those observed for Cu etching, although unlike the other metals that we have attempted to etch in H_2 plasmas, Ag, like Cu, etches readily. In Cu etching, the etch rate decreases as the atomic or molecular weight of the plasma etch gas increases: 13 nm/min with H_2, 10 nm/min with He and 4 nm/min with Ar plasma (Figure 3.2). This trend is opposite to the observed increasing Ag etch rates with increasing atomic weight of plasma etch gases. In addition, while no differences in surface morphologies of Cu exposed to H_2 and Ar plasmas are apparent, the average Cu grain size decreases to several nanometers and the surface morphology is smoothed after He plasma treatments (Figure 3.3). This observation is appeared to be a result of the Cu surface being amorphized by He ions since metal amorphization during ion implantation has been observed previously [104]. However, since the estimated penetration depth of He ions at energies <1 keV is <10 nm [105], Cu morphology changes by He plasma exposure should be limited to a thin

surface layer. Indeed, a cross sectional image of the Cu layer after exposure to a He plasma (Figure 3.4-b1) shows a thin (~10 nm), distinct upper layer. A subsequent 3 min H_2 plasma etch to remove the amorphized layer results in the recovery of the original cross-sectional appearance, grain size, and morphology of the Cu film (Figure 3.4-c1 and 3.4-c2).

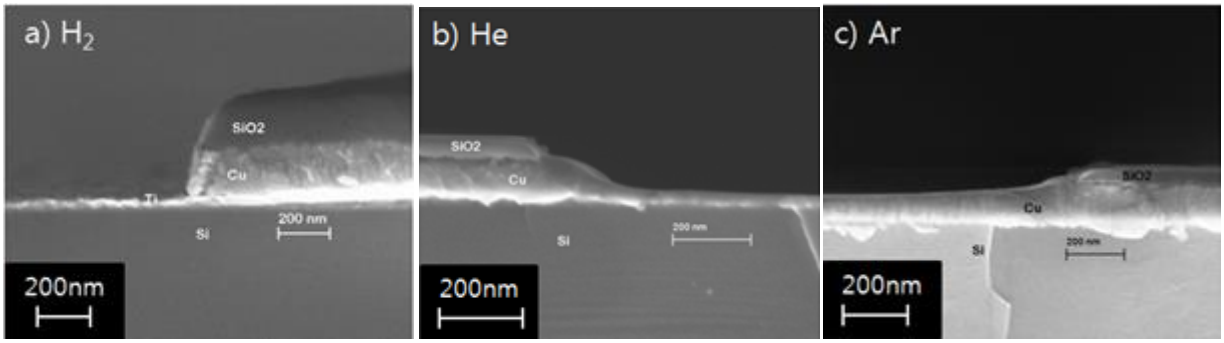

Figure 3.2 Cross-sectional SEMs of SiO_2 masked 100 nm Cu films. After 8 min plasma Cu etching with flows of (a) 50 sccm H_2, (b) 50 sccm He, (c) 50 sccm Ar. Other etch conditions were 100 W (platen)/500 W (coil), 20 mTorr pressure, and 10 ℃ electrode temperature [86, 87].

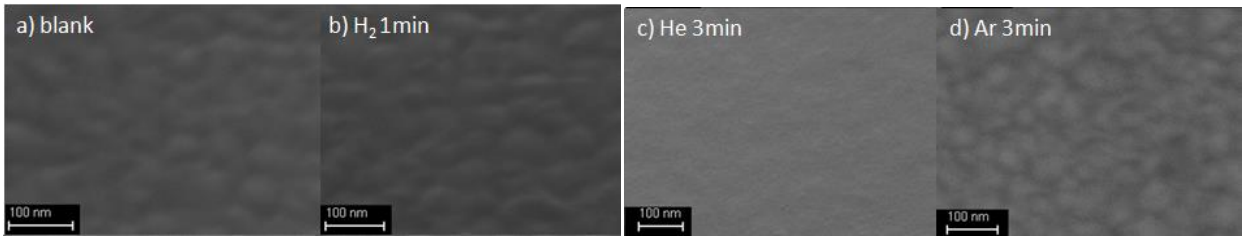

Figure 3.3 SEM images of surface of 100 nm thick Cu films. a) Cu surface before plasma etching; b) Cu surface after plasma etching with H_2 plasma for 1 min; c) Cu surface after He plasma etching for 3 min; d) Cu surface after etching with an Ar plasma for 3 min. All etch conditions were: 50 sccm gas flow, 100 W(platen)/500 W(coil) power, 20 mTorr pressure, and 10 ℃ electrode temperature.

In contrast to the Cu results, H_2 plasma etching smooths the Ag surface (Figure 3.1-b2), while the Ag surface etched/sputtered by the He plasma appears to be porous and the grain size decreases to 20-30 nm (Figure 3.1-c2). When exposed to an Ar plasma, the Ag grain size is also reduced (~30 nm) but no surface porosity is apparent (Figure 3.1-d2). The porosity created by the He plasma is likely due to back scattering of He+ ions that penetrate deeper into the bulk film

than do heavier ions such as Ar + [106]; this penetration may generate porosity as surface Ag atoms are sputtered. Currently, the reason for Ag surface smoothing is unclear, although if AgH molecules display higher diffusivity than do Ag atoms, surface smoothness will be enhanced. In addition, analogous to the observation that the low surface energy of thin Au films causes wetting of Ti surfaces when Au diffusivity is thermally increased [107], plasma exposure of Ag or AgH species can supply energy and thus promote spreading (or wetting) on Ti surfaces in order to mitigate the relatively high surface energy of Ti (2.5-2.27 J/m^2 for Ti; ~1.2 J/m^2 for Ag) [108].

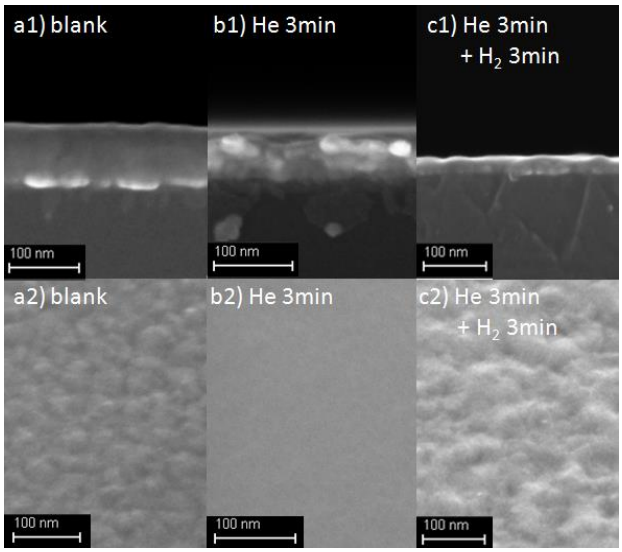

Figure 3.4 SEM images of cross section and surface of 80 nm thick Cu films. a1) cross section and Cu surface before plasma etching; b1) Cu cross section and b2) Cu surface after plasma etching with He plasma for 3 min; c1) Cu cross section and c2) Cu surface after consecutive He plasma for 3 min and H_2 plasma 3 min. All the etch conditions were: 50 sccm gas flow, 100 W(platen)/500 W(coil) power, 20 mTorr pressure, and 10 ℃ electrode temperature.

3.3.2 Au Etching Results

Additional plasma etch comparisons within Group 11 metals were performed with Au films. The same plasma gases (H_2, He, and Ar) and etch conditions were used to etch Au films as those described above for Cu and Ag etching. Because the self-diffusivity of Au is the lowest

among the metals Cu, Ag, and Au [109], Au thin films did not agglomerate during the SiO_2 mask layer deposition; as a result, their grain size (50-100 nm diameter) and film thicknesses were uniform (Figure 3.5-a). Due to the uniform surface, Au etch rates were easily measured by profilometry. The measured Au etch rates are 26 nm/min for the H_2 plasma, 55 nm/min for the He plasma, and 62 nm/min for the Ar plasma. Interestingly, the observed trend of Au etch rates is similar to that observed for Ag etch rates; that is, the etch rate increased as the atomic or molecular mass of the plasma etch gas increased.

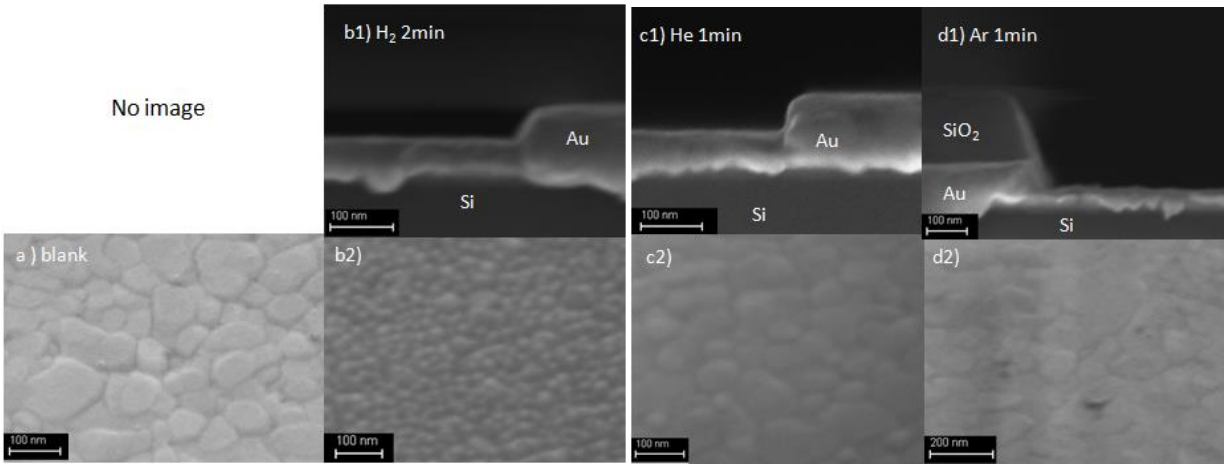

Figure 3.5 SEM images of cross section and surface of 100 nm thick Au films. a) Au surface before plasma etching. b1) Au cross section, and b2) Au surface after plasma etching with H_2 plasma for 2 min; c1) Au cross section, and c2) Au surface after He plasma etching for 1 min; d1) Au cross section, and d2) Au surface after etching with an Ar plasma for 1 min. All the etch conditions were: 50 sccm gas flow, 100 W(platen)/500 W(coil) power, 20 mTorr pressure, and 10 ℃ electrode temperature.

Figure 3.5 shows plasma etched Au surfaces and cross sectional images using H_2, He, and Ar plasmas both before and after etch. Because the SiO_2 layer did not adhere well to Au [110], it peeled easily from the Au surface when the etched samples were cross-sectioned to investigate etch profiles and rates. Therefore, no SiO_2 mask layers appear on the Au film surfaces in Figures 3.5-b1 and 3.5-c1. However, unlike the etched Cu and Ag surfaces, the grain size of Au film surfaces was reduced to 20-30 nm from their original (unetched) grain size of 50-

100 nm (Figure 3.5-b2) after exposure to the H_2 plasma. Reasons for the generation of smaller grain size are unclear but may be related to plasma damage since Au does not sputter efficiently.

Unlike Ag, exposure to He or Ar plasmas did not alter the Au surface morphology; rather, the surface was smoothed slightly while the grain size was not changed (Figure 3.5-c2 and d2). This result is similar to that observed during Cu etching where the grain size and surface of Cu films after H_2 or Ar plasma treatment are nearly identical to those of blanket Cu films (Figure 3.3).

3.3.3 Physical Etching Component (Ion Bombardment)

Etch rate dependence on atomic weight as observed in the Plasma Therm ICP plasma system is shown in Figure 3.6; for comparison, ion sputtering yields for H+, He+, and Ar+ ions [74] are shown in Table 1. In the PT-ICP system, the estimated maximum ion energy depends upon the dc bias, assuming that the plasma potential is constant and near 0 V; at a fixed pressure, the dc bias is controlled by the applied platen power. If no collisions occur during acceleration of the ions across the sheath in a single half rf cycle, the maximum ion bombardment energy is approximately equal to the platen potential. Although the platen/coil powers were fixed at 100 W/500 W for H_2, He, and Ar plasmas, the dc bias voltages differ: H_2 (360 V), He (250 V), and Ar (275 V). These differences arise because the electron concentration in a plasma depends upon the particular gas employed and to variations in the ionization energy of each gas. For these reasons, the maximum ion energies of 360 eV for H_2, 250 eV for He, and 275 eV for Ar are listed in Table 1 for a direct comparison to the measured ICP plasma etch rates.

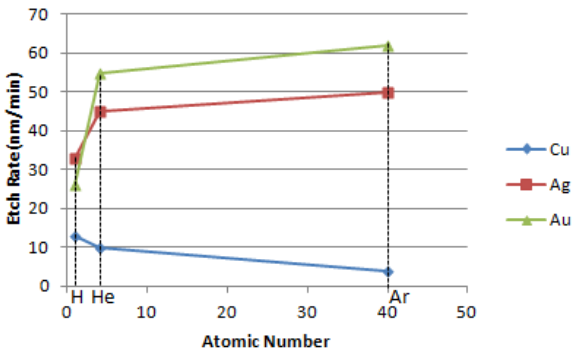

Figure 3.6 Cu, Ag, and Au etch rates in H_2, He, and Ar PT-ICP plasmas.

Table 3.1 H+, He+, and Ar+ ion sputtering yields for Cu, Ag, and Au at ion energies of 360 eV for H+ and 250 eV for He+ and 275 eV for Ar+ [74].

Sputtering Yield	H+(@360 eV)	He+(@250 eV)	Ar+(@275 eV)
Cu	0.02	0.15	1
Ag	0.015	0.15	1.9
Au	0.001	0.04	1.5

In ion sputtering processes, atoms are removed from the surface when the energy transferred exceeds the atom binding energy, normally 5-10 eV [72], and the ideal momentum transfer from the incoming ions to surface atoms in an elastic collision process is [111]

$$T = \frac{4M_1M_2}{(M_1+M_2)^2}E \tag{1}$$

where T is the transferred energy from the impinging ion of mass M_1 and energy E, and M_2 is the mass of the surface atom. Therefore, the threshold energy, E_{th}, at which sputtering is initiated is given by

$$E_{th} = E_B / \gamma \qquad \gamma = \frac{4M_1M_2}{(M_1+M_2)^2} \tag{2}$$

where E_B is the surface binding energy or the heat of sublimation. In addition, the widely accepted physical or ion enhanced chemical etching yield is given by [112]

$$Y = A(\sqrt{E} - \sqrt{E_{th}}) \tag{3}$$

where A is a constant that depends upon the particular ion/material combination.

As mentioned previously, the plasma etch rate trends of Ag and Au are similar in that the rates increase with an increase in atomic mass of plasma species, while Cu etching displays the opposite trend (Figure 3.6). These initial observations suggest that Ag and Au plasma etch rates depend significantly on ion sputtering or momentum transfer while Cu etching shows a clear dependence on chemical reactions. However, it is known that the metallic bond energy of Au is the highest among Cu, Ag, and Au (3.51 eV, 2.95 eV, and 3.77 eV respectively) and the kinetic energy transferred from hydrogen ions to Au is very low due to the substantial mass difference between Au atoms and H ions. Thus, despite the importance of atomic mass (physical aspects) in Au etch rates, chemical reactions of Au with H_2 plays an important role, because Au etch rates in an H_2 plasma are higher than those for Cu.

Since the mass of plasma etching species investigated varies widely, ion energies striking the etching surface will also vary among etchants due to the number of collisions experienced by the ions. That is, at 20 mTorr, the etch pressure is sufficiently high that accelerated ions are scattered by neutral gas collisions (charge transfer reaction) when the mean free path is shorter than the distance between the edge of sheath and the etching surface; ion momentum is therefore lost. For ions in the 200-300 eV range, the charge exchange cross sections of H+, He+ and Ar+ are $1x10^{-16}\,cm^2$, $1.5x10^{-15}\,cm^2$ and $4x10^{-15}\,cm^2$, respectively [113-115], and the calculated corresponding mean free path values at 20 mTorr are 18.3 cm, 1.2 cm, and 0.46 cm, respectively. As a result, Ar+ experiences more collisions and momentum loss than do H+ and He+ prior to impingement on the film surface. These collisions may be responsible for the observed similar etch rates of each metal (Cu, Ag, and Au) in Ar and He plasmas where ion and photon bombardment (physical effects) are primarily responsible for film etching. Specifically, for He

and Ar, Cu etch rates are 10 nm/min and 4 nm/min respectively, Ag etch rates are 45 nm/min and 50 nm/min respectively, and Au etch rates are 55 nm/min and 62 nm/min. These data are in contrast to the trend in Ar+ sputtering yield of Cu, Ag, and Au relative to the He+ sputtering yield of those metals (Table 3.1) when the pressure is sufficiently low that ions do not suffer extensive collisions that lead to momentum loss. Moreover, for Cu, the Ar plasma etch rate was lower than that for He [86, 87], despite the fact that the higher mass of Ar+ should yield more efficient sputtering than He+ as a result of momentum transfer [Equations (1) - (3) and Table 3.1]. Such considerations suggest that the reduction of Cu etch rate with higher ion mass may be related to the momentum loss of Ar ions during sheath transit, along with the energetic UV photon enhancement of Cu etching under He plasma exposure, as described previously [87].

Three different hydrogen ions, H+, H_2+, and H_3+, are formed in H_2 plasmas. The dominant ion species among them is determined by the pressure of the plasma gas. When the H_2 pressure is below 0.1 mTorr, the dominant hydrogen ion is reported to be H_2+ [116]. However, H_3+ is the major hydrogen ion (~80 %) when the pressure is greater than 15 mTorr due to a dissociative proton transfer reaction [115, 117].

$$H_2 + H_2^+ \rightarrow H_3^+ + H \quad (4)$$

As a result of these previous studies, we expect that H_3+ is the dominant ion species during Cu, Ag, and Au etching in an H_2 plasma under the conditions investigated in this study, since the H_2 pressure was 20 mTorr.

The ability of H_3+ ions to sputter Cu in the PT-ICP reactor can be estimated from the ion flux in a He plasma operating at 500 W coil power and 20 mTorr pressure. For this purpose, equation 5 was used to estimate the ion sputtering yield [118].

$$Y = Sd/(0.06JA), \quad (5)$$

where Y is the ion sputtering yield, S is the sputter rate, J is the ion beam current density, and d and A are the target density and molecular weight, respectively. The He ion sputtering yield of Cu at ion energies between 100 eV and 250 eV is 0.08~0.15 [74]; thus, the He ion flux from equation (5) is 1-2x10^{16} $cm^{-2}s^{-1}$, which is consistent with ion fluxes reported for ICP systems (1-5x10^{16} $cm^{-2}s^{-1}$ depending on the pressure, plasma power, and gas species) [119, 120].

Ion sputtering yield calculations indicate that even if the sputter yield of H_3+ is 3 times higher than that of H+ with an ion energy of 360 eV (Table 3.1), the estimated etch rate for H_3+ is too low to explain the observed plasma etch rates of Cu, Ag and especially Au. These considerations indicate that ion bombardment alone cannot account for the differences observed when plasma etching Cu, Ag, and Au in noble gases relative to H_2 plasmas. Therefore, effects such as chemical reactions and photon bombardment/excitation, appear to play important roles in Cu, Ag, and Au etch processes.

3.3.4 Chemical Etching Component

In order to investigate the chemical etching component of H_2 plasmas, two sets of experiments were performed. Blanket Cu, Ag, and Au films were etched without an SiO_2 mask layer. Consistent with the masked metal thin films, Cu, Ag, and Au were completely removed after 8 minutes of H_2 plasma, which suggests that the H_2 plasma etching mechanisms of Cu, Ag, and Au were not significantly affected by possible oxidation and/or fluorination during SiO_2 mask patterning. Blanket Cu, Ag, and Au films were also patterned using a borosilicate glass slide as a masking layer. Etch times were selected to allow complete removal of each of the 100 nm films; removal required 8 min for Cu, 4 min for Ag, and 6 min for Au. XPS analysis of the side of the glass slide that was in physical contact with the blanket metal film detected metal

species in each case. Figure 3.7 indicates that Cu, Ag, and Au were detected at the edge of the glass slide masks, while Cu and Au were also found at the center of the glass slide. Since the glass slide was held in place over the blanket Cu, Ag, and Au films by kapton tape at the edges of the slide, metal atoms must have deposited onto the glass slide by desorption from the metal surface and adsorption onto the slide. Because the gap between the glass slide and the blanket thin films was small (<3 μm), generation of reactive H species and ion bombardment in the gap are unlikely. As a result, formation of metal etch products that subsequently desorb from the surface and adsorb onto the slide requires the consideration of alternative mechanisms. For instance, diffusion of atomic hydrogen into the gap between the glass slide and the thin film will allow reaction with the metal to form hydrides which desorb; this process could be promoted by transmitted photons (through the glass slide). Alternatively, photons can excite surface metal atoms that react with either H or H_2 to form etch products [89]. Because the likely etch product AgH is the most unstable species among CuH, AgH, and AuH [90], the probability of desorption of AgH from Ag surface and adsorption onto the glass slide should be low at the center region of glass slide where very limited H radical concentration exists. Such considerations are consistent with the observed distribution of metal species on the slide surface.

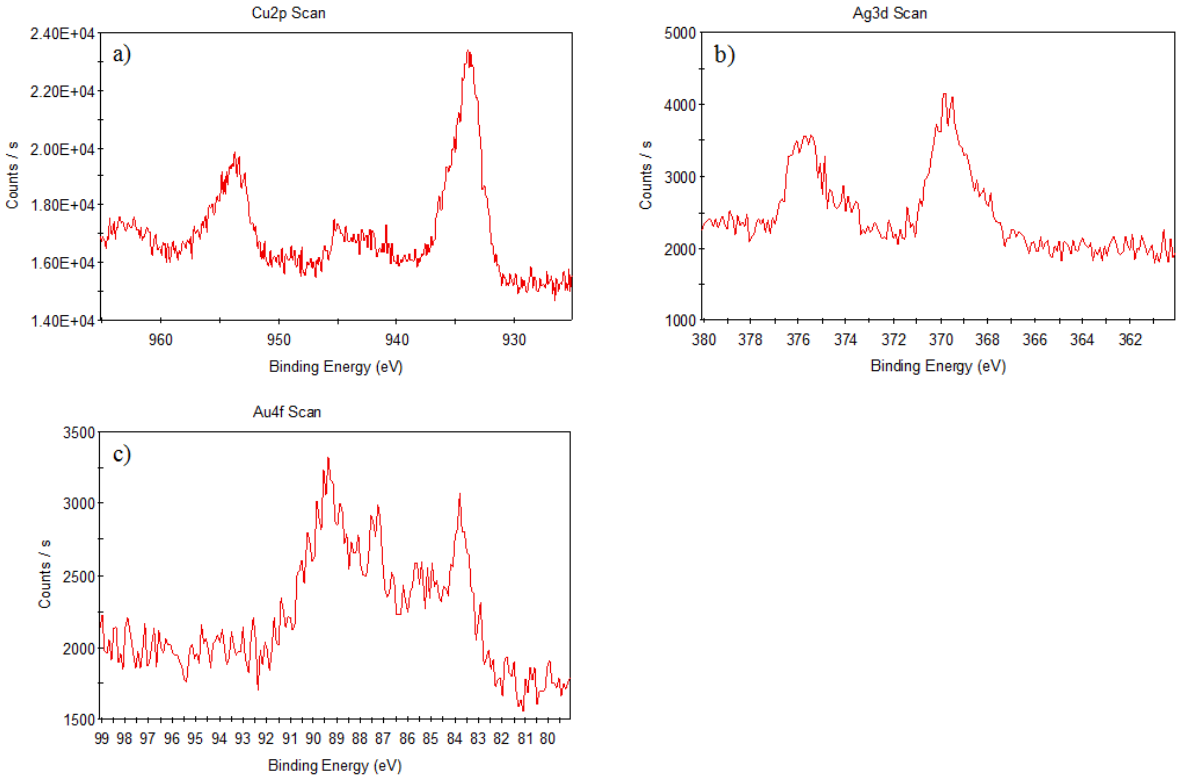

Figure 3.7 XPS of glass slide mask edge after H_2 plasma etching of blanket a) Cu for 8 min, b) Ag for 4 min, c) Au for 6 min.

As suggested by the current study as well as our previous work, H_2 plasma etching products of Group 11 species are likely metal (Cu, Ag, and Au) hydrides. Interestingly, Ag and Au are two of the metals that are reported not to form hydrides [121]. Nevertheless, caged Cu, Ag, and Au hydrides have been detected in a crystalline silicon lattice [122-124], and Cu, Ag and Au hydrides have been detected in solid Ar and Ne matrices by laser ablation. The relative stability of these hydrides has also been predicted by Density Functional Theory (DFT) [90, 125]. According to these calculations, all Cu, Ag, and Au hydride species are thermodynamically unstable, but among these three, Au hydrides are the most stable species followed by Cu hydrides and Ag hydrides as shown in Figure 3.8 [90]. These calculations predicted that metal dihydride anions and AuH_4^- are the stable compounds; small concentrations have been detected

using IR spectroscopy [90]. These data suggest a possible etching mechanism wherein Cu (Ag or Au) dihydride anions are first formed from exposure to an H_2 plasma. On the metal surface where electrons are abundant, Cu (Ag or Au) dihydride anion expulsion from the surface could be facilitated by electrostatic repulsion, despite the fact that the vapor pressure of Cu (Ag or Au) dihydride anions is relatively low. After formation of Cu (Ag or Au) hydrides on the surface, two competitive reaction paths are possible: dissociation of metal hydrides into M and H_x due to unstable Cu (Ag or Au) hydrides, and desorption of metal hydrides from the surface. Because AuH_2^- is the most stable among CuH_2^-, AgH_2^-, and AuH_2^- along with the formation of AuH_4^-, whose stability is similar to that of AuH_2^-, Au may display a higher etch rate than Cu if this reaction path is preferable to dissociation. Indeed, the Au etch rate is comparable to that of Ag despite the poor sputtering efficiency of Au by hydrogen ions and the relatively higher metal-metal bond strength compared to Cu and Ag.

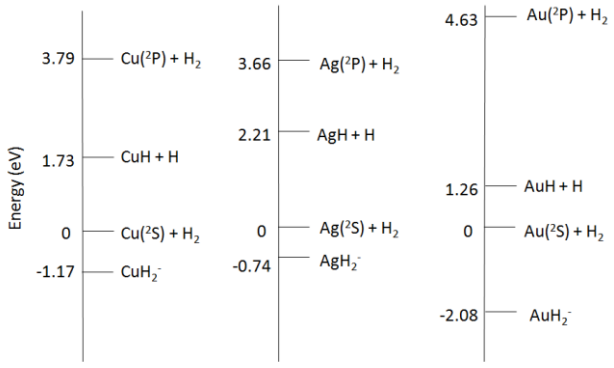

Figure 3.8 Relative energies of Cu, Ag, and Au + H_2 reactants and their reaction products [90].

CuH formation from a reaction between a photo-excited Cu atom and H_2 has been proposed to account for the generation of thermodynamically unstable CuH [89]. According to potential well calculations for CuH formation, ground and low level excited Cu state (^2D, $3d^9 4s^2$, and ^2S, $3d^{10} 4s^1$) interactions with H_2 are repulsive even if their total energy is lowered, but higher

excited Cu states (^2P, $3d^{10}4p^1$) display attractive interactions with H_2, to generate CuH + H [89]. In H_2 plasma etching of Cu, energetic UV photons are present along with highly reactive H radicals. Thus a similar scenario to that postulated for the proposed mechanism of CuH (AgH or AuH) formation exists and may be operative in the plasma atmosphere.

Table 3.2 Calculated Standard Sublimation Enthalpy of CuH, AgH, and AuH, and that of pure metals (Cu, Ag, and Au).

	CuH	AgH	AuH
Sublimation ΔH^o (eV)	2.07	2.01	2.12
	Cu	Ag	Au
Sublimation ΔH^o (eV)	3.51	2.95	3.77

Generally, plasma etching relies on the formation of volatile compounds on the surface of the material being etched. However, little work has been reported on vapor pressures of Cu, Ag, and Au hydrides due to their thermodynamic instability. Recently, Cu, Ag, and Au hydride crystal standard atomization enthalpies (467 kJ/mol, 417 kJ/mol, and 519 kJ/mol, respectively) have been calculated based upon linear relations between the crystal standard atomization enthalpy of MH, $\Delta_{at}H°(MH)$, and the diatomic bond dissociation enthalpy of MH, D°(MH) [9]. Here, $\Delta_{at}H°(MH)$ is the sum of the sublimation enthalpy of MH solid, $\Delta_{sub}H°(MH)$, and D°(MH). In addition, the experimental D° values are 267 kJ/mol, 223 kJ/mol, and 314 kJ/mol for CuH, AgH, and AuH, respectively [126]. From this information, $\Delta_{sub}H°(MH)$ is 200 kJ/mol (2.07 eV) for CuH, 194 kJ/mol (2.01 eV) for AgH and 205 kJ/mol (2.12 eV) for AuH. Comparison of these values to $\Delta_{sub}H°$ (3.51eV, 2.95eV, and 3.77eV for Cu, Ag, and Au, respectively) at 25 ºC shows that the calculated $\Delta_{sub}H°(MH)$ values are lower than those for the metals (Table 3.2). This (admittedly equilibrium) calculation indicates that if MH forms on the Cu, Ag, and Au surface, ion- (or photon-) assisted removal of etch product species during plasma etching is plausible;

indeed, such possibilities are consistent with observations of ion-assisted H_2-based plasma (chemical) Cu etching described previously [93].

3.4 Conclusions

Results for H_2, He and Ar plasma-assisted etching of Ag and Au at low temperature were compared to those previously reported for Cu etching to allow similarities and differences of Group 11 metal etching to be assessed. Under the same plasma conditions, H_2 plasmas displayed higher etch rates for Ag and Au (33 nm/min and 26 nm/min) than for Cu (13 nm/min). Due to variation in physical (mass) and chemical (reactivity, stability, and volatility) characteristics of Cu, Ag, and Au, insight into plasma-assisted etch mechanisms for these metals can be gained. Specifically, different etch trends are observed in that Ag and Au etch rates increase as the atomic or molecular mass of the plasma gas increases while Cu etch rates decrease with increasing atomic weight of the etch gas. Similar to Cu, Ag and Au etching is dependent upon a combination of chemical and physical etching components.

Although Ar is a more efficient sputtering gas than is He, little variation in etch rate is observed among each of the metals Ag, Au, or Cu when rates are compared in these two gases. This similarity appears to arise from the short mean free path and thus momentum loss in an Ar plasma combined with energetic UV photon enhancement in a He plasma. In an H_2 plasma, the dominant ion species is likely H_3+, but low ion flux under the plasma etching conditions demonstrates that hydrogen ion sputtering cannot account for the observed high etch rates of Cu, Ag, and especially Au.

Studies to investigate the chemical etching aspect of Group 11 metals in H_2 plasmas utilized a glass slide that was placed over the metal surface during exposure to the plasma. In all cases, metal (Cu, Ag and Au) species appeared on the bottom edge of the glass slide indicating

transport of metal beneath the mask. Because Cu (Ag or Au) hydrides are thermodynamically unstable, formation of more stable products that transport, dissociate or desorb, appear to be important in H_2 plasma etching. Also, formation of thermodynamically stable CuH_2^-, AgH_2^-, and AuH_2^- species may offer an additional etch mechanism, since electrostatic repulsion between metal hydride anions and electrons in the etching metal surface can assist product desorption. Thus, the formation of stable etch products, AuH_x or AuH_x^- among Cu, Ag, and Au hydrides or hydride anions are likely responsible for the higher etch rate of Au relative to that of Cu in H_2 plasmas. Such considerations may also account for the importance of a chemical component in Au etching to yield relatively high etch rates in spite of poor Au sputtering efficiency. Finally, the calculated low binding energy of CuH, AgH, and AuH implies that desorption of etch products can be facilitated by ion and photon bombardment in H_2 plasma etching.

CHAPTER 4.

LOW TEMPERATURE Cu ETCHING USING CH_4-BASED PLASMAS

4.1 Introduction

H_2-based plasma Cu etching studies [86, 87, 93, 127] have demonstrated the viability of etching and patterning Cu in H_2 plasmas at low (especially below room) temperatures, although the profile displays an ~80^o sidewall angle when using an SiO_2 etch mask. An increase in sidewall angle might be possible if a residue-forming gas is employed to etch Cu, analogous to processes developed to control the profiles of other film materials [128]. Because chemical reaction between Cu and H radicals appears to be a critical component of the etching mechanism in an H_2 plasma process [86, 87, 93, 127], hydrogen-containing gases such as CH_4, might result in effective Cu etching and patterning, but with different etch rate, selectivity, and etch profile. In addition, unlike an H_2 plasma, a CH_4 plasma should not be as physically and chemically damaging to photoresist (PR) masks which would simplify the etch and thus fabrication process.

Indeed, there are several reports describing CH_4 or methyl group-containing plasma etching of Cu. Mitura et al. etched Cu foils with a CH_4 plasma, although quantitative information regarding etching conditions, etch rate, selectivity, etch profiles and possible etch products were not discussed [129]. Recently, Nishimura suggested that under CH_4 plasma exposure, Cu can be removed by a chemical reaction involving hydrogen. Because the author postulated that CuCOO can be formed by reaction between Cu and an organic acid and that CuCOO is a volatile compound, the proposed etch product was believed to be CuCOO [130]. In order for this reaction to be plausible in the etch system described, oxygen is required. This mechanism therefore seems unlikely, because the O needed to form an organic acid can only be generated from the SiO_2

mask [130]. On the other hand, Druschke reported that CH_3Cu or CH_2Cu may be etch products when Cu is etched in a CH_3I plasma [131]. Because the mask employed was polymeric, organic acids cannot be formed in these experiments. Furthermore, the other possible etching product, CuI, is volatile only at high temperatures (vapor pressure of CuI is 20 mTorr at 700 ℃) [132], and the substrate temperature was maintained at 50℃; under these conditions, the reported etch rate was 36 nm/min [131]. Such results suggest that the etch product of CH_3I plasma etching of Cu is not likely CuI, but may be CH_3Cu or CH_2Cu as suggested.

Previous studies have reported the formation of CH_3Cu or related compounds in the gas phase or in a solid matrix at cryogenic temperatures [133-137]. Parnis et al. co-condensed CH_4 and Cu atoms generated from a tantalum filament and observed the formation and dissociation of CH_3CuH by photolysis of Cu atoms, thereby demonstrating that an electronically excited state of $Cu(^2P)$ is sufficiently reactive to form CH_3CuH; further photolysis or heating led to dissociation of CH_3CuH into CH_3 + CuH or CH_3Cu + H [133, 134]. Using DFT calculations, Cho et al. reported the relative stability of CH_3CuH, CH_3Cu and CH_3CuH^- species from laser ablated Cu atoms in an Ar matrix, where CH_3CuH is thermodynamically unstable but CH_3Cu and CH_3CuH^- are stable species [135]; these calculations support Parnis' CH_3CuH studies. In addition, Rijs and O'Hair observed gas phase CH_3CuH^- from fragmentation of $CH_3CuCH_2CH_3^-$ [136] and $CH_3CuCH_3^-$ derived from $CH_3CO_2CuO_2CCH_3^-$ [137] using mass spectrometry. These studies suggest that if Cu surface atoms exposed to a CH_4 plasma are excited into higher energy states due to energetic ion, electron, and photon bombardment, CH_3CuH, CH_3CuH^-, CH_3Cu, CH_3CuCH_3 or other methylated copper species may be generated.

In this chapter, we report Cu etch rates and pattern profiles using a pure CH_4 plasma and various CH_4 gas mixtures with H_2 or Ar at low temperature (10 ℃). In order to gain insight into

the Cu etching mechanism by CH_4 plasmas, platen/coil powers and etch pressures were varied, and the gas phase species present during etching were observed by optical emission spectroscopy (OES).

4.2 Experimental Procedure

100 nm thick Cu thin films were deposited onto a 20 nm thick Ti layer on a 4inch Si wafer by evaporation using a CVC E-Beam Evaporator. Copper patterns were generated using both hard (SiO_2) and soft (photoresist) masking layers. Specifically, a 176 nm thick SiO_2 was plasma deposited in a Unaxis PECVD system onto Cu layers from 400 sccm SiH_4 and 900 sccm N_2O at 25 W applied power, 900 mTorr pressure and a platen temperature of 250 ℃. Subsequently, the SiO_2 layer was patterned using a C_4F_8/CO_2/Ar- (15, 28, and 5 sccm, respectively) based plasma with 80 W and 400 W applied to the platen and coil, 5mtorr pressure, while16℃ substrate temperature was maintained during the process in a Plasma Therm ICP(PT-ICP). In addition, a 1.6μm thick photoresist (*Microposit* sc1813) layer was spin coated onto the Cu film, and exposed to 405 nm wavelength light from a Karl Suss MA6 Mask Aligner. The exposed pattern was developed by immersion into MF-319 base for 1 minute. These samples were cut into sections of ~1 cm^2 and attached to a 4 inch diameter Si carrier wafer by *cool grease* 7016 (AI Technology Inc.).

In order to compare the Cu etch results from CH_4-based plasmas with the previously reported Cu etching studies using H_2 plasmas, CH_4 plasma etching investigations were performed in the same PT-ICP reactor under the following etch conditions: 65 sccm CH_4 gas flow rate, 100 W(platen)/500 W(coil) power, 20 mTorr pressure, and 10 ℃ substrate temperature . A substrate temperature of 10 ℃ was employed to allow direct comparison with results

obtained from H_2 plasma etching of Cu, where the etch product, likely CuH_x, is unstable at temperatures near room temperature[93].

Additional experiments were performed to investigate the chemical selectivity and etch mechanism of CH_4 plasmas. First, blanket Cu, Ti, Si, and SiO_2 films were etched by CH_4 plasmas. Cu (100 nm) and Ti (40 nm) films were e-beam evaporated onto Si wafers, and 150nm SiO_2 films were plasma deposited onto Si wafers. Mixtures of CH_4 with 50 % or 10 % (33 and 6 sccm) H_2 gas and 10 % or 3 % (6 and 2 sccm) Ar gas were investigated; in all cases a fixed total flow rate of 65 sccm was used. In these experiments, the same plasma conditions used previously to pattern masked Cu films were applied. Finally, various platen/coil powers and pressures of CH_4 plasmas were studied. The platen power was varied from 100 to 200 W with a fixed 500 W coil power at 20 mTorr pressure; various coil powers from 500 to 700 W with a fixed 100 W platen power at 20 mTorr were also used. Finally, a pressure range of 10 to 60 mTorr range was investigated with fixed 100 W/ 500W applied power.

During etching, plasma species were identified using optical emission spectroscopy (OES) (Verity SD2048DL Spectroscopy system). Etched film profiles were examined with a scanning electron microscope (Zeiss Ultra60 FE-SEM), and etch rate and deposition rate were determined by both SEM and Dektak 150 Profilometer measurements after removing the SiO_2 mask with a dilute HF solution (2 volume %). Chemical analyses of blank films were conducted using X-ray photoelectron spectroscopy (Thermco Scientific K-Alpha XPS).

4.3 Results and Discussion

4.3.1 Cu Etching with Hard (SiO_2) and Soft (photoresist) Masks

Figure 4.1 shows SiO_2 and photoresist (PR) masked 100 nm thick Cu films etched by a CH_4 plasma for 6min at 65 sccm CH_4 gas flow rate, 100 W(platen)/500 W(coil) power, 20 mTorr pressure, and 10 ℃ substrate temperature. Due to non-uniform thickness of the Cu film, Cu residues and the underlying Ti layer between Cu grains were observed as shown in Figures 4.1-a2 and 4.1-b2. The Cu etch rate was 17 nm/min for both mask materials. CH_4 plasmas are often employed for hydrocarbon film deposition [138], and thus can be invoked for sidewall passivation in plasma etching processes to generate anisotropic etch profiles [128]. Hydrocarbon deposition on the PR surface (132 nm) and sidewall (83 nm) is evident in Figures 4.1-b and 4.2-b. The carbonaceous layer protects the PR mask from substantial H radical etching, in contrast to the situation with H_2 plasma etching of Cu. In comparison, a 137 nm hydrocarbon film was observed on top of the SiO_2 mask layer, while deposited films are not visible on the SiO_2 sidewall; in addition, ~18 nm of the SiO_2 mask layer was etched during the start of the CH_4 plasma process (Figure 4.1-a1). These observations indicate that CH_x radicals do not form a thick polymer film on the SiO_2 sidewall but rather react with the SiO_2 sidewall causing lateral SiO_2 mask etching. The combination of such chemical reactions and physical sputtering is believed to result in the rounded edge of the SiO_2 mask observed in Figure 4.1-a1. This effect combined with edge removal of the SiO_2 due to mask slope creates a sidewall slope in the underlying Cu layer. Interestingly, a hydrocarbon film was not observed on sidewalls of the etched Cu films nor on Cu surfaces for either SiO_2 or PR masked Cu patterning. As a result, the measured sidewall angle for SiO_2 masked Cu was ~80° (Figure 4.1-a1) which is the same slope as that observed during Cu etching by H_2 plasmas [86]. The sidewall angle of PR masked Cu films varies from 60-85°

(Figure 4.1-b1), apparently due to PR sidewall roughness that results from the CH_4 plasma. The observed Cu sidewall roughness for both SiO_2 and PR masked Cu films in Figure 4.1, is primarily due to the roughness of the patterned SiO_2 or PR mask layers which was transferred directly into the Cu film by the CH_4 plasma etch process.

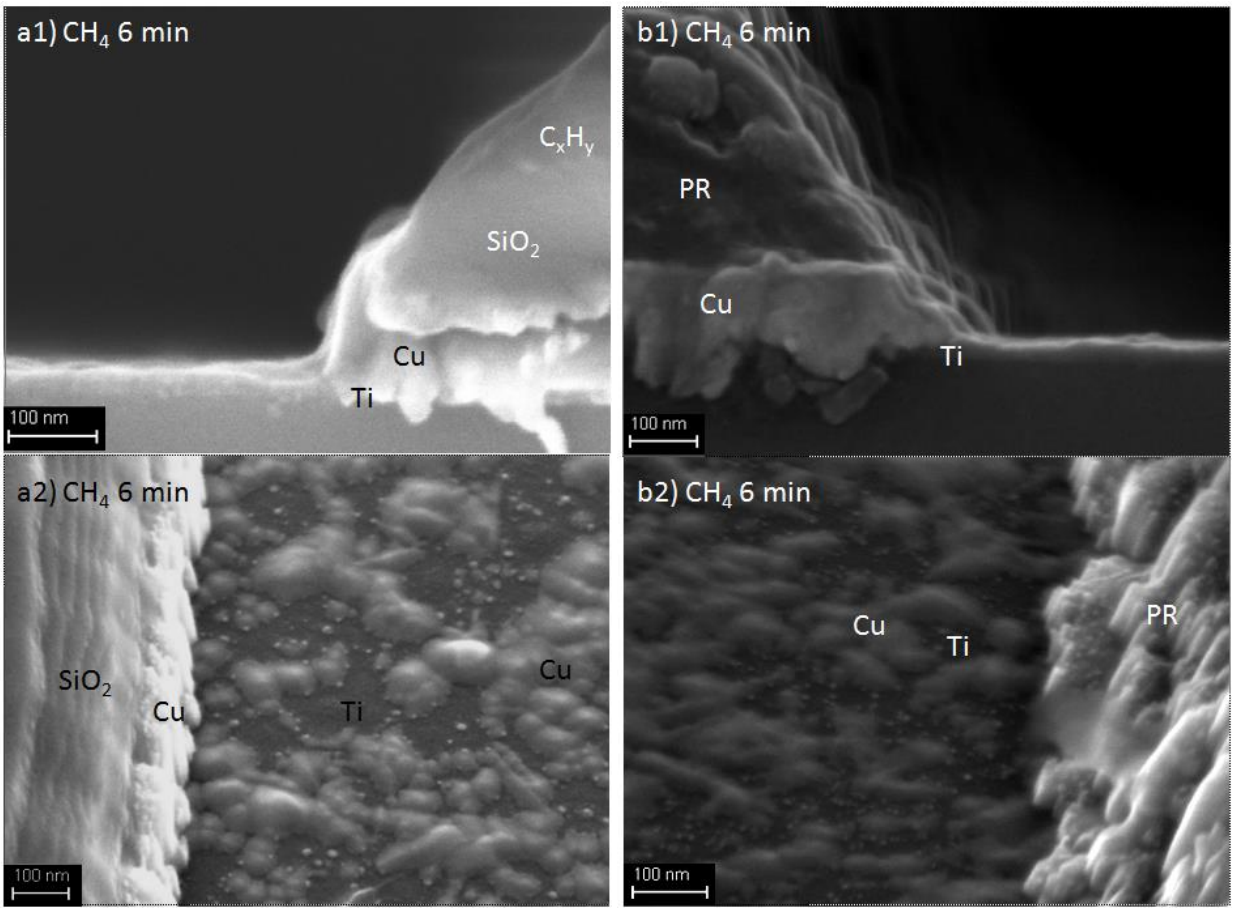

Figure 4.1 SEM images of cross sections and surfaces of 100 nm Cu films. a1) cross section and a2) surface of SiO_2 masked Cu after 6 min of CH_4 plasma etching; b1) cross section and b2) surface of PR masked Cu after 6 min of CH_4 plasma etching. All etch conditions were: 65 sccm CH_4 gas flow rate, 100 W(platen)/500 W(coil) power, 20 mTorr pressure, and 10 ℃ substrate temperature.

In order to compare/contrast the effect of CH_4 versus H_2 plasmas on PR mask layers, several Cu etch studies were performed. The thickness and sidewall angle of an as-developed (prior to plasma exposure) PR pattern (hereinafter "blank PR"), and PR patterns after 6 min of

CH_4 plasma or 6 min of H_2 plasma under the same plasma conditions were compared. PR exposure to the CH_4 plasma removed 70 nm of PR but deposited 132 nm of hydrocarbon on the PR surface. In addition, the PR sidewall slope increased relative to that of the blank PR, while the hydrocarbon layer deposited (83 nm) was thinner than that on the PR top surface. By comparison, 1000 nm of PR was etched by the H_2 plasma and the profile displayed a low (50° degree) sidewall angle.

Although a hydrocarbon film was not evident by SEM (or XPS) on Cu after CH_4 plasma etching (Figure 4.1), hydrocarbon species adsorption certainly occurs on Cu surfaces during the etching process. It is expected that these species will hinder both formation of the Cu etch product as well as escape/removal of etch product from the Cu surface. Therefore, the Cu etch rate of 17 nm/min by CH_4 plasma is very surprising because it is higher than the 13-14 nm/min H_2 plasma etch rate of Cu under the same etch conditions [86] where no film deposition from the plasma gas occurs. Moreover, unlike an H_2 plasma, a CH_4 plasma does not substantially degrade or etch a PR mask (Figure 4.2), which suggests that CH_4 plasmas may facilitate the implementation of plasma-based Cu etching processes in device manufacture.

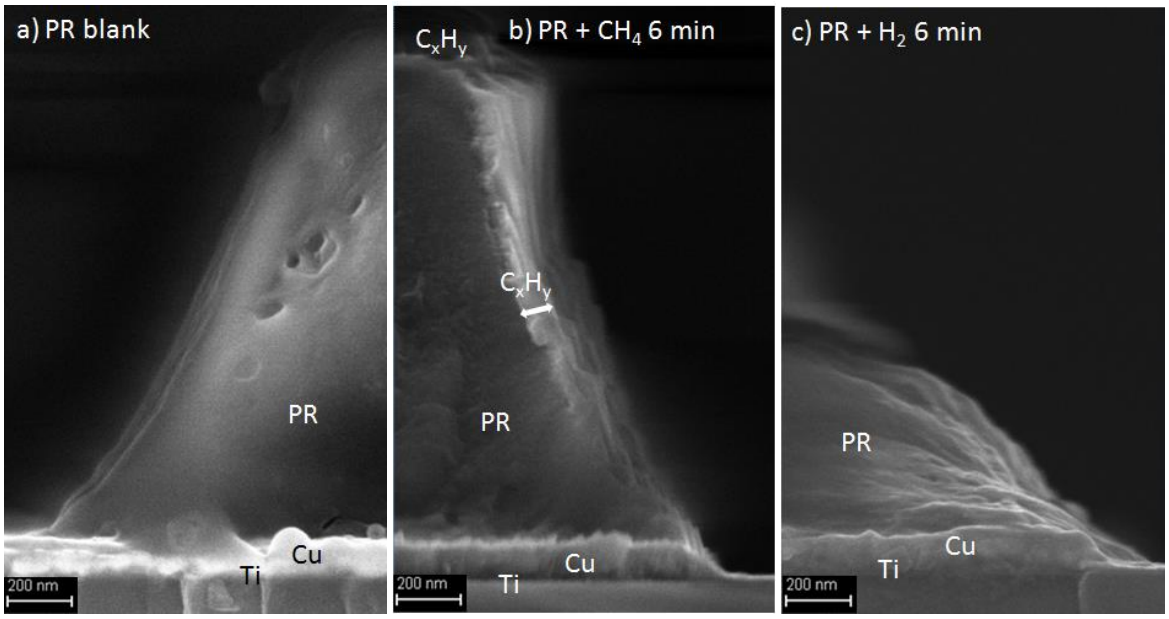

Figure 4.2 Cross sectional SEM images of PR masked 100 nm Cu films. a) blank (prior to Cu etching) PR, b) PR masked Cu after 6 min of CH_4 plasma etching, and c) PR masked Cu after 6 min of H_2 plasma etching. Etch conditions were: 65 sccm CH_4 or H_2 gas flow rate, 100 W(platen)/500 W(coil) power, 20 mTorr pressure, and 10 ℃ substrate temperature.

Cu etch rates are altered with CH_4 exposure times longer than 6 min. Cu etch rates and hydrocarbon deposition rates on SiO_2 mask layers were constant for etch times between 3 and 6 min: 17 nm/min and 22 nm/min, respectively, and the measured Cu thickness decreases linearly up to an etch time of 6 min (Figure 4.3). Subsequently, hydrocarbon deposition occurs within the etched trench. These observations demonstrate that hydrocarbon film deposition occurs after complete removal of the 100 nm thick Cu layer, indicating that unlike Cu, Ti is not etched by a CH_4 plasma under these plasma conditions.

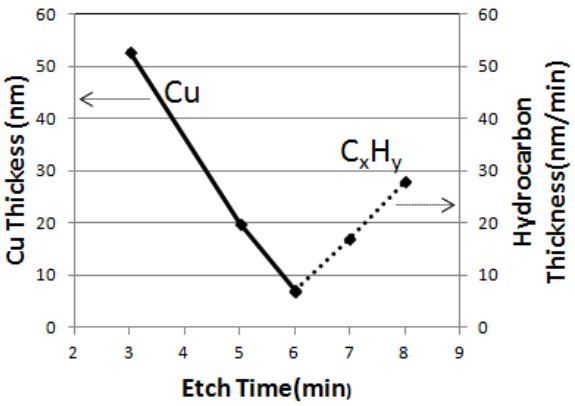

Figure 4.3 Cu film thickness (initially 100 nm) after CH_4 etching of SiO_2 masked Cu for etch times between 3 and 8 min.

4.3.2 CH_4 Selectivity on Cu, Ti, Si, and SiO_2

In order to gain more insight into hydrocarbon film formation on Ti after 6 min of CH_4 plasma etching of a patterned Cu film, blanket Cu, Ti, Si, and SiO_2 films were etched by CH_4 plasmas under the same conditions used for the SiO_2 and PR masked Cu samples. Possible cross contamination of samples by etch products or sputtering of film materials was avoided by conducting separate etch experiments with 6min of Cu etching, and 5min of Ti, Si, and SiO_2 etching. The different exposure time used for Cu etching was to ensure complete etching of the 100nm thick Cu film. Figure 4.4 shows cross sectional SEMs of each etched sample. Blank 100 nm Cu layers were completely etched by the CH_4 plasma in 6 min without visible hydrocarbon deposition (Figure 4.4-a). The 40 nm Ti layer was not etched by 7 min of CH_4 plasma, but 144 nm of hydrocarbon was observed on the Ti surface (Figure 4.4-b). Similarly, a 150 nm thick hydrocarbon film was formed on Si after 7 min of CH_4 plasma treatment (Figure 4.4-c). With SiO_2, 5 min of CH_4 plasma removed 18 nm, while a 109 nm thick hydrocarbon layer was formed (Figure 4.4-d). Therefore, the average hydrocarbon deposition rate on blank Ti, Si, and SiO_2 surfaces is 19-22 nm/min which is equal to the hydrocarbon deposition rate on the SiO_2 mask in

the Cu patterning experiments. These results indicate that for the substrates/films investigated, only Cu is etched significantly by a CH_4 plasma under the specific plasma conditions invoked. Furthermore, except for Cu, the hydrocarbon deposition rate was ~22 nm/min irrespective of the substrate material. Such results suggest that CH_4 etching of Cu is capable of excellent etch selectivity to other materials.

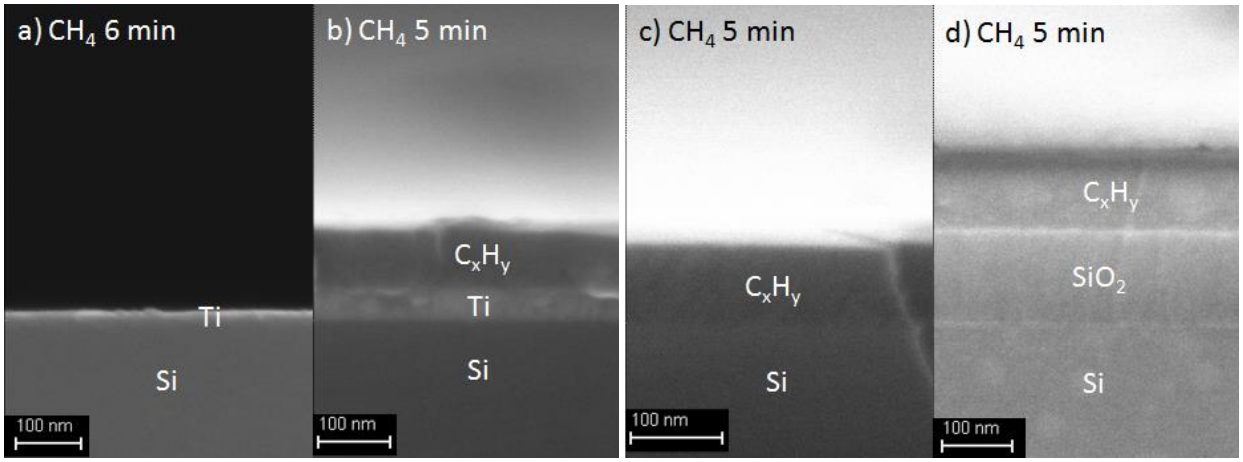

Figure 4.4 SEM cross sectional images of a) 100 nm thick blank Cu on thin Ti layer after 6 min of CH_4 plasma etching, b) 40 nm thick blank Ti and c) Si wafer after 7 min of CH_4 plasma etching, and d) 150 nm SiO_2 after 5 min of CH_4 plasma etching. Etch conditions for all experiments: 65 sccm CH_4 gas flow rate, 100 W(platen)/500 W(coil) power, 20 mTorr pressure, and 10 ℃ substrate temperature.

CH_4 plasma etch selectivity was further investigated using XPS surface analysis for time resolved blanket Cu etching. After 5 min of CH_4 plasma exposure, Cu peaks were detected at 932.5 eV and 952.3 eV (Figure 4.5-a), which are assigned to partially oxidized Cu [139], while no Ti peaks were detected (Figure 4.5-b). In addition, the most intense line at 284.8 eV is due to elemental carbon or hydrocarbon [140]; adsorbed CO on CuO is also observed (288.3 eV) [141] in Figure 4.5-c. Since the sampling depth of XPS is <10 nm, these observations indicate that at least a 10 nm thick Cu layer exists above the Ti, which agrees well with the Cu etch rates of 17 nm/min measured for SiO_2 or PR masked Cu. Also, the CO detected is likely a result of etched sample air exposure prior to XPS analysis

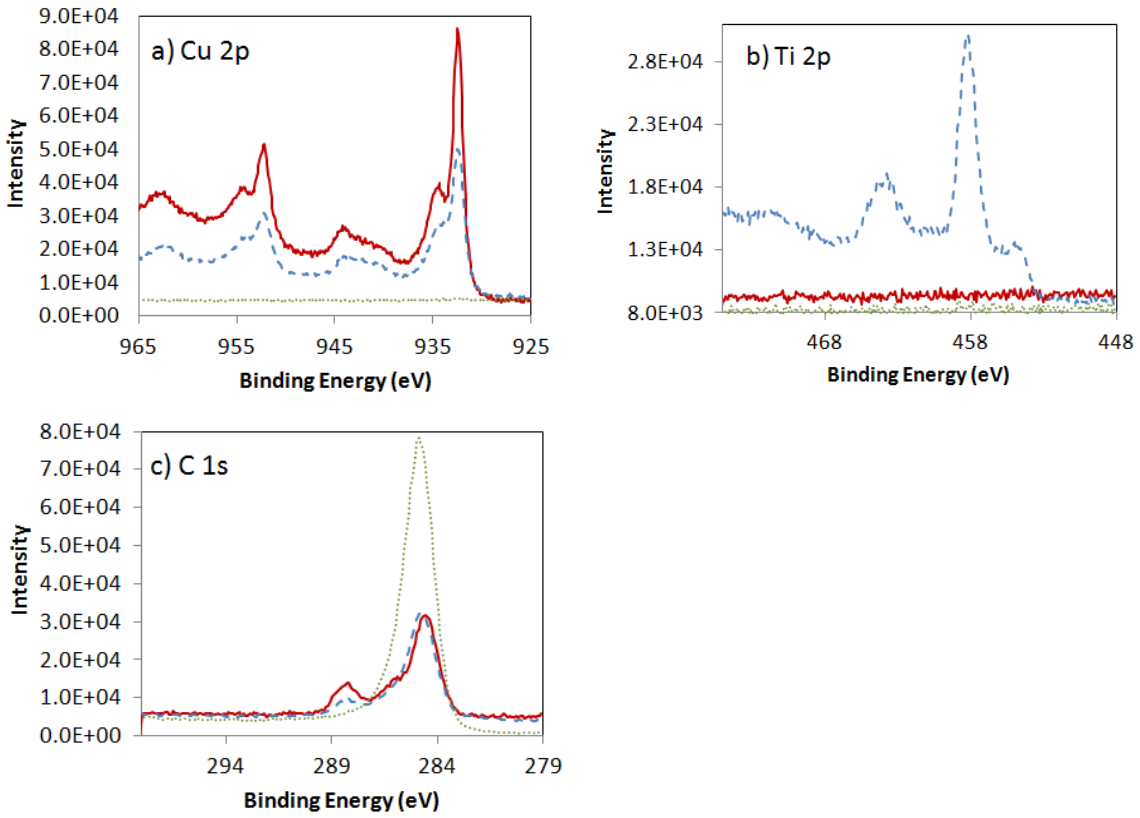

Figure 4.5 XPS scans of 100 thick blank Cu film etching by a CH_4 plasma for 5 min (red line), 6 min (blue dash line), and 10 min (green dot line) where peak intensities of a) Cu 2p, b) Ti 2p, and c) C 1s were measured for each etch time. All etch conditions were: 65sccm CH_4 gas flow rate, 100 W(platen)/500 W(coil) power, 20 mTorr pressure, and 10 ℃ substrate temperature.

When a Cu film was etched for 6 min, both Cu and Ti (oxidized Ti at 458.3 eV and 463.8 eV [139]) were detected (Figures 5-a and b), but the Cu and CO/CuO peak intensities were reduced (Figures 4.5-a and c). Because the Cu etch rate is 17 nm/min, the 100 nm Cu film should have been completely removed; detection of a trace amount of Cu is likely due to a non-uniform Cu film thickness. Moreover, the exposed Ti surface was covered by hydrocarbon as discussed previously (Figure 4.4b). This result is consistent with reduced intensity CO peaks. Since Ti was covered by a hydrocarbon layer, CO adsorption is limited to regions where Cu residues exist. However, after 10 min of CH_4 etching, no Cu, Ti, or CO peaks were detected, but hydrocarbon films were evident (Figure 4.5); these XPS data indicate that more than 10 nm of hydrocarbon

was deposited on Ti. Considering CH_4 plasma selectivity results and XPS analyses, a schematic, Figure 4.6, describing the time sequence involved in SiO_2 masked Cu etching can be proposed.

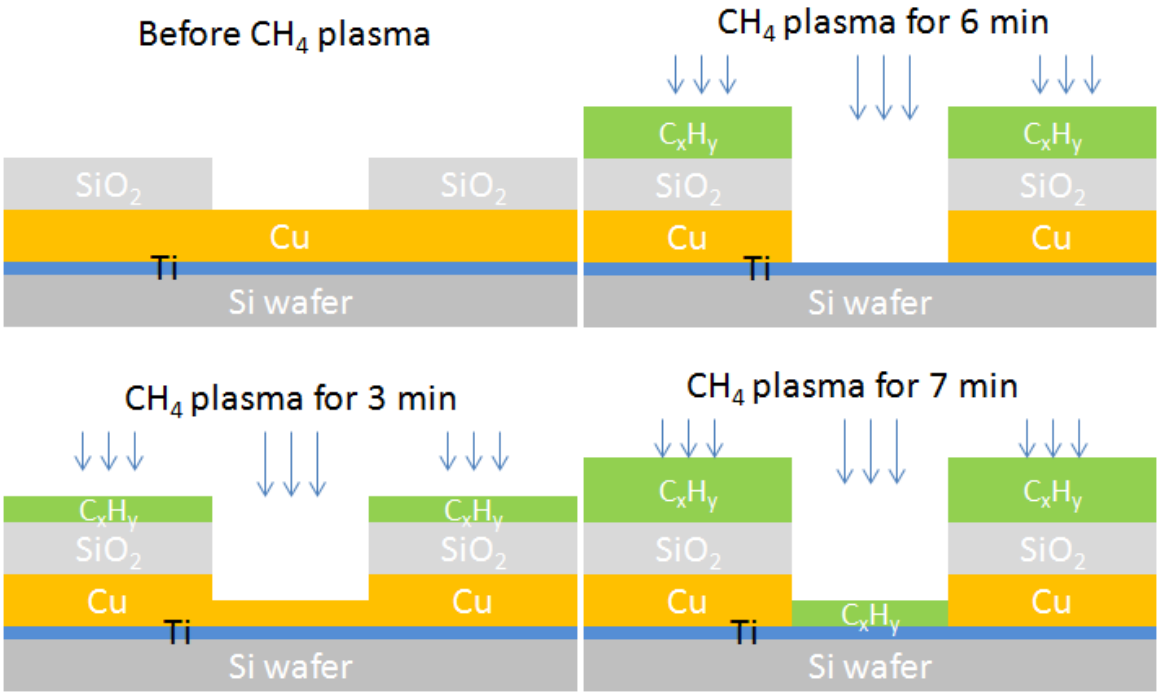

Figure 4.6 Schematic of Cu etching/patterning and hydrocarbon deposition during CH_4 plasma exposure for 3-8 min.

4.3.3 Cu Plasma Etching Using CH_4/H_2 and CH_4/Ar Mixtures

Cu etching by CH_4 plasmas without hydrocarbon deposition is difficult due to comparable Cu etch and hydrocarbon deposition rates (17 nm/min vs 22 nm/min) and the non-uniform thickness of Cu films. However, introducing H_2 or Ar gas into CH_4 plasma might inhibit hydrocarbon deposition and allow alteration of etch rates and profiles relative to those from pure CH_4 plasma etching. Thus, CH_4:H_2(1:1), CH_4:H_2(9:1), and CH_4:Ar(9:1) gas mixtures were employed for Cu patterning; etch results are shown in Figure 4.7.

A 120 nm thick patterned Cu film was etched with a 33 sccm:33 sccm CH_4:H_2 plasma; the etch rate was 20 nm/min with a side wall slope of 75°. The DC bias was 357 V, which was similar to the DC bias of a pure CH_4 plasma (350 V). No hydrocarbon film was observed on

either the sample surface or the carrier wafer by SEM. Because the likely etch product (CuH_x) is unstable and H ion sputtering is inefficient due to its low atomic mass, the Cu etch rate in an H_2 plasma is low: 13~14 nm/min [86, 87, 93, 127]. Moreover, because the CH_4 inlet concentration is 50 % that of the pure CH_4 plasma, the overall concentration of CH_4-related neutral and ion species will be reduced relative to those in the pure CH_4 plasma. The higher Cu etch rate observed in the CH_4:H_2 (5:5) plasma compared to that of the pure CH_4 plasma can be ascribed to a reduction of hydrocarbon deposition due to H atom generation within the H_2 plasma; removal of carbon residues by reaction with H is thereby facilitated. Additional evidence for this postulate arises from the results of Cu etching in CH_4:H_2 and CH_4:Ar with 9:1 ratio gas mixtures.

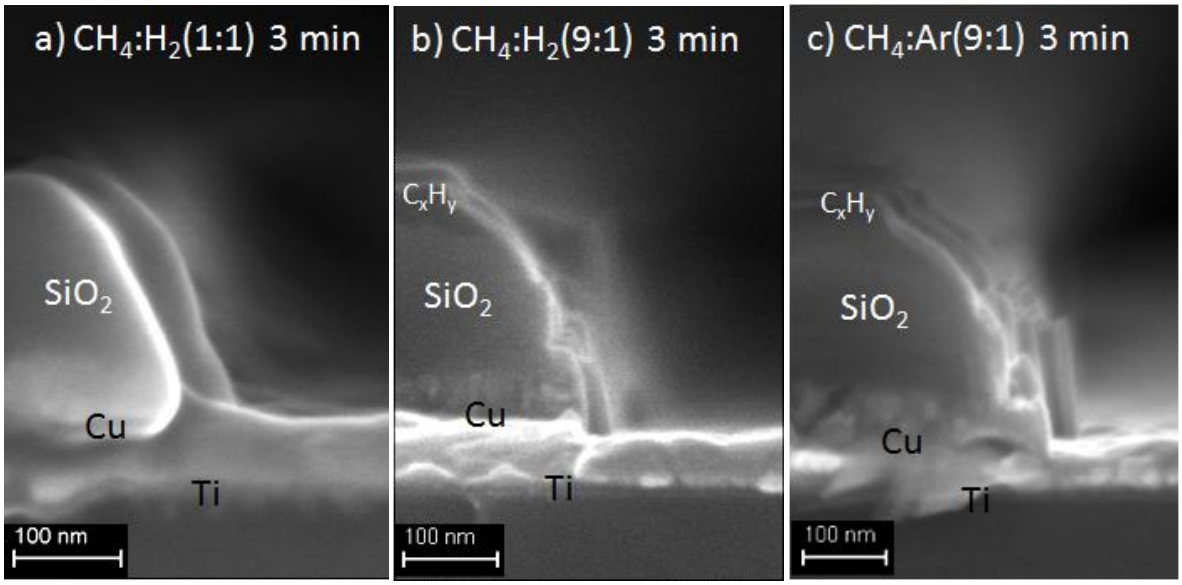

Figure 4.7 SEM Cross sectional images of a) 120 nm thick Cu film after 3min of 33 sccm CH_4+33 sccm H_2 (1:1) plasma etching, b) 100 nm thick Cu film after 3 min of 59 sccm CH_4 + 6 sccm H_2 (9:1) plasma etching, and c) 100 nm thick Cu film after 3 min of 59 sccm CH_4 + 6 sccm Ar (9:1) plasma etching. The steps observed in b) and c) are due to the viewing angle effect. Etch conditions were: 100 W(platen)/500 W(coil) power, 20 mTorr pressure, and 10 ℃ substrate temperature.

A mixture of 59 sccm of CH_4 and 6sccm of H_2 or Ar was used to etch Cu. For these two cases, measured etch rates and sidewall slopes were identical: 17 nm/min and 80°. The only

minor differences observed were the hydrocarbon deposition rate on the SiO_2 mask (19 nm/min for H_2) and 22 nm/min for Ar) and DC bias voltages of 375 and 360 V for H_2 and Ar, respectively (Figures 4.7-b and c). The Cu etch rate, side wall angle and carbon film deposition rate are also identical to those of the pure CH_4 plasma. Clearly, a 10 % addition of either H_2 or Ar did not prevent hydrocarbon formation on the SiO_2 surface and thus had essentially no impact on Cu etching, despite the reactive nature of H_2 for polymer removal and the efficiency of Ar sputtering. These gas mixture experiments suggest that >10 % H_2 must be added to CH_4 to effectively suppress hydrocarbon deposition and thereby yield enhanced Cu etch rates as well as better etch control.

4.3.4 Variation in Platen or Coil Power

Previous studies have demonstrated that Cu etch rates increased gradually from 13-20 nm/min in an H_2 plasma, when either platen power or coil power was increased from 100-200 W (platen) or 500-700 W(coil) [87]. For increasing platen power, the resulting higher ion energy enhanced both Cu sputtering and SiO_2 mask ablation and thereby degraded the anisotropy. However, increasing coil power generated higher electron, photon, reactive neutral and ion species concentrations or fluxes, which enhanced Cu etch rates, but sidewall angles did not change [87]. Results from these studies suggest that Cu etch rate, hydrocarbon deposition rate, and anisotropy of CH_4 plasma etching will also depend upon the ion energy and flux of photons, electrons, ions and neutrals.

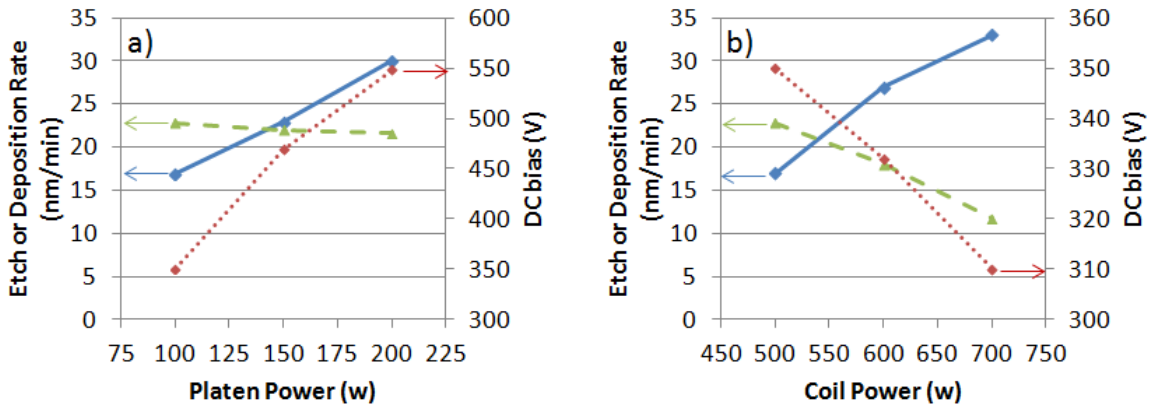

Figure 4.8 Cu etch rate (blue line) and hydrocarbon deposition rate on SiO_2 mask (green dashed line) and the resulting DC bias (red dotted line) a) platen power variation with fixed 500 W coil power, and b) coil power variation with fixed 100 W platen power. Other conditions are 65 sccm CH_4 gas flow rate, 20 mTorr pressure, and 10 ℃ substrate temperature.

When platen power was increased from 100 W to 200 W at 500 W coil power, the DC bias increased from 350 V to 550 V. This change caused a linear increase in Cu etch rate from 17 to 30 nm/min, although hydrocarbon deposition rates on the SiO_2 mask were nearly constant at ~22 nm/min (Figure 4.8-a). That is, higher ion energy enhanced the Cu etch rate but did not affect hydrocarbon deposition. When coil power was increased from 500 W to 700 W at 100 W platen power, Cu etch rates increased from 17 to 33 nm/min. Although this trend is similar to that for platen power changes, hydrocarbon deposition rates decreased from 22 to 11 nm/min, and the DC bias decreased from 350 to 310 V (Figure 4.8 b). These etch and deposition rate trends indicate that higher applied coil power increases photon, electron, neutral species, and ion flux, thereby enhancing both the chemical and physical components of Cu etching. Moreover, higher ion flux effectively facilitates removal of hydrocarbon fragments or films, despite the increased CH_x radical flux that promotes formation of polymeric layers on the SiO_2 surface. In addition, unlike H_2 plasma etching, despite increases in platen and coil power, the Cu sidewall angle remains at ~80°. Although a CH_4 plasma etched the sidewall of SiO_2, a thin layer of

hydrocarbon was likely formed to passivate the sidewall from reactive and/or energetic species flux.

Cu etch results due to variations in platen and coil power are consistent with OES data shown in Figure 4.9. Photons are collected through a pyrex window which blocks wavelengths <300 nm. Observed emission peaks are at 336.5 nm and 357.5 nm (N_2), 388.5 nm and 431.2 nm (CH), 516.2 nm (C_2), 486.2 nm, (H_β), and 656.5 (H_α),and bands at 600 nm is H_2[142]. Because the Cu sample size is ~1 cm^2, the small concentration of Cu-related gas phase species was not observed. Also, N_2 is likely present as a result of purge step prior to CH_4 plasma ignition or to minor vacuum system chamber leaks.

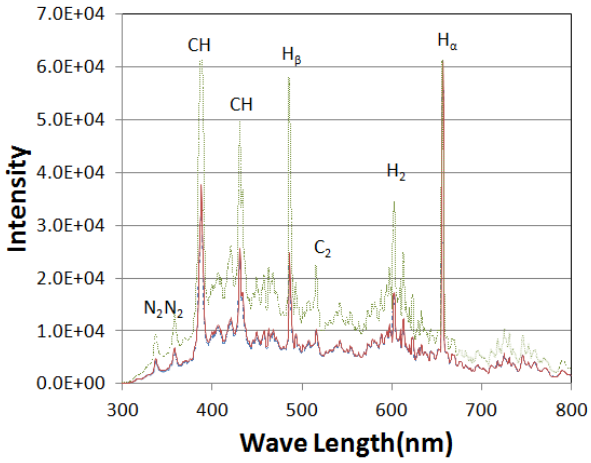

Figure 4.9 Optical emission spectra of various platen/coil power Cu etching in CH_4 plasmas. Blue dash line, red line, and green dot line represent 100 W/500 W, 200 W/500 W, and 100 W/700 W for each CH_4 plasma(blue dash line and red line are overlapped); other conditions are 65 sccm CH_4 gas flow rate, 20 mTorr pressure, and 10 ℃ substrate temperature.

In Figure 4.9, the most intense emission peaks are due to CH, C_2 and H, but according to the mass spectrometry study by Morrison et al., C and CH are the dominant radicals followed by CH_2, CH_3, and C_2, and the number of corresponding ions is ~1 order of magnitude lower in a 1.5 mTorr CH_4 plasma [143]. Thus, the most abundant neutral (and ion) species in our CH_4 plasma

appear to be CH (CH^+) and H (H^+). The overall CH_4 plasma emission intensities for the standard power level of 100 W/500 W (blue dash line) overlap with those of the higher platen power of 200 W/500 W (red line). On the other hand, with 100 W/700 W conditions, the overall intensity doubled relative to the intensity of the standard and high platen power operation. These results indicate that increasing platen power increases ion energy while increasing coil power is ascribed to enhanced flux of plasma species. Thus, higher platen power increases ion energy and thereby enhances Cu etch rates, while high coil power increases the flux of neutral and ion species; these changes increase Cu etch rates but reduce hydrocarbon deposition rates.

It is instructive to compare the Cu etch rate dependence on platen and coil power for both H_2 and CH_4 plasma etch gases. The etch rate increase per watt of platen power is greater for CH_4 etching than for H_2 etching. Specifically, in the range of 100 W-200 W platen power, the etch rate gradient of Cu in an H_2 plasma is 0.07 nm/min W [87], but 0.13 nm/min W in a CH_4 plasma. Similarly, in the range of 500 W-700 W coil power, the etch rate gradient of Cu in an H_2 plasma is 0.035 nm/min W [87], but 0.08 nm/min W in a CH_4 plasma. Such differences can be ascribed to different ion energy transfer efficiency and chemical reactivity between H_2 and CH_4.

In ion enhanced chemical etching, elastic collision-based momentum transfer and ion momentum loss due to charge transfer reactions are important as discussed previously [127]. That is, increased atomic mass and longer mean free paths of gaseous ions promote effective sputtering of Cu species. In the current study, the exact mean free path of C^+ or CH^+, the primary ions in CH_4 plasmas, is difficult to predict due to complicated charge transfer reaction paths. Nevertheless, approximate values can be estimated from consideration of charge transfer cross sections and charge transfer reaction constants. The reported rate constant of the gas phase charge transfer reaction $H^+ + H_2 \rightarrow H_2^+ + H$ is 6.02×10^{13} cm^3/mol s, for $C^+ + C_xH_y \rightarrow C_xH_y^+ + C$

is $1x10^{13}$-8x 10^{14} cm^3/mol s, and for $CH^+ + CH_y \rightarrow C_2^+ + H_x$ 4-7x is 10^{14} cm^3/mol s [143]. Thus, the mean free path of C^+ and CH^+ ions in our CH_4 plasma should be ~1 order of magnitude lower than that of H^+. In our previous study, at 200-300 eV range and 20 mTorr pressure, the mean free path of H^+ was estimated to be 18 cm [127]; the mean free path of C^+ and CH^+ ions will be ~1 cm which is similar to the that of He^+ (1.2 cm) [127]. This implies that momentum losses of C^+ and CH^+ ions accelerated toward the sample surface will be greater than those of H^+ in an H_2 plasma. However, because the atomic mass of C^+ and CH^+ are 12 and 13 which are substantially greater than the atomic masses of He and H, the sputtering efficiency of C^+ and CH^+ will be enhanced relative to those of He^+ and H^+ under our plasma conditions. These considerations can account for the larger increase in etch rate of Cu in CH_4 plasmas (17 nm/min to 30 nm/min) when the platen power is increased from 100 W to 200 W; by comparison the same platen power increase yields a smaller etch rate enhancement of Cu in an H_2 plasma (13 nm/min to 20 nm/min) [87].

In an H_2 plasma, Cu etch products, presumed to be CuH_x, are unstable [90], but the possible etch products formed in CH_4 plasmas, CH_3Cu and CH_3CuH^-, are presumed to be stable species [135]. Thus, the decomposition probability of the etch product before it escapes the Cu surface in an H_2 plasma is expected to be higher than that of etch products in CH_4 plasmas. Etch product stability may thus account for the more rapid increase in Cu etch rate in CH_4 plasmas relative to the Cu etch rate in H_2 plasmas when coil powers are increased from 500 W to700 W.

4.3.5 Variation in Etch Pressure

The hydrocarbon deposition rate in CH_4 plasmas has been reported to be a linearly increasing function of the square root of pressure in the 30-600 mTorr range [138], suggesting

that Cu etch profiles and etch rates should also be dependent upon CH_4 pressure. In the current investigation, Cu etching in CH_4 plasmas in the pressure range 10 to 60 mTorr was studied; 3% Ar was added to the CH_4 plasma to serve as an actinometer [144, 145] for OES analysis. The Cu etch results and OES spectra are shown in Figures 4.10 and 4.11. In contrast to the results in Ref. 29, the hydrocarbon deposition rate decreased with increasing pressure between 10 and 40 mTorr (Figure 4.10-a). Likewise, Cu etch rates gradually decreased with increasing pressure. At 40 mTorr, no Cu film etching was observed, but a 65 nm hydrocarbon film was deposited over the entire sample surface including Cu (Figure 4.10-b). The observed higher DC bias (380 V) at increased pressure implies that ion (and other plasma-generated species) flux decreased, resulting in a reduction in both Cu etch and hydrocarbon deposition rates. However, between 40 mTorr and 60 mTorr, the hydrocarbon deposition rate increased (with no apparent Cu etching) while the DC bias dropped to 333 V. The increase in hydrocarbon deposition rate within this range is consistent with Catherine's observation [138]. Most likely, a shift in the electron energy distribution function that reduces the plasma ionization fraction occurs. This change lowers the ion flux and DC bias, and thereby inhibits the removal of deposited hydrocarbon.

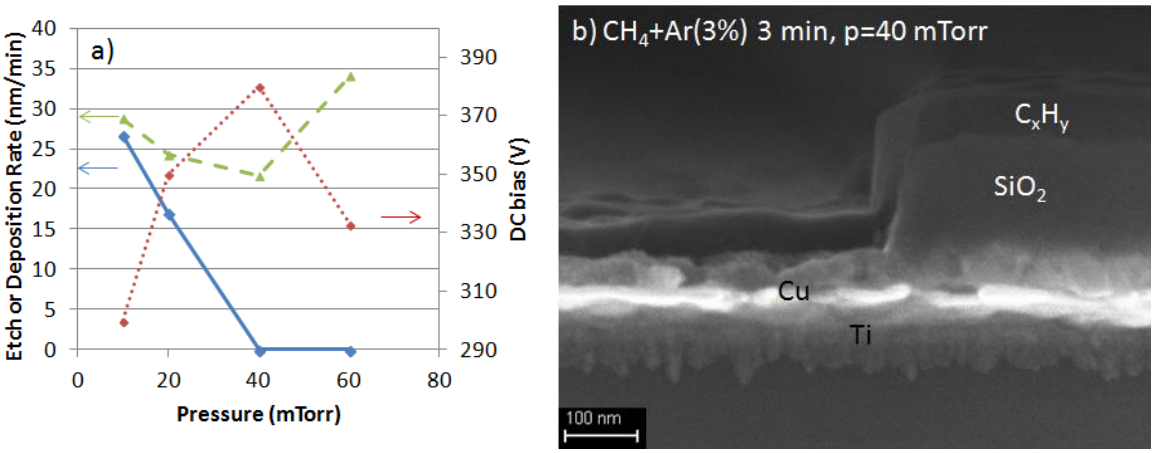

Figure 4.10 a) Cu etch rate (blue line), hydrocarbon deposition rate on SiO_2 mask (green dash line), and DC bias (red dot line) in a 3 % Ar/CH_4 plasma as a function of pressure. b) SEM cross section of Cu film exposed to a 3 % Ar/CH_4 plasma for 3min ; other conditions were 63 sccm CH_4 + 2 sccm Ar gas flow rate, 100 W(platen)/500 W(coil) power , and 10 ℃ substrate temperature.

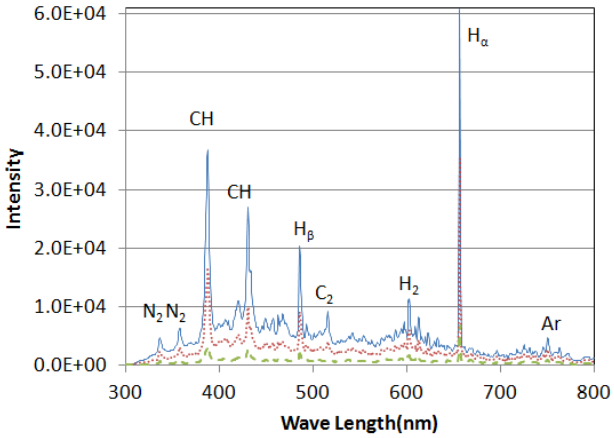

Figure 4.11 Optical emission spectra during Cu etching in CH_4 with 3 % Ar added to the plasma. Blue lines, red dot lines, and green dash lines represent 10 mTorr, 20 mTorr, and 40 mTorr plasma, respectively; other conditions are 63 sccm CH_4 + 2 sccm Ar gas flow rate, 100 W/500 W power, and 10 ℃ substrate temperature.

OES data in Figure 4.11 demonstrate the reduction of plasma species concentrations with increasing pressure. Since shorter integration time was used for collection of these data relative to the data shown in Figure 4.9, direct emission intensity comparisons cannot be made. The highest intensity peaks were observed at 10mTorr followed by 20 mTorr, and 40 mTorr. CH

and H peak intensities at 10mTorr are approximately twice those at 20 mTorr, and 8 times higher than those at 40 mTorr. This trend has been further investigated by using an Ar tracer (750.5 nm) [144] to perform actinometry using the CH emission peak at 388.5 nm. The CH/Ar peak intensity ratio is 7.6, 6.2 and 3.5 for 10 mTorr, 20 mTorr and 40 mTorr, respectively, indicating an increased density of plasma species at lower CH_4 pressures over the range investigated. These results are consistent with shifts in the electron energy distribution function (EEDF) with rf power and pressure. For example, at higher coil powers, the electron density increases, which leads to a higher density of all plasma species [146, 147]. A lower gas pressure increases the electron mean free path and reduces the electron collision rate. Thus, EEDF is shifted to higher average electron energy, thereby generating higher reactive species concentrations even at lower CH_4 concentration [146, 147]. Such changes in EEDF result in a higher Cu etch rate (27 nm/min) and hydrocarbon deposition rate (29 nm/min) at 10 mTorr than those at 20 mTorr pressure (17 nm/min etch rate and 22 nm/min deposition rate).

Above 40 mTorr, the CH_4 plasma did not etch Cu; rather, under these conditions, a hydrocarbon film was deposited on the Cu surface, analogous to results on SiO_2 surfaces. This indicates that between 40 mTorr and 60 mTorr, the net hydrocarbon deposition rate exceeds the Cu etch rate. That is, the ion, electron, and photon bombardment energy/flux is insufficient to ensure that the Cu etch rate and hydrocarbon removal rate are greater than or equal to the hydrocarbon formation rate on the Cu surface.

4.3.6 Low Pressure and High Platen Power

In various power and pressure studies, we demonstrated that increased Cu etch rates can be achieved by either lowering pressure or increasing platen/coil powers. In order to investigate

synergetic effects of pressure and power control, the combination of low pressure and high platen power CH_4 plasma etching was performed(Figure 4.12). After CH_4 plasma etching for 1 min at 10 mTorr and 200 W/500 W (platen/coil power), the measured Cu etch rate and hydrocarbon deposition rate were 40 nm/min and 30 nm/min, respectively, with 472 V DC bias.

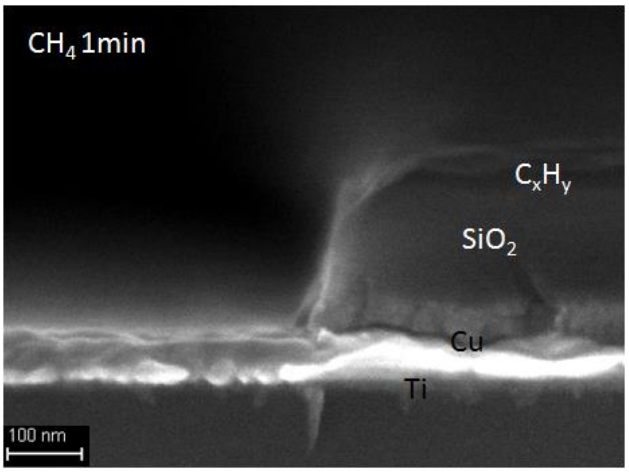

Figure 4.12 SEM cross sectional image of SiO_2 maked Cu etching by CH_4 for 1min at low pressure(10 mTorr) and high platen power(200 W); other conditions were 65 sccm CH_4 gas flow rate, 500 W coil power , and 10 ℃ substrate temperature.

The DC bias of 472 V is higher than the 295 V for the CH_4 plasma at 10 mTorr with 100 W/500 W but lower than the 550 V at 20 mTorr with 200 W/500 W, which implies that the ion energy increased with increased platen power (472V vs 295V), but decreasing pressure in this regime also leads to an increased ion flux, and thereby a reduction in the DC bias (472V vs 550V) at constant applied power. Thus, higher ion flux and energy yield a Cu etch rate of 40 nm/min which can be compared to 27 nm/min at 10 mTorr pressure and 30 nm/min at 200 W paten power. In addition, 30 nm/min hydrocarbon deposition rate is similar to 29 nm/min at 10 mTorr, although the platen power was increased to 200 W. This observation is consistent with the constant hydrocarbon deposition rate observed in the platen power variation study. Likewise,

the measured Cu side wall angle was also ~80°, regardless of increased ion flux and energy, which indicates that the degradation of SiO_2 mask side wall is limited by net removal and passivation of hydrocarbon layers as discussed in the previous section.

4.3.7 CH_4 Plasma Etch Chemistry

Small Cu samples (~1 cm^2) were used for power and pressure parametric studies; as a result, Cu-related emission peaks were not detected in OES spectra. In order to observe the gaseous CH_4 plasma etch products, blanket 100 nm thick Cu films deposited on 4 inch wafers were etched and OES data compared to those of a CH_4 plasma without Cu samples present (Figure 4.13). In this study, a quartz window was used to allow detection of 200-300 nm photons; as a result, an additional CH peak at 315.5 nm[142] was observed compared to those observed using a pyrex window. With the larger Cu sample, two Cu emission peaks at 324.7 nm and 327.4 nm [142] were detected (Figure 4.13). However, in agreement with OES spectra from H_2 plasma etching of Cu, no CuH_x peaks were observed. Furthermore, no CH_3-functionalized Cu moieties were evident in the OES spectrum. Such results suggest that most if not all Cu hydrides or methylated compounds formed that desorb or are sputtered from the surface, dissociate due to electron collisions so that only Cu emission is detected.

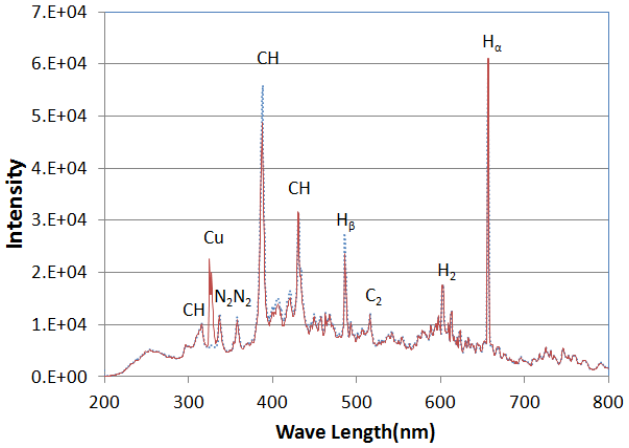

Figure 4.13 Optical emission spectra of a CH_4 plasma without a Cu sample (blue dot line) and with a 4 inch Cu film present (red line); other conditions are 65 sccm CH_4 gas flow rate, 100 W/500 W power, 20 mTorr pressure and 10 ℃ substrate temperature.

Cu photolysis investigations by Parnis et al. indicated that Cu could insert into CH_4 in a solid CH_4 matrix to form CH_3CuH upon photo-excitation of Cu(^{2}p) using photons in the range of 300-700 nm [133, 134]. In addition, depending upon the wavelength used, secondary photolysis decomposed the CH_3CuH into CH_3Cu+H (dominant) and CH_3+ CuH (minor) between 300 and 500 nm, and into CH_4 + Cu for wavelengths >500 nm. These authors also calculated dissociation energies of ~59 kcal/mol (2.6 eV) for Cu-CH_3, and ~65 kcal/mol (2.83 eV) for Cu-H [133, 134], whose values are similar to 2.5-3.0 eV, which represents the average electron energy for a plasma at p=20 mTorr [147, 148]. These data support our expectation that desorbed gaseous Cu etch products are readily dissociated and thereby are not detected by OES.

Cho and Andrews also reported the formation and decomposition of CH_3CuH in solid argon. [135] In this study, the IR signal of the CH_3CuH formed was not observed due to secondary photolysis at wavelengths >420 nm but reappeared within the UV wavelength range 240 and 380 nm. Formation of CH_3Cu was most prevalent in the UV range, and CH_3CuH^- was decomposed with UV but not visible radiation. Moreover, based on Density Functional Theory,

Cho and Andrews investigated the thermodynamic stability of CH_3CuH, CH_3Cu, and CH_3CuH^- and reported that CH_3CuH is unstable while CH_3Cu and CH_3CuH^- are stable species. These results are analogous to those reported by Parnis.

The various reports of stable Cu compounds that can be formed by exposure of Cu to CH_4 fragments, along with our current plasma studies suggest possible mechanisms for Cu etching in CH_4 plasmas. Cu surface atoms can be excited by energetic ion bombardment or by photons from the plasma; OES results indicate emissions at 315.5 nm, 388.5 nm and 431.2 nm by CH radiation and at 486.2 nm, 600 nm bands, and 656.5 nm by H_2. Excited states of Cu can then react with CH_4 plasma-created fragments such as CH_3 to form CH_3CuH or stable CH_3Cu and CH_3CuH^- species on the Cu surface. Since CH_3Cu and CH_3CuH^- species have higher thermodynamic stability than does CuH_x, these etch products may be more easily desorbed by ion, electron, or photon bombardment. Such considerations may result in higher Cu etch rates in CH_4 plasmas than in H_2 plasmas (17 nm/min vs 13 nm/min) under the same etching conditions, while minimizing hydrocarbon film formation on the Cu surface.

4.4 Conclusions

Blanket PR and SiO_2, as well as PR and SiO_2 masked Cu thin films were etched by CH_4 plasmas at low substrate temperature and their etch results compared to those of an H_2 plasma under the same plasma conditions. Unlike H_2 plasmas, a PR mask can withstand exposure to a CH_4 plasma due to the passivation/deposition of hydrocarbon layers. The Cu etch rate in a CH_4 plasma was 17 nm/min, which is higher than the 13 nm/min Cu etch rate by an H_2 plasma, even though hydrocarbon deposition occurs which should hinder Cu etch rates. In addition, the Cu side wall angle was ~80° which is essentially equivalent to that observed with H_2 plasma etching.

Also, CH_4 plasmas display excellent selectivity for Cu etching relative to Si, SiO_2 and Ti films. By adding 50 % H_2 to a CH_4 plasma, hydrocarbon deposition can be prevented while maintaining the Cu etch rate and sidewall profile achieved in a pure CH_4 plasma.

In platen and coil power dependence studies, higher energy ion bombardment by increasing platen power enhanced Cu etching but hydrocarbon deposition rate was nearly constant with increasing ion energy. On the other hand, increasing coil power generated higher electron, photon, reactive neutral and ion species concentrations or fluxes and thereby increased Cu etch rates while the net hydrocarbon deposition rate decreased as a result of the enhanced ion flux. However, the Cu sidewall angle remained at ~80° during increased platen or coil power probably because SiO_2 sidewall etching was suppressed by hydrocarbon passivation. The etch rate gradient with power in a CH_4 plasma was greater than that in an H_2 plasma due to more effective momentum transfer of CH^+ and C^+ relative to H^+ and better thermodynamically stability of the likely etch product, CH_3Cu, compared to CuH_x in an H_2 plasma.

Changes in pressure shifted EEDF which caused variations in electron, photon, reactive neutral and ion fluxes. Cu etch and hydrocarbon deposition rates in CH_4 plasmas increased at low pressure (10 mTorr) but decreased at higher pressure (40 mTorr); Cu etching was not observed above 40 mTorr. A reasonable Cu etch rate of 40 nm/min was achieved at 10 mTorr and 200 W platen power, while the sidewall angle remained at ~80°.

Etch products such as CH_3Cu or CH_3CuH^- are thermodynamically stable, and can be formed on Cu surfaces by excitation of Cu atoms using high energy ion or photon bombardment followed by reaction with CH_3 fragments. However, methyl-containing copper species were not detected in OES; rather, only Cu emission lines were observed, most likely because the Cu-CH_3 bond (2.83 eV) is readily dissociated by electron impact collisions.

CHAPTER 5.

ETCHING OF Ag AND Au FILMS IN CH_4-BASED PLASMAS AT LOW TEMPERATURE

5.1 Introduction

In chapter 3, a Ag and Au film patterning approach that employs an H_2 plasma at 10 ℃ was demonstrated. Unfortunately, severe degradation of organic PR masks by H_2 plasmas [149] prevents the use of a PR mask, while the high temperature process during SiO_2 mask deposition onto Ag films results in Ag agglomeration [127]. Therefore, precisely controlled Ag film patterning by H_2 plasmas is difficult to implement. In addition, the etch rates for Ag and Au in H_2 plasmas are too low for large scale device manufacture.

In order to address these limitations, Ag and Au etching with CH_4 plasmas has been investigated, since this etch gas has demonstrated improved performance for Cu etching relative to that of H_2 plasmas by suppressing PR degradation and enhancing the Cu etch rate [149]. Because Cu, Ag, and Au display similar chemical properties and electronic structures, CH_4 plasmas may facilitate Ag and Au etching and patterning, as we observed in H_2-based plasmas, while allowing the use of PR masks. Indeed, several previous studies suggest the likely success of this approach. For instance, Ag and Au removal by a CH_4 plasma with the observed formation of carbon cones on top of Ag and Au surfaces has been reported, although quantitative information such as etching conditions, etch rate, etch selectivity, and possible etch products were not discussed [129]. In addition, a plasma etch gas mixture of $H_2/CH_4/Ar$ etched blanket Ag thin films 10-20 % faster than did a pure Ar plasma at 1.5 mTorr, apparently due to a chemical reaction of Ag with CH_4 or H_2 radicals [150].

In this chapter, we report the plasma-assisted etching of Ag and Au films by CH_4 plasmas at low temperature (10 ℃) and describe their etch rates and pattern profiles. Variation of etch pressure and platen/coil powers identifies the similarities and differences in chemical reactivity of Cu, Ag, and Au and thus offers insight into the chemical and physical etching mechanisms of these difficult to plasma etch metal layers.

5.2 Experimental Procedure

Ag (100-230 nm) and Au (100 nm) films were deposited onto a 20 nm thick Ti layer on a 4 inch Si wafer using electron beam evaporation (CVC or CHA E-Beam evaporator). Photoresist (PR) mask patterned Ag and Au films were also prepared. After a 1.6 µm thick photoresist (*Microposit* sc1813) layer was spin coated onto the Ag and Au films, PR patterns were generated by exposure to 405nm wavelength light from a Karl Suss MA6 Mask Aligner. Immersion of the PR in MF-319 base for 1 min developed the exposed pattern. Etch samples were prepared by cutting the wafer into sections of ~1 cm^2; each was attached to a 4 inch diameter Si carrier wafer by *cool grease* 7016(AI Technology Inc.) prior to plasma etching.

A Plasma Therm inductively coupled plasma (PT-ICP) system was used for etch studies; this allowed direct comparison of results with those from previously reported Cu etching in CH_4 plasmas and Ag and Au etching in H_2 plasmas [127, 149]. The standard etch conditions were 100 W platen power, 500 W coil power, 20 mTorr pressure, 65 sccm of H_2 or CH_4 gas flow and 10 ℃ platen temperature. Twenty minutes of the standard etch recipe was used for CH_4 plasma conditioning/seasoning. Before H_2 plasma etching, a manual cleaning procedure that involved scraping the chamber wall with a razor blade followed by wiping with isopropanol and acetone was instituted. Subsequently, an O_2/Ar plasma cleaning process was performed prior to etch

studies. During pressure variation experiments, the pressure was altered from 10 to 60 mTorr at fixed 100 W (platen)/500 W (coil) power. Platen power was varied from 100 to 200 W at a fixed 500 W coil power; coil powers between 500 and 700 W were investigated while pressure was maintained at 20 mTorr in both cases. For Au fluorination studies, 50 sccm CF_4 or 5/28/15 sccm $Ar/CO_2/C_4F_8$ was used at 5 mTorr, 80 W/400 W platen/coil power, and 10 ℃ substrate temperature.

In order to gain additional insight into the chemical reactions and photon effects in CH_4 plasma etching, borosilicate glass slides and Si wafers were employed as hard masks on blanket Ag and Au thin films; these masks were affixed by kapton tape onto the carrier wafer. Standard etch conditions were used for these experiments.

Ag and Au film patterns and etch depths were examined with scanning electron microscopes (Zeiss Ultra 60 FE-SEM and LEO 1530 TFE-SEM) after exposure to CH_4 plasmas. Surface analyses of the glass slide and Si wafer masks in contact with the metal film surfaces were performed by X-ray photoelectron spectroscopy (Thermo Scientific K-Alpha XPS).

5.3 Results and Dission

5.3.1 PR masked Ag and Au Etching at Standard CH_4 Plasma Etch Conditions

Figure 5.1 shows the surface morphologies and etch profiles of PR masked 100 nm thick Ag and Au films after 3 min and 40 sec and 8 min and 20 sec of CH_4 plasma exposure, respectively, at 65 sccm CH_4 gas flow rate, 20 mTorr pressure, 100 W (platen) /500 W (coil) power, and 10 ℃ substrate temperature. The etch times used for masked films were determined from pre-etching of blanket Ag and Au films. Since the patterns were large, etch rates of masked layers will be very similar to those of blanket films. Thus, the Ag was over etched less than 20

seconds but Au was not over etched. Similar to the results of etching Cu in a CH_4 plasma [149], a ~90 nm thick hydrocarbon film formed on top of the PR mask, which suppressed PR degradation and ensured good selectivity between PR and Ag. Simultaneously, the 100 nm thick Ag film was etched although a small amount of Ag residue remained. Several factors may promote the formation of Ag residues. For instance, nonuniform Ag film thickness, Ag interaction with underlying Ti, and encapsulation of Ag by hydrocarbon layers formed can account for the Ag residue remaining. The Ag etch rate was ~27 nm/min and the hydrocarbon deposition rate on the PR mask was ~ 24 nm/min. However, a large amount of Ag was redeposited, as detected by XPS, on the Ag film near the PR mask and on the PR side wall as shown in Figures 5.1-a), b). Indeed, redeposition is expected when the etch products are relatively nonvolatile, [50]. This Ag redeposition indicates that the Ag etch products generated in the CH_4 plasma have low volatility, which requires physical ion sputtering to assist removal.

In Au etching, a ~190 nm thick hydrocarbon layer formed on top of the PR mask with ~23 nm/min deposition rate; the 100 nm thick Au film was removed, although Au residue remains on the underlying Ti layer in Figures 5.1-c) and d); similar explanations as those described above for Ag residues can be ascribed to the Au residue formation. The Au etch rate was 12 nm/min and redeposition of Au etch products near the PR mask resulted in sloped Au side wall profiles. Unlike Ag, however, Au redeposition was mostly on the PR sidewall; of more interest is the fact that the redeposited Au is not a film, but displays the shape of pillars as is evident in Figures 5.1-c), d). Redeposition of Au has been reported previously when relatively nonvolatile Au etch products are sputtered during etching by plasmas such as mixtures of HBr/Ar or Cl_2/Ar gases, where a thick layer of Au etch products is redeposited on the PR side wall. However, according to a previous study, a thick film of Au etch products is redeposited on

the PR side wall when relatively nonvolatile Au etch products are sputtered during etching by plasmas such as HBr/Ar or Cl_2/Ar mixtures [64]. Thus, the cylindrical shape of the structures formed on the PR side wall in Figures 5.1-c), d) implies that the deposited materials are likely a combination of Au and hydrocarbon. That is, initially some Au etch products were redeposited on the PR sidewall, but methyl radicals adsorbed in the regions devoid of Au etch products; subsequently, polymerization to form C – C bonds, results in the generation of cylindrical structures along the PR side wall. This explanation for the formation of cylindrical deposits is consistent with the formation of hydrocarbon cones or hills on Au at high CH_4 plasma pressures as discussed in a later section of this manuscript.

The Ag etch rate of 27 nm/min was higher than the Cu etch rate, but since the volatility of Ag products is limited, Ag etching is more dependent upon physical sputtering in CH_4 plasmas than is Cu etching. However, the fact that the Au etch rate is comparable to Cu (12 nm/min vs 17 nm/min) despite the higher mass and metal bond strength of Au demonstrates that chemistry plays some role in the Au etch mechanism although most of etching comes from the physical sputtering of etch products in a CH_4 plasma. In addition, the lack of a detectable hydrocarbon film on Au (or Ag) implies that carbon is present in the etch products for Ag and Au, evidently as methyl groups, analogous to related studies for Cu.

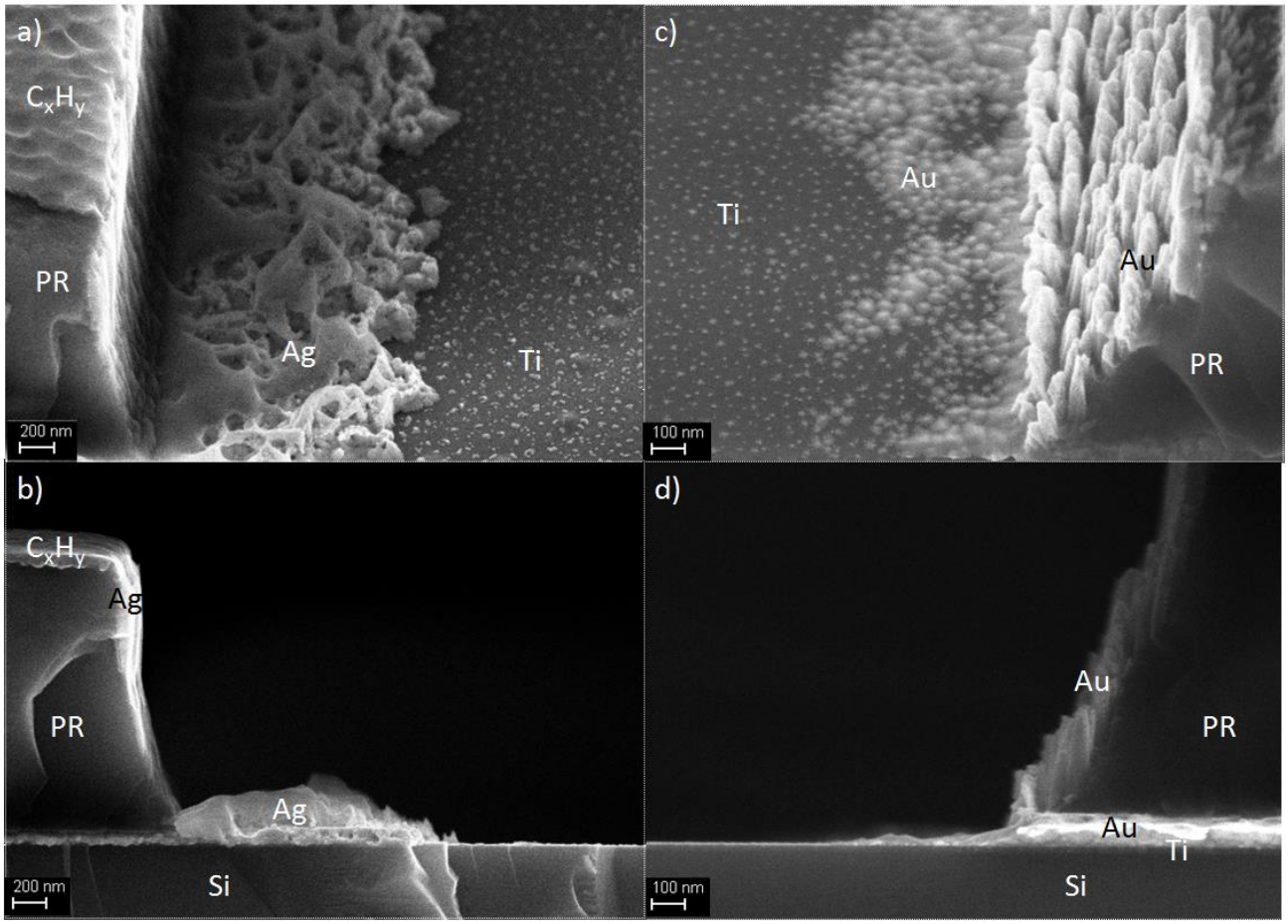

Figure 5.1 SEM images of (a) photoresist masked Ag surface and (b) cross sectional image after CH_4 plasma exposure for 3 min and 40 sec and photoresist masked (c) Au surface and (d) cross sectional image after 8 min and 20 sec of CH_4 plasma. Other conditions were maintained at 65 sccm of CH_4, 20 mTorr pressure, 100 W/ 500 W for platen/coil powers, and 10 ℃ platen temperature.

5.3.2 Pressure Variation

Previous investigations have demonstrated that the primary Cu etching mechanism in a CH_4 plasma involves competition between hydrocarbon formation on the Cu surface and Cu etching by CH_x plasma fragments [149]. When a high ion bombardment flux is present, the formation of hydrocarbon polymer on Cu surfaces is suppressed, thereby favoring Cu etching. Low ion flux at high pressures cannot effectively remove the hydrocarbon formed on Cu surfaces

during CH_4 plasma etching; thus, the hydrocarbon film formed inhibits Cu etching [149]. Such mechanisms should also be operative in Ag and Au etching.

In order to minimize unintended effects from chemical contamination during PR or SiO_2 masked patterning, blanket 120 nm thick Ag and 100 nm thick Au film etching experiments in the pressure range of 10 to 60 mTorr were performed. The etch rate of blanket Ag films at 20 mTorr was slightly higher than the PR masked Ag films (31 nm/min vs 27 nm/min). This reduction in etch rate appears to result from oxidation of the Ag film during the 5 min soft bake at 125 ℃ following PR spin coating, which inhibits Ag etching. Figure 5.2 indicates that hydrocarbon deposition rates decrease as the pressure increases from 10 to 30 mTorr, in agreement with our previous Cu etch studies. Figure 5.2 also shows that both Ag and Au etch rates drop rapidly in the 10 - 30 mTorr range. However, above 30 mTorr, hydrocarbon deposition rates increase, which is consistent with hydrocarbon deposition rate trends reported for CH_4 plasmas [138]. In addition, the etch rate gradient of Ag and Au with pressure decreases over this pressure range. At 60 mTorr, hills or cone-shaped hydrocarbon formations are sparsely observed on the Ag and Au films as the etch rates fall (Figure 5.3); the existence of these etch features is consistent with previous reports, although etch conditions in those reports were not specified [129]. The size (< 70 nm diameter) and areal density of hydrocarbon cones detected on Ag films are smaller than those observed on Au surfaces (Figure 5.3). Furthermore, at 60 mTorr, the etch rate of Ag is 12 nm/min while the Au etch rate is nearly zero.

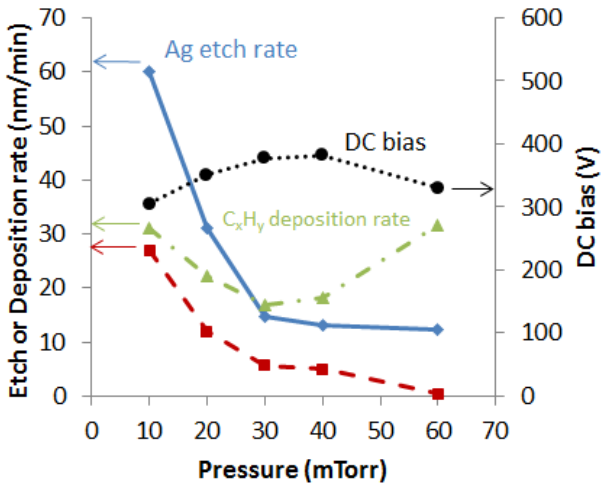

Figure 5.2 Ag etch rate (blue line), Au etch rate (red dash line), hydrocarbon deposition rate on Si wafer (green dash dot line), and DC bias (black dot line) in CH_4 plasmas as a function of pressure. Other conditions were 65 sccm CH_4 flow rate, 100 W(platen)/500 W(coil), and 10 ℃ platen temperature.

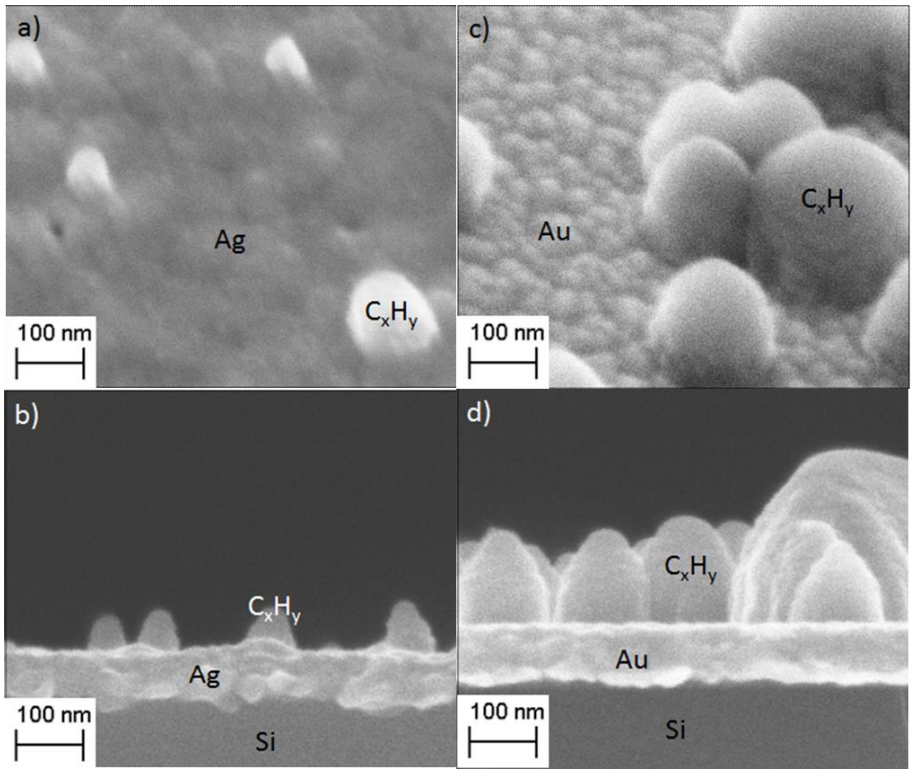

Figure 5.3 SEM surface cross sectional images Ag and Au film. a) Ag surface and b) Ag cross section, and c) Au surface and d) Au cross section after exposure to a CH_4 plasma for 5 minutes at 60 mTorr pressure, 65 sccm CH_4 flow rate, 100 W(platen)/500 W(coil), and 10 ℃ platen temperature.

The variations in Ag and Au etch rates and hydrocarbon deposition rates are ascribed to the change in plasma-generated chemical species concentrations with increasing plasma pressure. The electron energy distribution function (EEDF) varies with rf power and pressure; an increase in rf power increases the electron density, leading to a higher concentration and flux of neutral radicals and ion species [146, 147]. At lower gas pressures, the longer electron mean free path reduces electron collision rates and thereby shifts the EEDF to higher energies, resulting in enhanced neutral and ion generation [146, 147]. As the CH_4 pressure increased from 10 to 30 mTorr, emission intensities of plasma-generated CH_4 fragments decreased [149]. This observation combined with the increasing DC bias shown in Figure 5.2, suggests that both neutral radical and ion concentrations are reduced over this pressure range. As a result, both hydrocarbon deposition rate and Ag or Au etch rate should decrease. However, because the ionization potential of CH_4 is >10 eV while the dissociation energy is ~5 eV [143], the shift in EEDF to lower energies at higher pressure may result in a relatively high flux of neutral species compared to ion fluxes with increasing CH_4 pressure. Therefore, hydrocarbon deposition rates increase as the pressure is increased above 30 mTorr (Figure 5.2).

Additional evidence for the explanation offered for the trends observed in Figure 5.2 arises from previous studies of CH_4 plasmas in the pressure range 10 to 40 mTorr, where electron density increased while plasma potential decreased as the EEDF shifted to lower energies [147]. However, because the CH_4 vibrational excitation cross section peaks at ~6 eV [151], a large fraction of the low energy electrons attach to CH_4, which leads to a decrease in electron density but an increase in plasma potential in the lower EEDF energy regime above 40 mTorr [147]. These trends are consistent with a reduction in DC bias above 40 mTorr (Figure 5.2) that occurs in order to compensate for this raised plasma potential.

At 60 mTorr, although the net Ag (or Au) etch rate is higher than hydrocarbon deposition rates, the relatively low energy and flux of ions, electrons and photons are unable to fully remove hydrocarbon and Ag (or Au) layers; as a result, low Ag and especially Au etch rates are observed and hydrocarbon cones form. These observations indicate that the primary etch mechanism of Ag and Au in CH_4 plasmas depends critically on the competition between hydrocarbon deposition and Ag (or Au) etching.

The etch rate data demonstrate that the specific pressure where hydrocarbon films or structures form is different for each (Cu, Ag or Au) surface. A thick hydrocarbon film is deposited on a Cu surface at 40 mTorr [149], but only hydrocarbon cones are observed even at 60 mTorr on Ag and Au surfaces; as mentioned above, an increased density of hydrocarbon structures forms on Au compared to Ag. Since hydrocarbon ion sputter rates are independent of the underlying film and the CH_4 plasma conditions are the same, hydrocarbon formation should depend upon the adsorption and dissociation energy of the C-H bond for CH_x radicals (x=1, 2 or 3) on each metal. That is, the formation of hydrocarbon films on substrate surfaces requires high adsorption energy and low C-H bond dissociation energy for CH_x radicals on the specific metal surface. Compared to other transition metals such as Ru, Os, Rh, Ir, Pd and Pt, the overall CH_x radical adsorption energies on (111) crystal orientation of Cu, Ag, and Au are 1-3 eV lower and their dissociation energies 1-2 eV higher [152]; this implies that hydrocarbon formation on Cu, Ag, and Au is unfavorable relative to formation on other metals. Moreover, among Cu, Ag, and Au, the adsorption energy of CH_x radicals on Cu is the highest followed by Au and Ag, while the lowest C-H bond dissociation energy of CH_x radicals on metals is on Cu, followed by Au and Ag [152]. These energetics indicate that hydrocarbon layers form more easily on Cu than they do on Au and Ag, which is consistent with our observations.

The formation of cone- or hill-shaped hydrocarbon structures at specific regions on surfaces of Ag and Au, rather than the film formation, suggests that adsorption of methyl radicals were favored by certain crystal orientations, oxidation states or defects on the Ag and Au surfaces. In addition, while the adsorption energy of CH_3 and CH_2 on a carbon surface (100 oriented diamond) is above 4 eV [153], adsorption energies of those radicals on Ag and Au are lower (<1 eV and ~2 eV, respectively) [152]. This implies that after methyl radicals nucleate on at certain regions on Ag and Au surfaces, hydrocarbon polymerization occurs on these structures rather than on the Ag or Au. This preferred methyl radical nucleation at certain Ag and Au surface sites and the preferred polymerization on carbon materials results in hills or cone-shaped hydrocarbon formation on Ag and Au as shown in Figure 5.3.

The different cone sizes on Ag and Au might be ascribed to hydrocarbon structure formation on limited areas of the Ag and Au surfaces and ion bombardment that occurs on the structure edges. As shown in figure 5.2, hydrocarbon deposition rate on a Si wafer is 31.6 nm/min; this leads to the ~160 nm hydrocarbon film thickness observed for 5 min of CH_4 plasma exposure. However, the typical height and diameter of most hydrocarbon structures are ~60 nm on Ag and ~140 nm on Au, although several hydrocarbon structures are larger. Since the edge of the hydrocarbon structure is etched readily by ion bombardment, thereby generating the slope on the hydrocarbon structure, the original diameter of the hydrocarbon structure determines the structure height. The low CH_x adsorption energy on Ag did not allow the formation of high density hydrocarbon clusters or large areas of nucleation. Therefore, smaller diameters and heights (~60nm) of hydrocarbon cones formed on Ag relative to the 160 nm thick hydrocarbon film formed on the Si wafer. Similarly, ~140 nm height and diameter of the hydrocarbon structures on Au are ascribed to the more favored hydrocarbon structure formation compared to

Ag. In addition, the unusually large hydrocarbon structure size (~260 nm height and ~400 nm diameter) were observed at locations where hydrocarbon structures are closely spaced as indicated in figure 5.3; this observation suggests aggregation of smaller hydrocarbon structures to generate these larger structures on Au surfaces. Such considerations and observations support our hypothesis that hydrocarbon formation on Cu, Ag, and Au is inhibited at low pressure, thereby enabling CH_4-based plasma etching.

5.3.3 Platen or Coil Power Variation

The results of pressure variation indicate that Ag and Au etch rate and chemistry in CH_4 plasmas depend upon the energy and flux of ions, electrons, neutral radicals, and photons; these parameters can be controlled by changes in platen or coil power. In addition, comparison of Cu, Ag, and Au etch results with H_2 and CH_4 plasmas should offer insight into plasma etch mechanisms due to similarities and differences in etch characteristics among these metals.

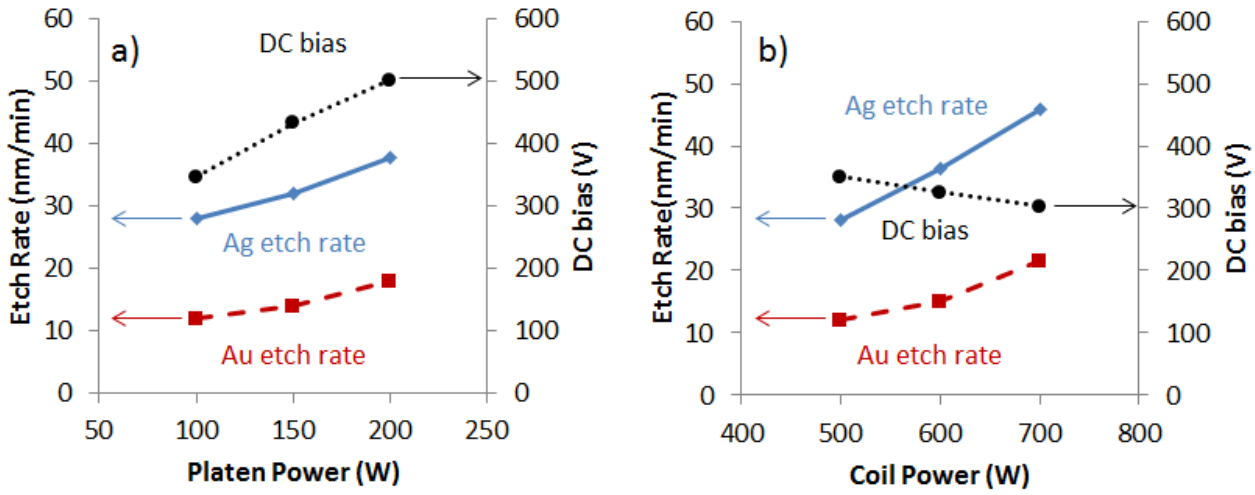

Figure 5.4 Ag etch rate (blue line), Au etch rate (red dashed line), and DC bias (black dotted line) under H_2 plasma exposure; a) platen power variation with fixed 500 W coil power, and b) coil power variation with fixed 100 W platen power. Other conditions are 65 sccm CH_4 flow rate, 20 mTorr pressure, and 10 ℃ substrate temperature.

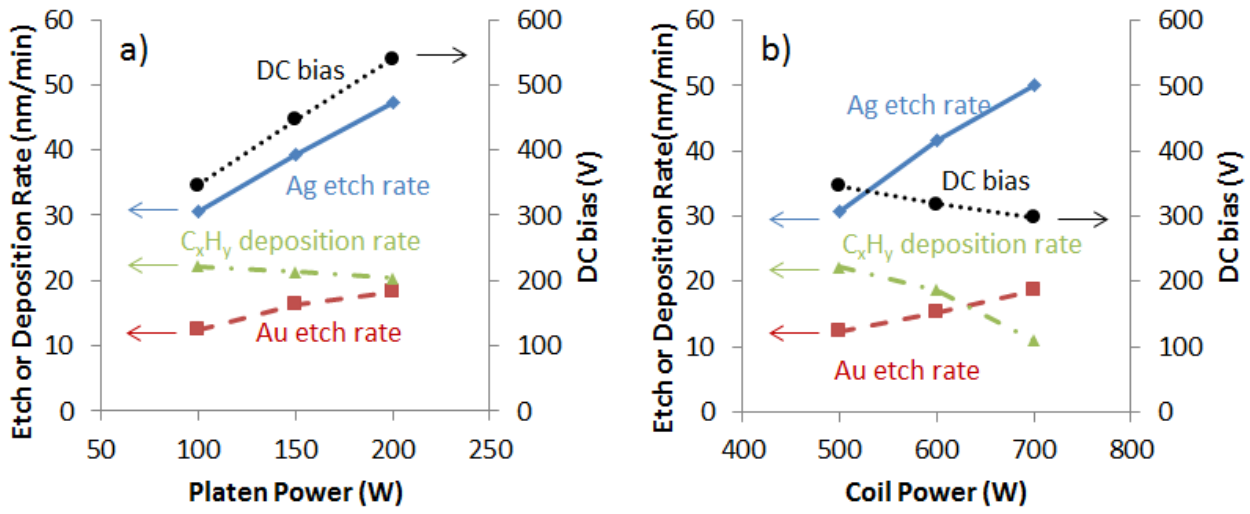

Figure 5.5 Measured Ag etch rate (blue line), Au etch rate (red dashed line), hydrocarbon deposition rate on Si wafer (green dashed dotted line), and DC bias (black dotted line) after CH_4 plasma etching of Ag and Au with a) varied platen power with fixed 500 W coil power and b) varied coil power with fixed 100 W platen power. Other conditions are 65 sccm CH_4 flow rate, 20 mTorr pressure, and 10 ℃ substrate temperature.

Figures 5.4 and 5.5 show the effect of platen and coil power variation on the etching of 200 nm thick blanket Ag and 100 nm thick blanket Au films using H_2 and CH_4 plasmas. Generally an increase in platen power enhances the ion bombardment energy by increasing DC bias. An increase in coil power increases the concentration of plasma species such as electrons, neutral radicals, photons, and ions but reduces the DC bias due to a higher ion flux. Thus, the increase of Ag and Au etch rates and DC bias with increasing platen power at fixed coil power with the H_2 plasma (Figure 5.4-a) can be ascribed to enhanced ion bombardment energy. In addition, the increase in plasma species flux due to increasing coil power at fixed platen power can account for the increase of Ag and Au etch rates (Figure 5.4-b).

Similar etching trends to those observed for H_2 are evident for CH_4 plasma etching as shown in Figure 5.5. Both Ag and Au etch rates increased with an increase in platen power while the hydrocarbon deposition rate was nearly constant (Figure 5.5-a); the hydrocarbon deposition

rate is essentially independent of ion bombardment energy within the range of 300 – 500 V, consistent with etch results for Cu [149]. Likewise, higher plasma species flux due to increased coil power results in increases in Ag and Au etch rates, as shown in Figure 5.5-b. However, although higher coil power increases the CH_x radical flux to Ag and Au surfaces, the effective removal of hydrocarbon layers by the higher ion flux reduced the net hydrocarbon deposition rate on the Si substrate.

Comparison of Ag etch rates in H_2 and CH_4 plasmas (Figures 5.4 and 5.5) indicates that CH_4 etch rates for both platen and coil power variations were higher than those of H_2 plasmas, despite the likely formation of hydrocarbon residues that inhibit Ag etching. Most likely, the enhanced momentum transfer efficiency of ions and the chemical reactivity of CH_4 plasmas are responsible for these results. In ion enhanced plasma etching, the ions accelerated by the electric field sputter the metals due to elastic momentum transfer; thus, higher ion mass and longer mean free path facilitate effective sputtering [127]. The higher etch rate and etch rate gradient of Ag in CH_4 plasmas relative to those in H_2 plasmas implies that like Cu, the higher mass of CH_5+ or C_2H_5+, which are the primary ions formed in CH_4 plasmas above 15 mTorr [154], improves the sputter efficiency of Ag etch products compared to sputtering by less massive hydrogen ions. That is, increases in platen power for CH_4 plasmas enhance Ag removal rates despite the fact that CH_5+ or C_2H_5+ loses momentum due to charge transfer reactions because of their shorter mean free path within the 200-300 eV ion energy range at 20 mTorr pressure; this conclusion follows from the relationship between charge transfer cross sections and charge transfer reaction constants [143, 149]. Although increasing coil power reduces the ion energy due to increased ion flux at constant power, the higher ion flux can remove adsorbed species and thereby suppress hydrocarbon deposition which will increase the net Ag etch rate. Also, the most probable etch

product, CH_3Ag in CH_4-based plasma etching, is thermodynamically stable [135], unlike AgH [90] which is formed in H_2 plasmas. This fact suggests that CH_3Ag is less likely to decompose before desorbing from the Ag surface, which leads to an overall increase in CH_4 plasma Ag etch rate compared to the etch rate in an H_2 plasma when the coil power is increased.

Au etch rates and trends in both H_2 and CH_4 plasmas are nearly identical as shown in Figures 4 and 5. Such results were unexpected, because CH_5+ or C_2H_5+ are more efficient sputtering ions than is H_x^+ and the postulated etch product, CH_3Au, is also thermodynamically stable [135]. As discussed in the previous pressure variation section, hydrocarbon formation is more favored on Cu than on Au under the same CH_4 plasma conditions; since hydrocarbon inhibition during Au etching is reduced relative to Cu etching, hydrocarbon formation cannot account fully for this observation. However, the net result of formation and inhibition of hydrocarbon residue could mitigate the anticipated higher Au etch rate because of low momentum transfer efficiency. Ideally, the momentum transfer efficiency also depends on the relative mass difference between impinging ions and sputtered metals [111] but the atomic mass difference between CH_5+ or C_2H_5+ (17 or 29 g/mol) and Au (197 g/mol) is large compared to the difference between Cu and Ag (63 and 108 g/mol). Moreover, the atomic mass of H_3+, which is the dominant ion in H_2 plasmas at 20 mTorr [115], and CH_5+ or C_2H_5+ in a CH_4 plasma are also low relative to the atomic mass of Au. As a result, the relative increase in ion sputtering efficiency when comparing H_2 and CH_4 plasmas is limited in the case of Au etching. Therefore, the virtually identical Au etch rates in H_2 and CH_4 plasmas appear to arise from the combination of hydrocarbon inhibition and low ion sputter efficiency. The lower Au etch rate in a CH_4 plasma compared to the removal rate in a He plasma [127] under the same plasma conditions also supports this hypothesis (12 nm/min vs 55 nm /min).

5.3.4 Effect of Fluorine on H_2 Plasma Etching of Au

In previous Au plasma etch studies, the etch rate of SiO_2 masked Au was 26 nm/min for a 2 min H_2 plasma exposure [127]. However, the H_2 plasma etch rate of a blanket Au film in the current study is approximately half that rate: ~12 nm/min (Figure 5.5). The increase in Au etch rate in an H_2 plasma may result from chemical contamination during SiO_2 mask patterning because the underlying Au film is exposed to an $Ar/CO_2/C_4F_8$ plasma mixture at the end of the mask etch process. This possibility was investigated by exposing blanket Au films to $Ar/CO_2/C_4F_8$ or CF_4 plasmas prior to H_2 plasma etching.

In order to investigate the fluorine effect on Au etching in H_2 plasma, CF_4 or $Ar/CO_2/C_4F_8$ plasmas was pretreated on Au flim prior to H_2 plasma etching. The thickness (100 nm) of the Au film did not change after 10 sec of CF_4 plasma exposure because of the low volatility of AuF_x (AuF_3 sublimes > 300℃) [155]. However, after H_2 plasma exposure for either 2 or 4 min, the etch rates of CF_4 plasma pretreated Au films were 18-19 nm/min which is 50% higher than the etch rate of the untreated Au film in an H_2 plasma (12 nm/min). When a Au film was pretreated in an $Ar/CO_2/C_4F_8$ plasma for 10 sec, ~4 nm of the film was removed, probably due to Ar sputtering. Subsequent etching in an H_2 plasma for 2 min yielded an etch rate of 19.5 nm/min, which is similar to the etch rate of the CF_4 plasma pretreated Au film; however, the etch rate decreased to 16 nm/min for the sample that was etched in H_2 for 4 min. Because the etch depth after 4 min of H_2 plasma etching was 64 nm, while 39 nm of Au film was etched during the first 2 min of H_2 plasma etching, the estimated etch rate of the last 2 min of H_2 plasma etching was ~12 nm/min; that is, after 2 min of H_2 plasma etching, the H_2 plasma etch rate returned to that of the untreated blanket Au film.

During 10 sec of CF_4 or $Ar/CO_2/C_4F_8$ plasma exposure, fluorocarbon layers were deposited onto the reactor chamber wall. Although outgassing from such layers releases F or CF_x, hydrogen species within the chamber will be significantly greater during the plasma etch process and so outgassing will not likely affect Au etch rates. In addition, the chamber wall was cleaned manually to remove deposited polymer layers after the SiO_2 etch process, prior to performing H_2 plasma etching. As a result, outgassing from the chamber wall is limited; thus outgassing from the chamber wall cannot adequately explain the substantial increase in Au etch rate observed after the SiO_2 etch process. Alternatively, fluorocarbon polymerization on Au or Au fluorination and F diffusion into the Au film during CF_4 or $Ar/CO_2/C_4F_8$ plasma pretreatment may have changed the surface and film reactivity with the H_2 plasma, thereby altering the Au etch rate.

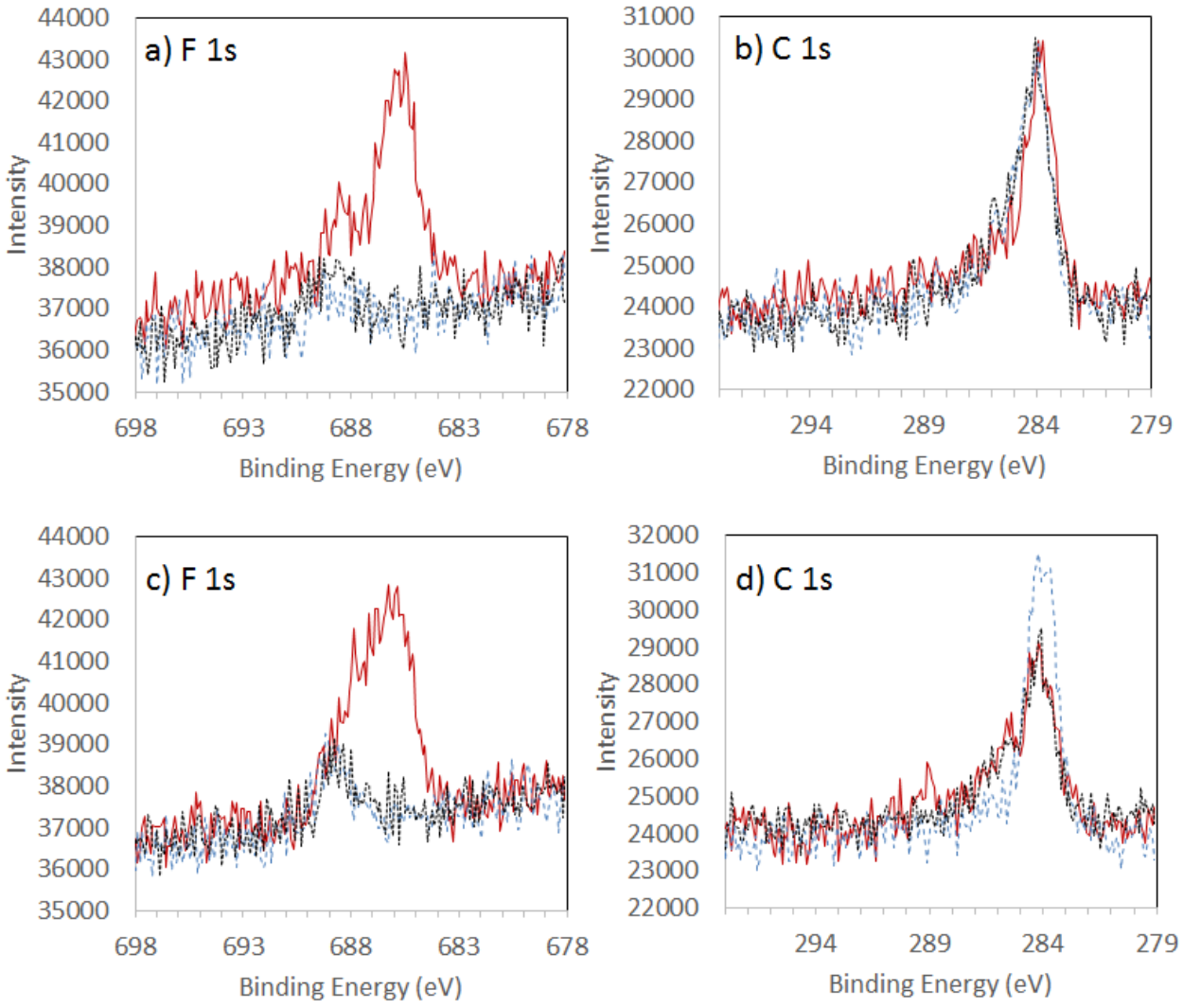

Figure 5.6 XPS spectra of Au films. a) F 1s peak and b) C 1s peak after CF_4 plasma pretreatment for 10 sec (red line), subsequent H_2 plasma exposure for 2 min (blue dashed line) and 4 min (black dotted line). c) F 1s peak and d) C 1s peak after $Ar/CO_2/C_4F_8$ plasma pretreatment for 10 sec (red line), subsequent H_2 plasma exposure for 2 min (blue dashed line) and 4min (black dotted line).

The changes of F 1s and C 1s XPS peaks due to plasma treatment and Au film etching are shown in Figure 5.6. After 10 sec of CF_4 plasma, 68.5 % Au, 11.5 % F, and 20 % C were detected on the Au film surface. The primary fluorine species is AuF_x at 686.4 eV, and C-F at 688.7 eV is also detected [156]. The AuF_x peak disappeared after 2 and/or 4 min of H_2 plasma exposure but C-F is still detected (Figures 5.6-a and 5.6-c). The elemental C peak at 284.1 eV

[157] and hydrocarbon peak at ~285.2 eV [156] were not changed despite H_2 plasma etching. Since the elemental C peak observed after 2 min of H_2 plasma exposure but without a CF_4 pretreatment was similar to that of detected after CF_4 exposure, the C detected appears to have originated primarily from atmospheric contamination after removal of the sample from the plasma reactor. The increase in H_2 plasma etch rate after CF_4 exposure suggests that F bonded to Au may assist reaction of Au with hydrogen species, perhaps by reacting with hydrogen to form HF which creates reactive Au sites for subsequent reaction with hydrogen atoms. Fluorine enhancement of the etch rate was only observed for Au etching, not for Cu and Ag etching. This distinction is probably a result of the lower Au-F bond strength compared to those of Cu-F and Ag-F (Bond dissociation energy of CuF is 431 kJ/mol [158], AgF is 354.8 kJ/mol [159], AuF is ~290 kJ/mol [160]). Apparently, the existing C layer allows both diffusion of hydrogen species to the Au-F bonds and diffusion of AuH_x products to the etching film surface for subsequent desorption.

The $Ar/CO_2/C_4F_8$ plasma treated Au surface had 62.7 % Au, 7.7 % F, and 29.6 % C. The lower F level and higher level of C on the Au surface reflects the dissociation pathway of C_4F_8 plasmas where less atomic F is generated but more CF_2 fragments are created relative to CF_4 plasmas [161]. As a result, enhanced polymer formation is observed. Indeed, the more extensive range of F 1s peaks from 685 to 689 eV (Figure 5.6-c) indicates the formation of various types of fluorocarbon moieties [162] along with AuF_x. Analogous to CF_4 plasma pretreated Au, H_2 plasma exposure removed F attached to Au, but fluorocarbon polymers are still detected at 688.7 eV. In Figure 6-d, the C 1s fluorocarbon peak at 288.6 eV [163] that was initially present after the Ar/CO2/C_4F_8 treatment, was not detected after H_2 plasma etching, although the elemental C peak at 284.1 eV [162] and the hydrocarbon peak at 285.2 eV [156], were evident.

XPS analysis of $Ar/CO_2/C_4F_8$ plasma treated Au films implies that the formation of AuF_x species on Au surfaces also promotes H_2 plasma etching as observed in CF_4 plasma pretreated Au film etching. However, the relatively lower F concentration in C_4F_8 plasma [161] limited F incorporation into the Au film; the incorporated F is likely depleted by the subsequent H_2 plasma etch. That is, after 2 min of H_2 plasma etch, the Au etch rate returned to that of the untreated blanket Au film. This result is different from that observed with the CF_4 treated Au film but is consistent with the extent of F incorporation expected in the film due to the higher F flux in CF_4 plasmas.

5.3.5 Chemical Etching Component and Photon Effects

In order to investigate chemical aspects and photon effects that occur in metal etching without ion bombardment, blanket Cu, Ag, and Au films were patterned using glass slides or Si wafers as masking materials during a 10 min CH_4 plasma exposure. After exposure, the edge and center of the glass slide and/or the Si wafer that was in contact with the metal films during etching were analyzed by XPS to determine if metals desorb from the underlying metal films and adsorb onto the mask surface. Because the gap between the glass slide (or Si wafer) and metal films is less than 3 μm, neither generation of reactive radicals nor ion bombardment will occur under the masking material. However, CH_x radicals can diffuse into the gap and photons with wavelengths >300 nm will be transmitted through the glass slide but light penetration through Si wafers is limited to wavelengths at and above the IR range. Therefore, a combination of chemical reaction and photon effects are expected under the glass slide but only chemical etching and/or IR radiation enhanced chemical reactions will occur beneath the Si wafer.

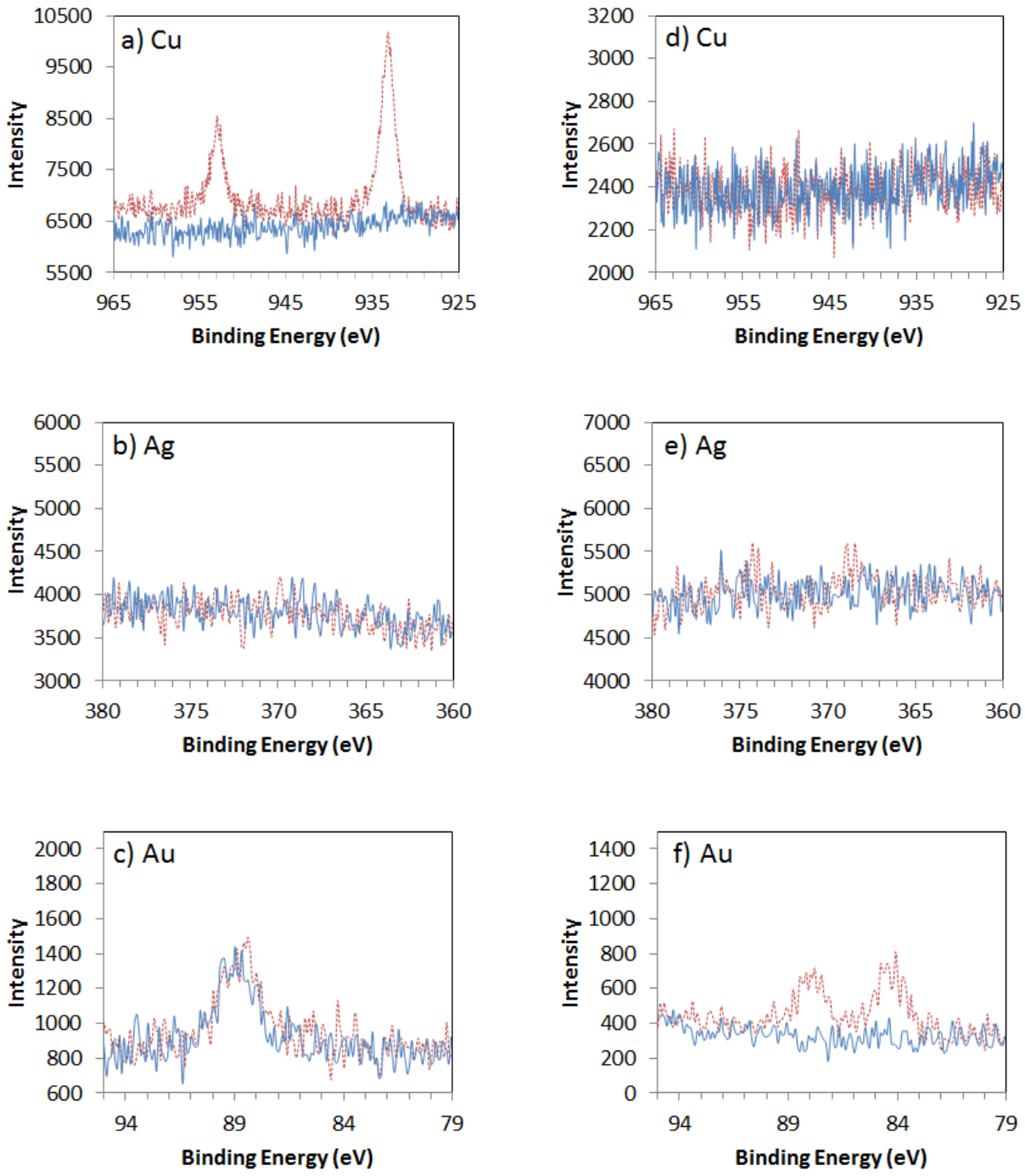

Figure 5.7 XPS of glass slide mask edge (red dotted line) and center (blue line) after 10 min of CH_4 plasma exposure on blanket a) Cu, b) Ag, c) Au. XPS spectra of Si mask on blanket d) Cu, e) Ag, f) Au.

Figure 5.7 shows XPS spectra of Cu, Ag, and Au species on the glass slide and Si wafer masks. Cu peaks at 953.1 eV and 933.1eV were detected only at the edge of the glass slide, but Ag was not detected on either the glass slide or the Si wafer. Au peaks were observed across the glass slide and across most of the Si wafer except at the center. Because Au peaks would appear at 87.7 and 84 eV [164], the broad XPS peak at 89 eV observed on the glass slide is likely shifted due to interaction between Au and oxygen in the glass slide (Figure 5.7-c). The high reactivity of CH_x radicals suggests that reaction/desorption of Au in the center area of the masks is unlikely relative to the edge area. Specifically, the high aspect ratio of the gap between the glass slide mask and the metal film and the lateral distance between center and edge of glass slide mask (1:1666), results in frequent collisions of radicals on glass slide or metal film surfaces prior to reaching the center of glass slide; this severely limits the radical concentration near the glass slide center relative to the edge. In addition, the negligible H_x+ ions concentration at > 15 mTorr in CH_4 plasma [154] implies that the concentration of neutral hydrogen atoms and molecule is small at 20 mTorr of CH_4 plasma. Furthermore, if the hydrogen species control the etch rate, the results from glass slide mask experiments using a CH_4 plasma should be similar to the results from an H_2 plasma but this is not what is observed. Therefore, detection of Cu only at the edge of the glass slide indicates formation of volatile etch products in a CH_4 plasma, but the etch process requires easy access to CH_x radicals and UV or visible light-induced chemical reaction and/or desorption. In addition, the inability to detect Ag peaks implies that physical ion bombardment is the dominant mechanism controlling etching of Ag in CH_4 plasmas. Finally, the observed Au peaks on the edge and center of the glass slide and the edge of the Si wafer demonstrate that Au etch products are stable with some, albeit limited, volatility and that their formation and desorption can be promoted by UV or visible light exposure.

Previous investigations on the formation of CH_3MH, CH_3M and CH_3MH^- (M = Cu, Ag, and Au) and their relative stability [135] support the current etch results using glass slide and Si masks, and suggest plausible etch products in CH_4 plasma etching of these metals. Further evidence of such etch products arises from the reaction of laser ablated Cu, Ag, and Au with CH_4 in an Ar matrix at 8 K where the products were detected by IR spectroscopy while varying UV and visible light doses. Unlike the reaction with H_2, stable CH_3M were identified and UV (<380 nm) photolysis enhances their formation where Cu (Ag or Au) ^2P state excitation is facilitated. Moreover, according to DFT calculations, CH_3Au is the most stable methylated product followed by CH_3Cu and CH_3Ag: the energy levels reported for CH_3Cu, CH_3Ag, and CH_3 Au are 2.1 eV, 1.6 eV, and 2.19 eV lower respectively than for M (M= Cu, Ag, and Au) + CH_3 [135]. This order of relative thermodynamic stability of CH_3M is consistent with the detected trends of metal deposition onto glass slides or Si wafers after CH_4 plasma etching. That is, chemical reaction of CH_4 plasma fragments results in Au etching but Cu etching requires chemical reactions that are enhanced by UV photons, while Ag etching appears to require ion bombardment. Furthermore, the difficulty in detecting Cu (or Au) beneath the Si wafer (but not beneath the glass slide) demonstrates that the likely etch product in a CH_4 plasma is CH_3Cu (or CH_3Au) and that UV photons may play a critical role in both Cu and Au etching.

5.4 Summary and Conclusions

PR masked and blanket Ag and Au thin film etching in CH_4 plasmas was investigated at low temperature (10 ℃) and their etch trends compared to Cu etching. The etch rates were 31 nm/min for Ag and 12 nm/min for Au. Although a CH_4 plasma ensured a highly selective etch of

Ag and Au films with PR masks, sloped sidewall profiles were obtained due to redeposition of Ag and Au.

The variation of electron, photon, neutral radical and ion concentrations due to pressure change also affected Ag and Au etch rates and hydrocarbon deposition rates. Similar to Cu etch results in CH_4 plasmas, Ag and Au etch rates and hydrocarbon deposition rates decreased rapidly as the pressure varied from 10 - 30 mTorr. Unlike Cu, however, hill or cone shaped hydrocarbon formation occurred above 60 mTorr with low Ag and nearly zero Au etch rates. The relative hydrocarbon formation tendency on Cu, Ag, and Au is consistent with the lower adsorption energy of methyl radicals and higher C-H bond dissociation energy for CH_x radicals on Ag followed by Au and Cu. The primary etch mechanism depends upon the competition between Ag (or Au) etching and hydrocarbon formation on Ag (or Au) surface.

Enhanced ion bombardment energy at high platen power and increased flux of plasma species at high coil power increased their etch rate for both Ag and Au. Relatively higher sputter yield of CH_5+ or C_2H_5+ species and stable etch product for Ag (CH_3Ag) result in higher etch rates and dependencies in CH_4 plasmas compared to those in H_2 plasmas when platen and coil powers were varied. However, essentially the same Au etch rate trends were observed when etching with CH_4 and H_2 plasmas. This result indicates that hydrocarbon inhibition of Au etching and the high mass difference between sputtering ions and Au atoms inhibited the expected higher etch rate that should have ensued from more efficient CH_5+ or C_2H_5+ sputtering and from stable etch product, CH_3Au. In addition, fluorination of Au films enhanced the H_2 plasma etch rate. This etch rate alteration was probably due to the lower Au-F bond dissociation energy which allowed ready formation of HF and thus generated reactive sites on the Au film, thereby promoting AuH_x formation.

Studies on blanket Cu, Ag, and Au film etching using glass slides and Si wafers as mask materials demonstrated that the formation of etch products such as CH_3MH, CH_3M and CH_3MH^- (M = Cu, Ag, and Au) in CH_4 plasmas is facilitated by UV photon exposure. The etch results are consistent with both the order of methylated Cu, Ag, and Au etch product stability, specifically that methylated Au is the most stable followed by Cu and Ag, and the redeposition of Ag due to the low etch product volatility in CH_4 plasmas, when PR masks were employed for pattering.

The higher Cu etch rate in CH_4 plasmas relative to the physical Ar plasma sputter rate (17 nm/min vs 4 nm/min) [86] demonstrates the importance of chemical effects in CH_4 plasma etching. However, the redeposition of Ag and Au on PR sidewalls in patterning studies, and the limited detection of Au on a Si mask when no ion bombardment occurs, imply that the volatility of Ag and Au etch products is low; as a result, physical sputtering of CH_x+ ions is a major contributor to Ag and Au etching in CH_4 plasmas. The advantage of CH_4 plasmas for etching Ag and Au relative to traditional sputtering processes stems from their high selectivity to PR masks and underlying Ti layers due to the hydrocarbon deposition that occurs on these materials.

CHAPTER 6.

CONCLUSIONS AND FUTURE WORK

6.1 Conclusions

Etching and patterning methods for Cu, Ag, and Au have been investigated. These group 11 metals are expected to behave similarly due to their common unique electronic and optical properties. Indeed, such commonalities lead to low electrical resistivity and tunable reflectivity in visible wavelength. However, traditional etching methods for these metals have several limitations for nm scale patterning. The isotropic nature of chemically controlled reactions prevented use of wet (liquid) chemical etching process for sub-nm scale patterning. Gas phase etch processes, e.g., ion beam and plasma, were also investigated, but low selectivity and redeposition on masks or substrates during ion beam process and the formation of low volatility etch products in halogen-based plasmas were obstacles for anisotropic etching process. The Damascene process arose as an alternative to the traditional subtractive etching approaches and successfully replaced those previous methods. However, nucleation and grain growth based upon Cu deposition into narrow trenches (<100 nm) increased the electrical resistivity. This so-called size effect that results from the Damascene process, provides a need for a subtractive metal etching method for Cu, and perhaps for Ag and Au as well.

Previous work in our group identified an H_2-based plasma etching process for Cu that can be carried out below room temperature; the suggested etch mechanism involves ion- and photon-assisted chemical etching to form volatile Cu hydrides. We have invoked an H_2 plasma to etch an ~60 nm Ta/Cu/Ta stack structure that could be used for IC manufacture; this work is described in chapter 2. A 3-step process was used for the stack etching, wherein a CF_4-based plasma was first

employed to etch the upper Ta layer, followed by an H_2 plasma to etch Cu layer, and finally another CF_4 based plasma to etch the underlying Ta layer. The final Cu structure had ~60 nm linewidth and ~70° sidewall angle but the multiple exposures by the fluorine-containing plasma completely removed the SiO_2 mask layer. This caused nonuniform etching of the Ta upper edge which resulted in the generation of a roughened Cu sidewall.

Chapter 3 describes the H_2 plasma etching process as applied to Ag and Au films; proposed etch mechanisms are compared to those of Cu. Considering the physical etching aspect of an H_2 plasma, the low mass, low flux and energy of H_x+ ion-induced physical sputtering of Ag and Au is unlikely. Indeed, Ag and Au etching trends were more dependent on ion bombardment than was Cu when etching was performed in H_2, He, and Ar plasmas. When a glass slide was placed over the film material to serve as a mask, we detected Cu, Ag, and Au by XPS analysis on the underside of the glass mask. This result suggests that the formation of volatile hydrides (or hydride anions) by photon-assisted processes in the H_2 plasma. Although CuH_x, AgH_x and AuH_x are thermodynamically unstable, stable hydride anions of these metals have been reported. In addition, the calculated standard sublimation energies of these metal hydrides were lower than those of the pure metals. These observations and calculations imply that group 11 hydrides can form in H_2 plasmas and could be easily sputtered by ion bombardment. We find that the observed etching phenomena of Cu, Ag, and Au in an H_2 plasma is unique among other metals such as Ti, Ta, Cr, Ni, and Al. We postulate that the lower hydride bond dissociation energy relative to the oxide dissociation energy of Cu, Ag, and Au as shown in Table 1.1 enables these group 11 metals to etch in H_2 plasmas despite the presence of oxides and thermodynamically unstable hydrides.

Although H_2-based etching of Cu, Ag, and Au was effective, low etch rate, low sidewall angle and the inability to utilize photoresist (PR) as a mask, precludes potential use of such etch processes in the manufacture of ICs or photonic devices. To address these limitations, we investigated the use of a residue-forming (CH_4) plasma to etch Cu; this work was discussed in chapter 4. The CH_4 plasma displayed a very high etch selectivity for Cu relative to both an SiO_2 hard mask and to a PR mask as a result of the formation of a thick hydrocarbon passivation layer on mask surfaces. In addition, an increased Cu etch rate was observed relative to that in an H_2 plasma despite hydrocarbon fragment adsorption and polymerization on Cu which was evident in CH_4 plasmas. From platen and coil power variations, we identified two primary factors that are responsible for this increased Cu etch rate. One factor is the more effective momentum or energy transfer that occurs due to the heavier CH_x+ ions, and the other is the formation of thermodynamically stable etch products (CH_3Cu) in CH_4 plasmas, which lowers the probability of decomposition prior to product desorption. Also, the higher Cu etch rate in CH_4 plasmas compared to that observed when etching with the more massive Ar plasma implies that chemistry plays an important role in Cu etching in a CH_4 plasma. Like CuH_x in H_2 plasma etching, however, the low bond strength of CH_3-Cu appears to preclude the detection of etch products by optical emission; rather, only Cu emission was detected. This result is consistent with the low bond energies of the hydrides or methylated compounds, since they will be readily dissociated by electron collision in the plasma. In addition, Cu sidewall angles were still ~80° with SiO_2 or PR masks due to sidewall etching of the mask layer.

In chapter 5, Ag and Au etching by CH_4 plasmas was investigated; these studies included pressure and power variation as well as the use of glass slides or Si wafers as masks to evaluate the effect of photons and ions on the etch process. The etch results of PR masked Ag and Au

films in CH_4 plasmas were similar to those of pure physical sputtering based upon the observation of redeposited Ag and Au on PR sidewalls. However, the difference in CH_x adsorption energy on metal surfaces when comparing Ag and Au generated different etching behaviors for these metals. The lower CH_x adsorption energy on Ag relative to Cu and Au, the higher CH_x+ ion bombardment energy at higher platen power and increased flux of neutral radicals and ions under high coil power conditions enhanced Ag etch rates in CH_4 plasmas when compared to the etch results from H_2 plasma etching. However, adsorption of CH_x radicals on Au surfaces inhibited sputtering of Au by ions and thereby yielded essentially identical etching behavior of H_2 and CH_4 plasmas. In addition, the detection of Au when using both glass slide and Si wafer masks indicates that volatile CH_3Au formation played a role in CH_4 plasma etching even though ion bombardment was a major contributor. This result is distinct from the results obtained with Ag etching, where ion bombardment/sputtering controls the etch process.

6.2 Future work

Based upon the discovery and mechanistic considerations of Cu subtractive etching in H_2 plasmas below room temperature, we have applied this process to Cu stack etching, and extended the H_2 plasma process to Ag and Au etching; these studies supplied insight into their etching mechanisms. Increased Cu etch rate and PR mask stability were achieved by employing a CH_4 plasma, which overcomes some of the disadvantages of the H_2 plasma etching process.

However, in order to effectively integrate H_2 or CH_4 plasma etching as a routine process in the IC or photonics industries, further understanding of the etch processes must be generated. For instance, the etching mechanism, including identification of etch products for both etchant gases, along with reaction kinetics must be established; this information will greatly facilitate

process optimization and control. Specifically, etch product volatility, will affect etch rates and the formation of residues on chamber walls and fixturing, and thereby determine the frequency and recipe(s) needed for chamber cleaning after Cu, Ag, or Au etching. In addition, for overall process efficiency and device performance, process optimization should be considered to achieve higher etch rate and improved anisotropy for metal sidewall profiles. We suggest below several methods that may establish a better understanding of the etching mechanism and lead to process optimization.

One effective method to investigate etching chemistry is to determine the dependence of etch rates on temperature. Depending upon chemical and/or physical effects involved in plasma processes, variation in effective activation energy is observed [95]. For example, the effective activation energy for Cu etching in an H_2 plasma demonstrates that the etching mechanism relies on a combination of chemical reactions and physical bombardment; to remove the expected etch product, CuH_x. Our XPS studies that used either a glass slide or Si mask, where detection of both Cu and Au without ion bombardment in H_2 or CH_4 plasmas indicates that their etching mechanisms are more dependent upon etch chemistry than is Ag etching, which depends critically on physical etch product removal. Therefore, a temperature study on Ag and Au etching in an H_2 plasma and Cu, Ag, and Au etching in a CH_4 plasma should indicate the importance of chemical reactions and thermal desorption of etch products relative to metal or metal etch product sputtering by physical ion bombardment.

Although temperature studies will supply insight into the etching mechanism, fundamental reactions and their kinetics remain undefined. Because an etch reactor such as the current ICP system does not allow control of the flux of neutral radicals, ions, and photons, a reactor designed to quantitatively control H atom flux, ion flux and energy, and photon flux and

energy would allow etch rates and kinetics to be investigated as a function of species fluxes and energies from H_2 or CH_4 plasmas. In addition, analogous to investigations performed by Winters and Coburn [165], synergistic effects of atom chemistry and ion bombardment could be studied for Cu, Ag, and Au etching. Indeed, the ion assisted chemical etching that we observed from the temperature study on Cu etching and the detection of small amounts of Cu on the glass slide mask under H_2 plasma without ion bombardment suggest synergetic effects of reactive H atom and ion bombardment. In addition, several experimental and theoretical studies demonstrated the UV assisted reaction between Cu (Ag or Au) and H_2 or CH_4 gases [89, 90, 135]. To reduce the influence of substrate heating due to the filament used to dissociate H_2, ion or UV bombardment and dissociation of unstable hydride etch products at elevated temperature, a controlled temperature sample stage is needed.

One advantage of a customized UHV system for beam studies is the addition of in-situ analysis equipment, which is not amenable to commercial ICP systems. In situ IR spectroscopy is an excellent analytical method for the detection of gaseous or surface metal hydrides or methylated compounds [90, 135]. If mass spectrometry is installed near the surface of etched metals, etch products might be directly detected. Moreover, the low collision frequency in a UHV system with H atom source, ion gun and UV lamp, will minimize dissociation of etch products but may allow implementation of OES in the UHV system.

Use of a deuterium plasma might also offer insight into the H_2 plasma etching mechanism. Deuterium, an isotope of hydrogen, has been extensively used in chemical reaction studies as a tracer to investigate a variety of hydrogen reaction mechanisms including metal hydride detection [166]. Although the chemical reactivity of deutrium to form CuD is slightly lower than that to form CuH [90], the chemical bond strength is somewhat stronger than CuH

[167]. Furthermore, in high pressure decomposition studies of CuH and CuD, a CuD crystal was thermodynamically more stable than a CuH crystal [168, 169]. In addition, corresponding energy levels in hydrogen and deuterium atoms differ only by 0.25% due to higher reduced mass of deuterium; therefore, the atomic emission lines of deuterium do not differ substantially from the emission lines of hydrogen. As a result, photon emission from a deuterium plasma is predicted to be virtually the same as that from a hydrogen plasma [170]. These facts suggest that optical emission from CuD might be detected at 428 nm, where both CuH and CuD emit [142].

Although there may be subtle differences in the OES signature of CuH and CuD, the chemical bond strength and length of the metal deuteride bonds are similar to those of the metal hydrides. Because of its factor of two heavier mass, deuterium ion sputtering yields of Cu, Ag, and Au with 500 eV ions are approximate 2-3 times higher compared with hydrogen ion sputtering yields [74]. Thus, any differences that are observed in the etch rates and profile control between H_2 and D_2 plasmas may result from the effect of ion bombardment on Cu (or Ag and Au) and etch mask etch rates and profiles.

In general, successful large scale manufacturing requires that several criteria be met: suitable etch rate, anisotropy, selectivity, surface uniformity, and reproducibility [34, 35]. Because the goal is to achieve pattern sizes <100 nm without an increase in resistivity, especially for Cu etching, development of methods to improve anisotropic etching is critical. Two major approaches to be considered are the optimization of H_2 or CH_4 plasma recipes and the formulation of new mask materials.

Without further etch mechanism studies on etch products in H_2 and CH_4 plasma, process optimization will be limited due to lack of specific desorbed species and their properties such as volatility and thermodynamic stability. Nevertheless, because the likely etch product, CuH, in H_2

plasma, is thermodynamically unstable with low volatility, the overall process should occur at low temperature, low pressure and relatively high energy (or momentum) ion bombardment. However, too low a temperature decreases Cu etch rates and a lower pressure changes the flux of plasma species, and the dominant ions (from H_3^+ to H_2^+) present in an H_2 plasma. High energy ion bombardment also degrades mask layers; these considerations must be considered in process optimization.

In our etching study, SiO_2 and PR masks were utilized for H_2 or CH_4 plasma processes. Although the SiO_2 hard mask displays high selectivity in H_2 plasmas, several disadvantages are present: a slight degradation of SiO_2 mask sidewalls that can generate a sloped profile in the underlying Cu layer, a high temperature SiO_2 deposition process that oxidizes Cu and Ag surfaces and promotes severe agglomeration of Ag films, and fluorine residues on Au surfaces that arise from SiO_2 mask patterning and affect subsequent Au etching by an H_2 plasma. Even a CH_4 plasma did not fully passivate SiO_2 sidewalls and displayed some etching of the sidewall edge In addition, Ag and Au redeposition on sidewalls of micrometer thick masks due to physical sputtering limits the utility of thick PR mask; instead, a thin hard mask is more appropriate. As a result, development of a highly chemically and physically selective etch mask for H_2 or CH_4 plasma processes may improve pattern fidelity and improve anisotropy.

Ta is a good candidate for a highly selective mask in H_2 plasma etching of Cu because we have already demonstrated that the Cu layer is selectively etched by an H_2 plasma during Ta/Cu/Ta stack etching. In addition, because Ta has been used as a diffusion barrier in IC manufacture [171], the Ta layer can function as both a mask for Cu etching and a diffusion barrier, thus eliminating the need for further processing to remove the Ta mask layer after Cu etching. However, fluorine based plasma etching to pattern the Ta mask also fluorinates the

underlying Cu surface which could influence the electrical resistivity of Cu and a non-uniform Ta mask pattern can result in roughened Cu sidewalls. Therefore, further study on Ta pattering methods and their effect on Cu properties would be beneficial.

Unlike SiO_2 deposition by PECVD, Ta deposition by physical sputtering methods such as PVD or e-beam evaporation should avoid thermal agglomeration of Ag layers. In addition, unlike a PR mask, a several nm thick Ta layer is easily deposited and this structure may minimize re-deposition of Ag or Au on mask sidewalls. However, selectivity of Ta to a CH_4 plasma must be investigated.

Finally, in order to replace the current damascene process, the anticipated (improved) electrical properties for Cu patterns <100 nm generated by subtractive etching using H_2 or CH_4 plasmas must be confirmed. Although we achieved <100 nm Ta/Cu/Ta stack structures by H_2 based plasma etching, ~70° sidewall profile and significant sidewall roughness were observed. These results must be improved, perhaps by optimization of Cu and Ta patterning; subsequent electrical tests on nm structures will determine the utility of plasma etch process for Cu and perhaps for Ag and Au as well.

APPENDIX A.

Ion Sputtering and H Atom Dosing of Cu Films

The H_2 plasma-induced Cu etching mechanism proposed is a combination of chemical reaction and ion and/or photon bombardment. One way to investigate the contributions of these different plasma components is to isolate each component and conduct individual and combination experiments. Since isolation of a single component within the plasma is not trivial, we set up an ultra high vacuum (UHV) system where an ion gun and an H_2 gas cracking tungsten (W) filament were installed to permit various etching experiments; that is, this system allowed ion beam studies, atom dosing experiments with the H atom source, and etch studies using a combination of these fluxes.

Experimental

A commercial ion gun, IQE 11/35, was installed on top of the 7" diameter spherical UHV chamber. In this configuration, the ion beam was perpendicular to the sample stage located in the center of the chamber and the working distance between the nozzle of ion gun and the sample stage was ~5 cm. The base pressure of the UHV system was ~1x 10^{-8} Torr and the operating pressure was from ~9 x 10^{-5} to 5 x 10^{-4} Torr. Ion fluxes were controlled by the operating pressure and Ar, H_2/N_2(1:9 gas mixture) and H_2 gases were used for ion (sputtering) sources. Applied ion energies were varied from 700 eV to 2 keV.

A heated tungsten (W) coil filament (0.375 mm diameter) with 2.5 cm height and 4 mm diameter was used to thermally crack H_2. The W filament was positioned at a 45° angle from the top plane of the UHV chamber. The working distance from the W filament and the sample stage

was ~4 cm. Current flow through the W filament was controlled by a variable autotransformer (Staco Energy).

Fifty nm and 100 nm thick Cu films were deposited from CHA 2 e-beam evaporator and Denton Explorer e-beam evaporator onto 4-inch Si wafers with a 20 nm thick Ti layer. The deposited Cu films were cut into 1.5 x 1.5 cm^2 samples. Step heights were measured by a Dektak 150 Profilometer.

Results and Discussion

Figure A.1 describes the results of Ar and H_2/N_2 ion beam exposure, and H atom dosing followed by H_2 ion beam exposure. After 30 min of Ar ion sputtering with 700 eV ion energy and 3.5 x 10^{-5} Torr and H_2/N_2 (1:9) ion sputtering with 1 keV and 8.9 x 10^{-5} Torr, 100 nm thick Cu film was sputtered; the crater is evident at the center of the Cu samples, and the color of the surface suggests that the Ti adhesive layer has been exposed. Because the full width half maximum (FWHM) of the ion beam is determined by ion energy, the size of the crater formed from in Ar ion sputtering of the Cu film is larger (figure A.1 a)) than that from H_2/N_2 (1:9) ion sputtering (figure A.1 b)). However, when a 50 nm thick Cu film was exposed to H_x+ ion sputtering at 2 keV and 5 x 10^{-4} Torr for 30 min, no visual indication of etching was observed despite the high ion (2 keV) energy. In collisionless ion sputtering, the Ar+ sputter yield at 700 eV is ~3 and the N+ sputter yield at 1 keV is ~ 1.5 [74]. Because of the smaller ionization cross section of N+ relative to N_2+ [172], the expected dominant ion in our system is N_2+ resulting in a similar sputtering yield relative to the Ar+ induced sputter yield. Considering the similar sputtering results from Ar and H_2/N_2 (1:9) ions, it appears that the addition of 10 % H_2 does not contribute to Cu sputtering. Indeed, the reported Cu sputtering yield at 2 keV is only 0.03 [74]

and therefore Cu sputtering by pure H_2 is unlikely even though the dominant ion is H_2+ in the pressure range used [116].

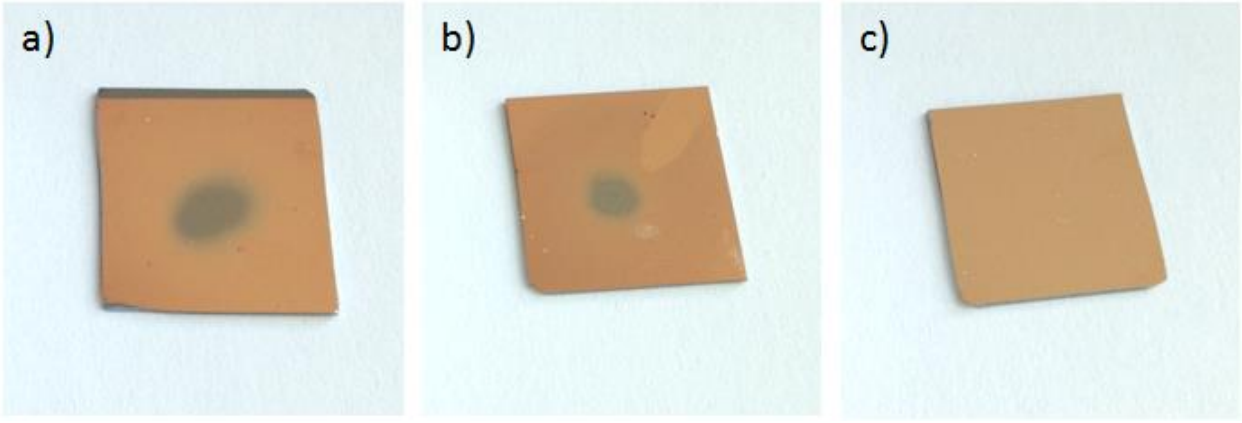

Figure A.1 Cu films after a) Ar ion sputtering with 700 eV ion energy for 30 min, b) H_2/N_2 (1:9) ion sputtering with 1 keV for 30 min and c) three cycles of 2 step process; a single cycle compose of H atom dose for 2 min and H_2 ion sputtering with 2 keV for 10 min.

In order to investigate possible H atom contribution to Cu etching, H atom dosing of the Cu surface followed by H_x+ ion exposure was performed. Although simultaneous exposure of a Cu film with H atom and H_x+ impingement is important in order to observe synergetic effects, electron generation from the W filament interfered with operation of the ion gun, rendering this experiment untenable. As a result, simultaneous operation of both beams could not be performed. Therefore, a single cycle consisting of 2 min H atom dose followed by 10 min of H_x+ ion beam exposure was designed. Hydrogen atoms impinging on the Cu may adsorb on the Cu surface and grain boundries, although some may penetrate into interstitial positions in the Cu lattice. In addition, unstable CuH_x may decompose during H_x+ ion flux. As a result, we ran more than one cycle of the short H atom dose followed by H_x+ ion sputtering in an attempt to form and maintain CuH_x more effectively than was deemed possible in one cycle of a longer exposure to H atoms followed by H_x+ sputtering. Despite these various approaches, a 50 nm thick Cu film

showed no visible indication that etching occurred after three cycles of this two-step process (figure A.1 c)).

There are several factors that may inhibit Cu etching in our current ion sputtering and H atom cracking system. First, the estimated ion flux from the ion gun is ~ 10^{-14} ions/cm^{2}s which is two orders of magnitude lower than the ion flux in the PT-ICP system. In addition, the cracking efficiency of the W filament is low (1-3 % in the temperature range 1500- 2000 ℃) [173]. Therefore, the expected H atom flux onto the Cu film at 5 x 10^{-4} Torr is also two or three orders of magnitude lower than H atom flux at 2 x 10^{-2} Torr in PT-ICP. Moreover, photon radiation from the filament heated the Cu film and likely decomposed any (unstable) CuH_x that formed. Finally, depending upon the crystal orientation of Cu, reduced ion sputter rates above 500K have been reported [174]. In order to perform controlled experiments to allow valid comparison of beam studies to ICP Cu etch studies, a sample stage with cooling capability and beams with improved isolation to reduce interference are required for further investigation of H_x+ and H atom induced Cu etching

REFERENCES

[1]. TRIGG, G.L. and E.H. IMMERGUT, "Encyclopedia of Applied Physics". Vol. 4. 1992, New York: VCH Publishers.

[2]. TRIGG, G.L. and E.H. IMMERGUT, "Encyclopedia of Applied Physics". Vol. 18. 1997, New York: VCH Publishers.

[3]. OMAR, M.A., "Elementary Solid State Physics", ed. D. Lazarus. 1975: Addison Wesley

[4]. KREIBIG, U. and M. VOLLMER, "Optical properties of metal clusters". 1995: Springer-Verlag.

[5]. JAIN, P., X. HUANG, I. EL-SAYED, and M. EL-SAYED, "Review of Some Interesting Surface Plasmon Resonance-enhanced Properties of Noble Metal Nanoparticles and Their Applications to Biosystems". Plasmonics, vol. 2(3), pp. 107-118, 2007.

[6]. MURARKA, S.P., "Multilevel interconnections for ULSI and GSI era". Materials Science and Engineering: R: Reports, vol. 19(3–4), pp. 87-151, 1997.

[7]. ADAMS, D. and T.L. ALFORD, "Encapsulated silver for integrated circuit metallization". Materials Science and Engineering: R: Reports, vol. 40(6), pp. 207-250, 2003.

[8]. KARIM, S., W. ENSINGER, T.W. CORNELIUS, and R. NEUMANN, "Investigation of size effects in the electrical resistivity of single electrochemically fabricated gold nanowires". Physica E: Low-dimensional Systems and Nanostructures, vol. 40(10), pp. 3173-3178, 2008.

[9]. VON SZENTPÁ LY, L., "Atom-Based Thermochemistry: Crystal Atomization and Sublimation Enthalpies in Linear Relationships to Molecular Atomization Enthalpy". Journal of the American Chemical Society, vol. 130(18), pp. 5962-5973, 2008.

[10]. SINKE, G.C., L.C. WALKER, F.L. OETTING, and D.R. STULL, "Thermodynamic Properties of Aluminum Hydride". The Journal of Chemical Physics, vol. 47(8), pp. 2759-2761, 1967.

[11]. BARBALACE, K. "Periodic Table of Elements", http://www.webelements.com. (Accessed August 2014)

[12]. WINTER, M. "Home of the Periodic Table", http://environmentalchemistry.com/yogi/periodic. (Accessed August 2014)

[13]. EHRENREICH, H., H.R. PHILIPP, and B. SEGALL, "Optical Properties of Aluminum". Physical Review, vol. 132(5), pp. 1918-1928, 1963.

[14]. LUKASIAK, L. and A. JAKUBOWSKI, "History of Semiconductros". Journal of Telecommunication and Information Technology, vol. 3, 2010.

[15]. MAY, G.S. and S.M. SZE, "Fundamentals of Semiconductro Fabrication". 2004, Hoboken: John Wiley & Sons, Inc

[16]. SCHALLER, R.R., "Moore's law: past, present and future". Spectrum, IEEE, vol. 34(6), pp. 52-59, 1997.

[17]. STAMPER, A.K., T.L. MCDEVITT, and S.L. LUCE. "Sub-0.25-micron interconnection scaling: damascene copper versus subtractive aluminum". in *Advanced Semiconductor Manufacturing Conference and Workshop, 1998. 1998 IEEE/SEMI*. 1998.

[18]. BRAUN, L., "Electromigration testing—A current problem". Microelectronics Reliability, vol. 13(3), pp. 215-228, 1974.

[19]. KELLY, K.L., E. CORONADO, L.L. ZHAO, and G.C. SCHATZ, "The Optical Properties of Metal Nanoparticles: The Influence of Size, Shape, and Dielectric Environment". The Journal of Physical Chemistry B, vol. 107(3), pp. 668-677, 2002.

[20]. SÖ NNICHSEN, C., T. FRANZL, T. WILK, G. VON PLESSEN, J. FELDMANN, O. WILSON, and P. MULVANEY, "Drastic Reduction of Plasmon Damping in Gold Nanorods". Physical Review Letters, vol. 88(7), pp. 077402, 2002.

[21]. JAIN, P.K., K.S. LEE, I.H. EL-SAYED, and M.A. EL-SAYED, "Calculated Absorption and Scattering Properties of Gold Nanoparticles of Different Size, Shape, and Composition: Applications in Biological Imaging and Biomedicine". The Journal of Physical Chemistry B, vol. 110(14), pp. 7238-7248, 2006.

[22]. YGUERABIDE, J. and E.E. YGUERABIDE, "Light-Scattering Submicroscopic Particles as Highly Fluorescent Analogs and Their Use as Tracer Labels in Clinical and Biological Applications: I. Theory". Analytical Biochemistry, vol. 262(2), pp. 137-156, 1998.

[23]. GHOSH, S.K., S. NATH, S. KUNDU, K. ESUMI, and T. PAL, "Solvent and Ligand Effects on the Localized Surface Plasmon Resonance (LSPR) of Gold Colloids". The Journal of Physical Chemistry B, vol. 108(37), pp. 13963-13971, 2004.

[24]. HAES, A.J. and R.P. VAN DUYNE, "A Nanoscale Optical Biosensor: Sensitivity and Selectivity of an Approach Based on the Localized Surface Plasmon Resonance Spectroscopy of Triangular Silver Nanoparticles". Journal of the American Chemical Society, vol. 124(35), pp. 10596-10604, 2002.

[25]. MALINSKY, M.D., K.L. KELLY, G.C. SCHATZ, and R.P. VAN DUYNE, "Chain Length Dependence and Sensing Capabilities of the Localized Surface Plasmon Resonance of Silver Nanoparticles Chemically Modified with Alkanethiol Self-Assembled Monolayers". Journal of the American Chemical Society, vol. 123(7), pp. 1471-1482, 2001.

[26]. LINK, S. and M.A. EL-SAYED, "OPTICAL PROPERTIES AND ULTRAFAST DYNAMICS OF METALLIC NANOCRYSTALS". Annual Review of Physical Chemistry, vol. 54(1), pp. 331-366, 2003.

[27]. HUANG, X., I.H. EL-SAYED, W. QIAN, and M.A. EL-SAYED, "Cancer Cell Imaging and Photothermal Therapy in the Near-Infrared Region by Using Gold Nanorods". Journal of the American Chemical Society, vol. 128(6), pp. 2115-2120, 2006.

[28]. TURKEVICH, J., P.C. STEVENSON, and J. HILLIER, "The Formation of Colloidal Gold". The Journal of Physical Chemistry, vol. 57(7), pp. 670-673, 1953.

[29]. GOIA, D.V., "Preparation and formation mechanisms of uniform metallic particles in homogeneous solutions". Journal of Materials Chemistry, vol. 14(4), pp. 451-458, 2004.

[30]. HUTTER, E. and J.H. FENDLER, "Exploitation of Localized Surface Plasmon Resonance". Advanced Materials, vol. 16(19), pp. 1685-1706, 2004.

[31]. ROSSNAGEL, S.M., "Thin film deposition with physical vapor deposition and related technologies". Journal of Vacuum Science & Technology A, vol. 21(5), pp. S74-S87, 2003.

[32]. KEATING, C.D. and M.J. NATAN, "Striped Metal Nanowires as Building Blocks and Optical Tags". Advanced Materials, vol. 15(5), pp. 451-454, 2003.

[33]. POULSEN, R.G., "Plasma Etching in Integrated-Circuit Manufacture - Review". Journal of Vacuum Science & Technology, vol. 14(1), pp. 266-274, 1977.

[34]. GRILL, A., "Cold Plasma in Materials Fabrication: from Fundamentals to Applications". 1994, Piscataway, NJ: IEEE Press.

[35]. LIEBERMAN, M.A. and A.J. LICHTENBERG, "Principles of Plasma Discharges and Materials Processing". Vol. 2nd ed. 2005, Hoboken, N.J: Wiley-Interscience.

[36]. LANGMUIR, I., "POSITIVE ION CURRENTS FROM THE POSITIVE COLUMN OF MERCURY ARCS". Science, vol. 58(1502), pp. 290-291, 1923.

[37]. BELKIND, A., "How Plasmas Are Made". Vacuum Technology and Coating, vol. November, pp. 80, 2007.

[38]. RANADE, R.M., S.S. ANG, and W.D. BROWN, "Reactive Ion Etching of Thin Gold Films". Journal of The Electrochemical Society, vol. 140(12), pp. 3676-3678, 1993.

[39]. XIA, Y., E. KIM, M. MRKSICH, and G.M. WHITESIDES, "Microcontact Printing of Alkanethiols on Copper and Its Application in Microfabrication". Chemistry of Materials, vol. 8(3), pp. 601-603, 1996.

[40]. GEISSLER, M., H. WOLF, R. STUTZ, E. DELAMARCHE, U.-W. GRUMMT, B. MICHEL, and A. BIETSCH, "Fabrication of Metal Nanowires Using Microcontact Printing". Langmuir, vol. 19(15), pp. 6301-6311, 2003.

[41]. WILLIAMS, K.R., K. GUPTA, and M. WASILIK, "Etch rates for micromachining processing-Part II". Microelectromechanical Systems, Journal of, vol. 12(6), pp. 761-778, 2003.

[42]. XIA, Y., E. KIM, and G.M. WHITESIDES, "Microcontact Printing of Alkanethiols on Silver and Its Application in Microfabrication". Journal of The Electrochemical Society, vol. 143(3), pp. 1070-1079, 1996.

[43]. LEE, H., D.S. BIEN, S. BADARUDDIN, and A. TEH, "Silver (Ag) as a novel masking material in glass etching for microfluidics applications". Microsystem Technologies, vol. 19(2), pp. 253-259, 2013.

[44]. HAUDER, M., W. HANSCH, J. GSTÖ TTNER, and D. SCHMITT-LANDSIEDEL, "Electromigration resistance of sputtered silver lines using different patterning techniques". Microelectronic Engineering, vol. 60(1–2), pp. 51-57, 2002.

[45]. GEISSLER, M., H. SCHMID, A. BIETSCH, B. MICHEL, and E. DELAMARCHE, "Defect-Tolerant and Directional Wet-Etch Systems for Using Monolayers as Resists". Langmuir, vol. 18(6), pp. 2374-2377, 2002.

[46]. EIDELLOTH, W. and R.L. SANDSTROM, "Wet etching of gold films compatible with high Tc superconducting thin films". Applied Physics Letters, vol. 59(13), pp. 1632-1634, 1991.

[47]. KUMAR, A., H.A. BIEBUYCK, and G.M. WHITESIDES, "Patterning Self-Assembled Monolayers: Applications in Materials Science". Langmuir, vol. 10(5), pp. 1498-1511, 1994.

[48]. WILLIAMS, K.R. and R.S. MULLER, "Etch rates for micromachining processing". Microelectromechanical Systems, Journal of, vol. 5(4), pp. 256-269, 1996.

[49]. PELHOS, K., V.M. DONNELLY, A. KORNBLIT, M.L. GREEN, R.B. VAN DOVER, L. MANCHANDA, Y. HU, M. MORRIS, and E. BOWER, "Etching of high-k dielectric Zr1−xAlxOy films in chlorine-containing plasmas". Journal of Vacuum Science & Technology A, vol. 19(4), pp. 1361-1366, 2001.

[50]. DONNELLY, V.M. and A. KORNBLIT, "Plasma etching: Yesterday, today, and tomorrow". Journal of Vacuum Science & Technology A, vol. 31(5), pp. -, 2013.

[51]. MACHIELS, A.J. and D.R. OLANDER, "Investigation of the tantalum-fluorine reaction by modulated molecular beam mass spectrometry". Surface Science, vol. 65(1), pp. 325-344, 1977.

[52]. KUO, Y. and S. LEE, "Room-temperature copper etching based on a plasma--copper reaction". Applied Physics Letters, vol. 78(7), pp. 1002-1004, 2001.

[53]. PARK, S., Y. LEE, and G. YEOM, "Effects of Additive Gases on Ag Etching Using Inductively Coupled Cl2-Based Plasmas". Joural of the Korean Physical Society, vol. 42, pp. S804-S2808, 2003.

[54]. ALDRIDGE, F.T., "High Speed Anisotropic Reactive Ion Etching of Gold Films". Journal of The Electrochemical Society, vol. 142(5), pp. 1563-1565, 1995.

[55]. LEE, J.W., Y.D. PARK, J.R. CHILDRESS, S.J. PEARTON, F. SHARIFI, and F. REN, "Copper Dry Etching with Cl2 / Ar Plasma Chemistry". Journal of The Electrochemical Society, vol. 145(7), pp. 2585-2589, 1998.

[56]. HOWARD, B.J. and C. STEINBRUCHEL, "Reactive ion etching of copper in SiCl[sub 4]-based plasmas". Applied Physics Letters, vol. 59(8), pp. 914-916, 1991.

[57]. BERTZ, A., T. WERNER, N. HILLE, and T. GESSNER, "Effects of the biasing frequency on RIE of Cu in a Cl2-based discharge". Applied Surface Science, vol. 91(1–4), pp. 147-151, 1995.

[58]. IGARASHI, Y., T. YAMANOBE, and T. ITO, "Dry Etching Technique for Subquarter-Micron Copper Interconnects". Journal of The Electrochemical Society, vol. 142(3), pp. L36-L37, 1995.

[59]. MIYAZAKI, H., K. TAKEDA, N. SAKUMA, S. KONDO, Y. HOMMA, and K. HINODE, "Copper dry etching with precise wafer-temperature control using Cl2 gas as a single reactant". Journal of Vacuum Science & Technology B, vol. 15(2), pp. 237-240, 1997.

[60]. MARKERT, M., A. BERTZ, and T. GESSNER, "Copper dry etching technique for ULSI interconnections". Microelectronic Engineering, vol. 35(1–4), pp. 333-336, 1997.

[61]. GAO, L., J. GSTOETTNER, R. EMLING, P. WANG, W. HANSCH, and D. SCHMITT-LANDSIEDEL, "Silver Patterning by Reactive Ion Beam Etching for Microelectronics Application". MRS Online Proceedings Library, vol. 812, pp. null-null, 2004.

[62]. ALFORD, T.L., P. NGUYEN, Y. ZENG, and J.W. MAYER, "Advanced silver-based metallization patterning for ULSI applications". Microelectronic Engineering, vol. 55(1–4), pp. 383-388, 2001.

[63]. PARK, S.D., Y.J. LEE, S.G. KIM, H.H. CHOE, M.P. HONG, and G.Y. YEOM, "Etch characteristics of silver by inductively coupled fluorine-based plasmas". Thin Solid Films, vol. 445(1), pp. 138-143, 2003.

[64]. WERBANETH, P., Z. HASAN, P. RAJORA, and M. ROUSEY-SEIDEL, "The Reactive Ion Etching of Au on GaAs Substrates in a High Density Plasma Etch Reactor", in *Internatinal Conference on Compound Semiconductror Manufacturing Technology*. 1999, CS MANTECH.

[65]. OHSHITA, Y. and N. HOSOI, "Lower temperature plasma etching of Cu using IR light irradiation". Thin Solid Films, vol. 262(1–2), pp. 67-72, 1995.

[66]. HAHN, Y.B., S.J. PEARTON, H. CHO, and K.P. LEE, "Dry etching mechanism of copper and magnetic materials with UV illumination". Materials Science and Engineering: B, vol. 79(1), pp. 20-26, 2001.

[67]. TANG, H. and I.P. HERMAN, "Anomalous local laser etching of copper by chlorine". Applied Physics Letters, vol. 60(17), pp. 2164-2166, 1992.

[68]. RAAF, H. and N. SCHWENTNER, "Efficiencies above unity in light-induced reaction of Cu with Cl2: excitation, amplification, and diffusion processes". Applied Surface Science, vol. 174(1), pp. 13-34, 2001.

[69]. SANGHEON, L. and K. YUE, "A New Hydrogen Chloride Plasma-Based Copper Etching Process". Japanese Journal of Applied Physics, vol. 41(12R), pp. 7345, 2002.

[70]. LEE, S. and Y. KUO, "Hydrogen bromide plasma–copper reaction in a new copper etching process". Thin Solid Films, vol. 457(2), pp. 326-332, 2004.

[71]. JAIN, A., T.T. KODAS, and M.J. HAMPDEN-SMITH, "Thermal dry-etching of copper using hydrogen peroxide and hexafluoroacetylacetone". Thin Solid Films, vol. 269(1–2), pp. 51-56, 1995.

[72]. SPENCER, E.G. and P.H. SCHMIDT, "Ion-Beam Techniques for Device Fabrication". Journal of Vacuum Science and Technology, vol. 8(5), pp. S52-S70, 1971.

[73]. LEE, R.E., "Microfabrication by ion beam etching". Journal of Vacuum Science and Technology, vol. 16(2), pp. 164-170, 1979.

[74]. YAMAMURA, Y. and H. TAWARA, "ENERGY DEPENDENCE OF ION-INDUCED SPUTTERING YIELDS FROM MONATOMIC SOLIDS AT NORMAL INCIDENCE". Atomic Data and Nuclear Data Tables, vol. 62(2), pp. 149-253, 1996.

[75]. EDELSTEIN, D., J. HEIDENREICH, R. GOLDBLATT, W. COTE, C. UZOH, N. LUSTIG, P. ROPER, T. MCDEVITT, W. MOTSIFF, A. SIMON, J. DUKOVIC, R. WACHNIK, H. RATHORE, R. SCHULZ, L. SU, S. LUCE, and J. SLATTERY. "Full copper wiring in a sub-0.25 μm CMOS ULSI technology". in *Electron Devices Meeting, 1997. IEDM '97. Technical Digest., International*. 1997.

[76]. ANDRICACOS, P.C., C. UZOH, J. DUKOVIC, J. HORKANS, and H. DELIGIANNI, "Damascene Copper Electroplating for Chip Interconnections". IBM Journal of Research and Development, vol. 42(p.567), 1998.

[77]. PETERS, L., Semiconductor International, vol. 21, pp. 64-74, 1998.

[78]. MALLIKARJUNAN, A., S. SHARMA, and S.P. MURARKA, "Resistivity of Copper Films at Thicknesses Near the Mean Free Path of Electrons in Copper Minimization of the Diffuse Scattering in Copper". Electrochemical and Solid-State Letters, vol. 3(9), pp. 437-438, 2000.

[79]. TELLIER, C.R. and A.J. TOSSER, "Size Effects in Thin Films". 1982, New York: Elsevier Scintific Publishing Company.

[80]. ZHANG, W., S.H. BRONGERSMA, T. CLARYSSE, V. TERZIEVA, E. ROSSEEL, W. VANDERVORST, and K. MAEX, "Surface and grain boundary scattering studied in beveled polycrystalline thin copper films". Journal of Vacuum Science & Technology B: Microelectronics and Nanometer Structures, vol. 22(4), pp. 1830-1833, 2004.

[81]. WU, W., D. ERNUR, S.H. BRONGERSMA, M. VAN HOVE, and K. MAEX, "Grain growth in copper interconnect lines". Microelectronic Engineering, vol. 76(1–4), pp. 190-194, 2004.

[82]. ZHANG, W., S.H. BRONGERSMA, N. HEYLEN, G. BEYER, W. VANDERVORST, and K. MAEX, "Geometry Effect on Impurity Incorporation and Grain Growth in Narrow Copper Lines". Journal of The Electrochemical Society, vol. 152(12), pp. C832-C837, 2005.

[83]. STEINHOEGL, W., G. SCHINDLER, and M. ENGELHARDT, "Unraveling the Mysteries Behind Size Effects in Metallization Systems. (cover story)". Semiconductor International, vol. 28, pp. 34-38, 2005.

[84]. KULKARNI, N.S. and R.T. DEHOFF, "Application of Volatility Diagrams for Low Temperature, Dry Etching, and Planarization of Copper". Journal of The Electrochemical Society, vol. 149(11), pp. G620-G632, 2002.

[85]. WU, F., G. LEVITIN, and D.W. HESS, "Patterning of Cu Films by a Two-Step Plasma Etching Process at Low Temperature". Journal of The Electrochemical Society, vol. 157(4), pp. H474-H478, 2010.

[86]. WU, F., G. LEVITIN, and D.W. HESS, "Low-Temperature Etching of Cu by Hydrogen-Based Plasmas". ACS Applied Materials & Interfaces, vol. 2(8), pp. 2175-2179, 2010.

[87]. WU, F., G. LEVITIN, and D.W. HESS, "Mechanistic considerations of low temperature hydrogen-based plasma etching of Cu". Journal of Vacuum Science & Technology B: Microelectronics and Nanometer Structures, vol. 29(1), pp. 011013-7, 2011.

[88]. FITZSIMONS, N.P., W. JONES, and P.J. HERLEY, "Studies of copper hydride. Part 1.-Synthesis and solid-state stability". Journal of the Chemical Society, Faraday Transactions, vol. 91(4), pp. 713-718, 1995.

[89]. RUIZ, M.E., J. GARCIA-PRIETO, and O. NOVARO, "Theoretical studies of photoexcited state Cu atom reactions. I. Excited state responsible for H[sub 2] capture". The Journal of Chemical Physics, vol. 80(4), pp. 1529-1534, 1984.

[90]. ANDREWS, L. and X. WANG, "Infrared Spectra and Structures of the Stable CuH2-, AgH2-, AuH2-, and AuH4- Anions and the AuH2 Molecule". Journal of the American Chemical Society, vol. 125(38), pp. 11751-11760, 2003.

[91]. CANDLER, C., "Atomic Spectra and the Vector Model". 2nd ed. 1964, Van Nostrand: Princeton, N.J.

[92]. PREUSS, S., A. DEMCHUK, and M. STUKE, "Sub-picosecond UV laser ablation of metals". Applied Physics A, vol. 61(1), pp. 33-37, 1995.

[93]. WU, F., G. LEVITIN, and D.W. HESS, "Temperature Effects and Optical Emission Spectroscopy Studies of Hydrogen-Based Plasma Etching of Copper". Journal of The Electrochemical Society, vol. 159(2), pp. H121-H124, 2012.

[94]. GREENE, J.E., "Optical spectroscopy for diagnostics and process control during glow discharge etching and sputter deposition". Journal of Vacuum Science and Technology, vol. 15(5), pp. 1718-1729, 1978.

[95]. VITALE, S.A., J. KEDZIERSKI, and C.L. KEAST, "High density plasma etching of titanium nitride metal gate electrodes for fully depleted silicon-on-insulator subthreshold transistor integration". Journal of Vacuum Science & Technology B: Microelectronics and Nanometer Structures, vol. 27(6), pp. 2472-2479, 2009.

[96]. BORAH, D., M.T. SHAW, S. RASAPPA, R.A. FARREL, C. O'MAHONY, C.M. FAULKNER, M. BOSEA, P. GLEESON, J.D. HOLMES, and M.A. MORRIS, "Plasma etch technologies for the develpoment of ultra-small feature size transistor devices.". Journal of Physics D: Applied Physics, vol. 44, pp. 174012, 2011.

[97]. ONO, H., T. NAKANO, and T. OHTA, "Diffusion barrier effects of transition metals for Cu/M/Si multilayers (M=Cr, Ti, Nb, Mo, Ta, W)". Applied Physics Letters, vol. 64(12), pp. 1511-1513, 1994.

[98]. CHANG, J.P., H.W. KRAUTTER, W. ZHU, R.L. OPILA, and C.S. PAI, "Integration of fluorinated amorphous carbon as low-dielectric constant insulator: Effects of heating and deposition of tantalum nitride". Journal of Vacuum Science & Technology A: Vacuum, Surfaces, and Films, vol. 17(5), pp. 2969-2974, 1999.

[99]. DOH, H.-H., J.-H. KIM, S.-H. LEE, and K.-W. WHANG, "Mechanism of selective SiO[sub 2]/Si etching with fluorocarbon gases (CF_4, C_4F_8) and hydrogen mixture in electron cyclotron resonance plasma etching system". Journal of Vacuum Science & Technology A: Vacuum, Surfaces, and Films, vol. 14(5), pp. 2827-2834, 1996.

[100]. KIANI, Z., Y. ABDI, and E. ARZI, "Low Temperature Formation of Silver and Silver-Copper Alloy Nano-Particles Using Plasma Enhanced Hydrogenation and Their Optical Properties". World Journal of Nano Science and Engineering, vol. 2, pp. 142-147, 2011.

[101]. KIM, H.C., T.L. ALFORD, and D.R. ALLEE, "Thickness dependence on the thermal stability of silver thin films". Applied Physics Letters, vol. 81(22), pp. 4287-4289, 2002.

[102]. ALFORD, T.L., L. CHEN, and K.S. GADRE, "Stability of silver thin films on various underlying layers at elevated temperatures". Thin Solid Films, vol. 429(1–2), pp. 248-254, 2003.

[103]. HOFFMAN, R.E. and D. TURNBULL, "Lattice and Grain Boundary Self-Diffusion in Silver". Journal of Applied Physics, vol. 22(5), pp. 634-639, 1951.

[104]. ZIEMANN, P., "Amorphization of metallic systems by ion beams". Materials Science and Engineering, vol. 69(1), pp. 95-103, 1985.

[105]. TERREAULT, B., J.G. MARTEL, R.G. ST-JACQUES, and J. L'ECUYER, "Depth profiling of light elements in materials with high-energy ion beams". Journal of Vacuum Science and Technology, vol. 14(1), pp. 492-500, 1977.

[106]. WEISSMANN, R. and R. BEHRISCH, "Contributions of backscattered ions to sputtering yields depending on primary ion energy". Radiation Effects, vol. 19(2), pp. 69-75, 1973.

[107]. KAMIKO, M., J.-W. KOO, J.-M. KIM, and J.-G. HA, "Atomic force microscopy and x-ray diffraction studies on agglomeration phenomena of ultrathin Au/Fe bilayers". Journal of Vacuum Science & Technology A: Vacuum, Surfaces, and Films, vol. 30(3), pp. 031512-4, 2012.

[108]. VITOS, L., A.V. RUBAN, H.L. SKRIVER, and J. KOLLÁ R, "The surface energy of metals". Surface Science, vol. 411(1–2), pp. 186-202, 1998.

[109]. MAKIN, S.M., A.H. ROWE, and A.D. LECLAIRE, "Self-Diffusion in Gold". Proceedings of the Physical Society. Section B, vol. 70(6), pp. 545, 1957.

[110]. STEPHEN, R.W., B. HANS, and G.M. W., "Monolayres of 11-trichlorosilylundecyl thioacetate: A system that promotes adhesion between silicon dioxide and evaprorated gold.". Journal of Materials Research, vol. 4, pp. 886-892, 1989.

[111]. HOTSTON, E., "Threshold energies for sputtering". Nuclear Fusion, vol. 15(3), pp. 544, 1975.

[112]. STEINBRUCHEL, C., "Universal energy dependence of physical and ion-enhanced chemical etch yields at low ion energy". Applied Physics Letters, vol. 55(19), pp. 1960-1962, 1989.

[113]. COPELAND, F.B.M. and D.S.F. CROTHERS, "CROSS SECTIONS FOR RESONANT CHARGE TRANSFER BETWEEN ATOMS AND THEIR POSITIVE IONS". Atomic Data and Nuclear Data Tables, vol. 65(2), pp. 273-288, 1997.

[114]. PHELPS, A.V., "Cross Sections and Swarm Coefficients for H[sup +], H[sub 2][sup +], H[sub 3][sup +], H, H[sub 2], and H[sup -] in H[sub 2] for Energies from 0.1 eV to 10 keV". Journal of Physical and Chemical Reference Data, vol. 19(3), pp. 653-675, 1990.

[115]. TANARRO, I. and V.J. HERRERO, "Ion energy distributions for the identification of active species and processes in low pressure hollow cathode discharges". Plasma Sources Science and Technology, vol. 18(3), pp. 034007, 2009.

[116]. EHLERS, K.W. and K.N. LEUNG, "High-concentration H2+ or D2+ ion source". Review of Scientific Instruments, vol. 54(6), pp. 677-680, 1983.

[117]. MENDEZ, I., V.J. HERRERO, and I. TANARRO. "Ion and Neutral Species in H2, H2+Ar and H2+N2 Plasmas Generate in Low Pressure DC Discharges.". in *28th ICPIG*. July 15-20, 2007. Prague, Czech Republic

[118]. VEISFELD, N. and J.D. GELLER, "Ion sputtering yield measurements for submicrometer thin films". Journal of Vacuum Science & Technology A: Vacuum, Surfaces, and Films, vol. 6(3), pp. 2077-2081, 1988.

[119]. CHEVOLLEAU, T. and W. FUKAREK, "Ion flux, ion energy distribution and neutral density in an inductively coupled argon discharge". Plasma Sources Science and Technology, vol. 9(4), pp. 568, 2000.

[120]. VENTZEK, P.L.G., M. GRAPPERHAUS, and M.J. KUSHNER, "Investigation of electron source and ion flux uniformity in high plasma density inductively coupled etching tools using two‐dimensional modeling". Journal of Vacuum Science & Technology B: Microelectronics and Nanometer Structures, vol. 12(6), pp. 3118-3137, 1994.

[121]. GRIESSEN, R. and A. DRIESSEN, "Heat of formation and band structure of binary and ternary metal hydrides". Physical Review B, vol. 30(8), pp. 4372-4381, 1984.

[122]. KNACK, S., J. WEBER, H. LEMKE, and H. RIEMANN, "Copper-hydrogen complexes in silicon". Physical Review B, vol. 65(16), pp. 165203, 2002.

[123]. YARYKIN, N., J.U. SACHSE, H. LEMKE, and J. WEBER, "Silver-hydrogen interactions in crystalline silicon". Physical Review B, vol. 59(8), pp. 5551-5560, 1999.

[124]. SVEINBJÖ RNSSON, E.Ö . and O. ENGSTRÖ M, "Reaction kinetics of hydrogen-gold complexes in silicon". Physical Review B, vol. 52(7), pp. 4884-4895, 1995.

[125]. ANDREWS, L., X. WANG, L. MANCERON, and K. BALASUBRAMANIAN, "The Gold Dihydride Molecule, AuH2: Calculations of Structure, Stability, and Frequencies, and the Infrared Spectrum in Solid Hydrogen†". The Journal of Physical Chemistry A, vol. 108(15), pp. 2936-2940, 2004.

[126]. HUBER, K.P. and G. HERZBERG, "Molecular Spectra and Molecular Sturcture Ⅳ. Constants of Diatomic Molecules ". 1979, Newyork: Van Nostrand Reinhold.

[127]. CHOI, T.-S., G. LEVITIN, and D.W. HESS, "Mechanistic Considerations in Plasma-Assisted Etching of Ag and Au Thin Films". ECS Journal of Solid State Science and Technology, vol. 2(6), pp. P275-P281, 2013.

[128]. BYUNG-TEAK, L., S.Y. JUNG, J.L. LEE, Y.J. PARK, M.C. PAEK, and K.I. CHO, "Reactive ion etching of vertical GaN mesas by the addition of CH 4 to BCl 3 /H 2 /Ar inductively coupled plasma". Semiconductor Science and Technology, vol. 16(6), pp. 471, 2001.

[129]. MITURA, S., L. KLIMEK, and Z. HAŚ, "Etching and deposition phenomena in an R.F. CH4 plasma". Thin Solid Films, vol. 147(1), pp. 83-92, 1987.

[130]. NISHIMURA, E., "Substrate Processing Method". 2012: United States. p. U. S. Patent Application Publication, 2012/0164839 A1.

[131]. DRUSCHKE, F., G. KRAUS, U. KUENZEL, W.D. RUH, and R. SCHAEFER, "Method of Dry Copper Etching And Its Implementation". 1985: United States. p. U.S. Patent 4,557,796.

[132]. ISHIDA, T., "Dry Etching Method of Copper or Copper Alloy Interconnection Layer Employing Plasma of An Iodin Compound". 1993: United States. p. U. S. Patent, 5,240,559.

[133]. OZIN, G.A., J.G. MCCAFFREY, and J.M. PARNIS, "Photochemistry of Transition-Metal Atoms: Reactions with Molecular Hydrogen and Methane in Low-Temperature

Matrices". Angewandte Chemie International Edition in English, vol. 25(12), pp. 1072-1085, 1986.

[134]. PARNIS, J.M. and G.A. OZIN, "Photochemistry of methylcopper hydride, CH3CuH: wavelength dependence of the product distribution". The Journal of Physical Chemistry, vol. 93(10), pp. 4023-4029, 1989.

[135]. CHO, H.-G. and L. ANDREWS, "Infrared spectra of CH3-MH, CH3-M, and CH3-MH- prepared via methane activation by laser-ablated Au, Ag, and Cu atoms". Dalton Transactions, vol. 40(42), pp. 11115-11124, 2011.

[136]. RIJS, N.J. and R.A.J. O'HAIR, "Unimolecular Reactions of Organocuprates and Organoargentates". Organometallics, vol. 29(10), pp. 2282-2291, 2010.

[137]. RIJS, N.J. and R.A.J. O'HAIR, "Dimethylcuprate-Catalyzed Decarboxylative Coupling of Allyl Acetate". Organometallics, vol. 31(22), pp. 8012-8023, 2012.

[138]. CATHERINE, Y. and P. COUDERC, "Electrical characteristics and growth kinetics in discharges used for plasma deposition of amorphous carbon". Thin Solid Films, vol. 144(2), pp. 265-280, 1986.

[139]. BIESINGER, M.C., L.W.M. LAU, A.R. GERSON, and R.S.C. SMART, "Resolving surface chemical states in XPS analysis of first row transition metals, oxides and hydroxides: Sc, Ti, V, Cu and Zn". Applied Surface Science, vol. 257(3), pp. 887-898, 2010.

[140]. KHASSIN, A.A., T.M. YURIEVA, V.V. KAICHEV, V.I. BUKHTIYAROV, A.A. BUDNEVA, E.A. PAUKSHTIS, and V.N. PARMON, "Metal–support interactions in cobalt-aluminum co-precipitated catalysts: XPS and CO adsorption studies". Journal of Molecular Catalysis A: Chemical, vol. 175(1–2), pp. 189-204, 2001.

[141]. NORTON, P.R. and R.L. TAPPING, "Photoelectron spectroscopic studies of the adsorption of CO and CO2 on nickel, platinum and copper". Chemical Physics Letters, vol. 38(2), pp. 207-212, 1976.

[142]. PEARSE, R.W.B. and A.G. GAYDON, "The Identification of Molecular Spectra". Vol. 4th ED. 1976, London: Chapman and Hall Ltd.

[143]. MORRISON, N.A., C. WILLIAM, and W.I. MILNE, "Methane chemistry involved in a low-pressure electron cyclotron wave resonant plasma discharge". Journal of Applied Physics, vol. 94(11), pp. 7031-7043, 2003.

[144]. GICQUEL, A., M. CHENEVIER, K. HASSOUNI, A. TSEREPI, and M. DUBUS, "Validation of actinometry for estimating relative hydrogen atom densities and electron energy evolution in plasma assisted diamond deposition reactors". Journal of Applied Physics, vol. 83(12), pp. 7504-7521, 1998.

[145]. ALCOUFFE, G., M. CAVARROC, G. CERNOGORA, F. OUNI, A. JOLLY, L. BOUFENDI, and C. SZOPA, "Capacitively coupled plasma used to simulate Titan's atmospheric chemistry". Plasma Sources Science and Technology, vol. 19(1), pp. 015008, 2010.

[146]. GODYAK, V.A., R.B. PIEJAK, and B.M. ALEXANDROVICH, "Electron energy distribution function measurements and plasma parameters in inductively coupled argon plasma". Plasma Sources Science and Technology, vol. 11(4), pp. 525, 2002.

[147]. OKADA, K., S. KOMATSU, and S. MATSUMOTO, "Langmuir probe measurements in a low pressure inductively coupled plasma used for diamond deposition". Journal of Vacuum Science & Technology A: Vacuum, Surfaces, and Films, vol. 17(3), pp. 721-725, 1999.

[148]. DONNELLY, V.M., "Plasma electron temperatures and electron energy distributions measured by trace rare gases optical emission spectroscopy". Journal of Physics D: Applied Physics, vol. 37(19), pp. R217, 2004.

[149]. CHOI, T.-S., G. LEVITIN, and D.W. HESS, "Low Temperature Cu Etching Using CH4-Based Plasmas". ECS Journal of Solid State Science and Technology, vol. 2(11), pp. P506-P514, 2013.

[150]. JUNG, K.B., J.W. LEE, Y.D. PARK, J.A. CABALLERO, J.R. CHILDRESS, S.J. PEARTON, and F. REN, "Patterning of Cu, Co, Fe, and Ag for magnetic nanostructures". Journal of Vacuum Science & Technology A, vol. 15(3), pp. 1780-1784, 1997.

[151]. MORGAN, W.L., "A critical evaluation of low-energy electron impact cross sections for plasma processing modeling. II: Cl4, SiH4, and CH4". Plasma Chemistry and Plasma Processing, vol. 12(4), pp. 477-493, 1992.

[152]. AU, C.-T., C.-F. NG, and M.-S. LIAO, "Methane Dissociation and Syngas Formation on Ru, Os, Rh, Ir, Pd, Pt, Cu, Ag, and Au: A Theoretical Study". Journal of Catalysis, vol. 185(1), pp. 12-22, 1999.

[153]. ALFONSO, D.R., S.E. ULLOA, and D.W. BRENNER, "Hydrocarbon adsorption on a diamond (100) stepped surface". Physical Review B, vol. 49(7), pp. 4948-4953, 1994.

[154]. TOYODA, H., H. KOJIMA, and H. SUGAI, "Mass spectroscopic investigation of the CH3 radicals in a methane rf discharge". Applied Physics Letters, vol. 54(16), pp. 1507-1509, 1989.

[155]. MIT'KIN, V.N., "Fluorine Oxidants in the Analytical Chemistry of Noble Metals". Journal of Analytical Chemistry, vol. 56(2), pp. 100-122, 2001.

[156]. CIOFFI, N., I. FARELLA, L. TORSI, A. VALENTINI, and A. TAFURI, "Correlation between surface chemical composition and vapor sensing properties of gold-fluorocarbon nanocomposites". Sensors and Actuators B: Chemical, vol. 84(1), pp. 49-54, 2002.

[157]. WITEK, G., M. NOESKE, G. MESTL, S. SHAIKHUTDINOV, and R.J. BEHM, "Interaction of platinum colloids with single crystalline oxide and graphite substrates: a combined AFM, STM and XPS study". Catalysis Letters, vol. 37(1-2), pp. 35-39, 1996.

[158]. HILDENBRAND, D.L., "Dissociation Energy of Copper Monofluoride". The Journal of Chemical Physics, vol. 48(6), pp. 2457-2459, 1968.

[159]. ZMBOV, K.F. and J.L. MARGRAVE, "Mass spectrometric studies at high temperatures. XIV. Vapor pressure and dissociation energy of silver monofluoride". The Journal of Physical Chemistry, vol. 71(2), pp. 446-448, 1967.

[160]. EVANS, C.J. and M.C.L. GERRY, "Confirmation of the Existence of Gold(I) Fluoride, AuF: Microwave Spectrum and Structure". Journal of the American Chemical Society, vol. 122(7), pp. 1560-1561, 2000.

[161]. MIYATA, K., M. HORI, and T. GOTO, "Infrared diode laser absorption spectroscopy measurements of CFX (X=1–3) radical densities in electron cyclotron resonance plasmas employing C4F8, C2F6, CF4, and CHF3 gases". Journal of Vacuum Science & Technology A, vol. 14(4), pp. 2343-2350, 1996.

[162]. SLEIGH, C., A.P. PIJPERS, A. JASPERS, B. COUSSENS, and R.J. MEIER, "On the determination of atomic charge via ESCA including application to organometallics". Journal of Electron Spectroscopy and Related Phenomena, vol. 77(1), pp. 41-57, 1996.

[163]. LINN, J.H. and W.E. SWARTZ, "An XPS Study of the Effects of CF4 Plasmas on Gold Surfaces". Applied Spectroscopy, vol. 39(5), pp. 755-760, 1985.

[164]. DARRAH THOMAS, T. and P. WEIGHTMAN, "Valence electronic structure of AuZn and AuMg alloys derived from a new way of analyzing Auger-parameter shifts". Physical Review B, vol. 33(8), pp. 5406-5413, 1986.

[165]. COBURN, J.W. and H.F. WINTERS, "Ion- and electron-assisted gas-surface chemistry---An important effect in plasma etching". Journal of Applied Physics, vol. 50(5), pp. 3189-3196, 1979.

[166]. D'ULIVO, A., Z. MESTER, J. MEIJA, and R.E. STURGEON, "Mechanism of Generation of Volatile Hydrides of Trace Elements by Aqueous Tetrahydroborate(III). Mass Spectrometric Studies on Reaction Products and Intermediates". Analytical Chemistry, vol. 79(7), pp. 3008-3015, 2007.

[167]. "Calculated Bond Strength of Metal-Hydrogen or Metal-Deutrium ", http://www.wolframalpha.com/input/?i=Cu-deuterium+bond. (Accessed 2014 August)

[168]. TKACZ, M. and R. BURTOVYY, "Decomposition of the hexagonal copper hydride at high pressure". Solid State Communications, vol. 132(1), pp. 37-41, 2004.

[169]. TKACZ, M. and R. BURTOVYY, "Isotope effect in a Cu–H(D) system with hexagonal hydride phase". Journal of Alloys and Compounds, vol. 404–406(0), pp. 368-371, 2005.

[170]. DUNHAM, J. "Atomic Hydrogen and Deuterium Spectra: The Mass of the Deuteron", http://cat.middlebury.edu/~PHManual/atomic.html. (Accessed 2014 August)

[171]. LIU, X., S.W. KING, and R.J. NEMANICH, "Thermal stability of Ti, Pt, and Ru interfacial layers between seedless copper and a tantalum diffusion barrier". Journal of Vacuum Science & Technology B, vol. 31(2), pp. 2166-2746, 2013.

[172]. KRISHNAKUMAR, E. and S.K. SRIVASTAVA, "Cross sections for the production of N + 2 , N + +N 2+ 2 and N 2+ by electron impact on N 2". Journal of Physics B: Atomic, Molecular and Optical Physics, vol. 23(11), pp. 1893, 1990.

[173]. ATSUSHI, S., O. YOSHITAKA, O. SHIGERU, and K. MITSUO, "Cracking Efficiency of Hydrogen with Tungsten Filament in Molecular Beam Epitaxy". Japanese Journal of Applied Physics, vol. 34(10B), pp. L1379, 1995.

[174]. WINDAWI, H.M., "Effect of temperature on the sputtering yield of copper". Surface Science, vol. 55(2), pp. 573-588, 1976.

VITA

Tae-Seop Choi

Tae-Seop Choi was born in Seoul, Korea. He attended Banpo High School in Seoul, and graduated cum laude with a B.S. in Chemical Engineering from Hanyang University, Seoul, Korea in 2009. In same year, he won a Korean Government Scholarship Program for Study Abroad and joined Georgia Tech to pursue a doctorate in Chemical Engineering in 2010. When he is not working in the lab, Tae-Seop enjoys a tea time with his friends and dating with his wife.